New Insights into enzymatic CO_2 reduction using protein film electrochemistry

Vincent Cho-Chien Wang

Wolfson College

TRINITY TERM 2013

A thesis submitted to the Board of the Faculty of Physical Sciences, for the degree of Doctor of Philosophy,

University of Oxford

Abstract

Carbon monoxide dehydrogenase (CODH) is known to catalyze CO oxidation and CO_2 reduction reversibly with the minimal overpotential. A great advantage of protein film electrochemistry (PFE) is its ability to probe catalysis over a wide range of potentials, especially in the low potential region required for CO_2 reduction. CODH I and CODH II from *Carboxydothermus hydrogenoformans* (*Ch*) and the composite enzyme acetyl-CoA synthase/carbon monoxide dehydrogenase (ACS/CODH) from *Moorella thermoacetica*(*Mt*) are intensively studied throughout this thesis .

The different catalytic redox-states in CODH, C_{ox} (inactive state), C_{red1} (for CO oxidation) and C_{red2} (for CO_2 reduction) as characterized by spectroscopy, are studied by PFE in the presence of substrate-mimic inhibitors. Cyanide, isoelectronic with CO, mainly inhibits CO oxidation, whereas cyanate, isoelectronic with CO_2, mainly targets CO_2 reduction. Sulfide inhibits CODH rapidly when the potential is more positive than –50 mV, which suggests that sulfide reacts to form a state at the oxidation level of C_{ox} in CODH and is not an activator for CODH catalysis as suggested before. Thiocyanate only partially inhibits CO oxidation. No inhibition of CODH by azide is detected, which is in contrast with previous studies with ACS/$CODH_{Mt}$. The main differences between CODH I_{Ch} and CODH II_{Ch} are the stronger CO product inhibition and inhibition of CODH II_{Ch} by cyanide. These discoveries might shed light on the possible role of CODH II_{Ch} in biological systems.

In comparison with bidirectional (reversible) electrocatalysis by CODH I_{Ch} and CODH II_{Ch}, only unidirectional electrocatalysis for CO oxidation by ACS/$CODH_{Mt}$ is observed with an overpotential of 0.1 V and the electrocatalytic current is much smaller. In order to identify whether ACS influences the performance of CODH, several chemical reagents, such as sodium dodecyl sulfate (which separates CODH and ACS partially), 1, 10-phenanthroline, (which inhibits the active site in ACS) and acetyl-CoA (the product of the reaction carried out by ACS/$CODH_{Mt}$) are added. However, we have yet to observe any electrocatalytic current from CO_2 reduction. Inhibition of ACS/$CODH_{Mt}$ by cyanide, cyanate and azide is consistent with previous studies by spectroscopy.

Oxygen attack toward the active site in CODH is proved by cyanide protection. The inactive state, C_{ox} can prevent oxygen attack and reductive reactivation restores CODH activity. In contrast, oxygen damages the active site irreversibly when CODH is in the C_{red1} state. The new substrate, nitrous oxide (N_2O), isoelectronic with CO_2, is reduced by CODH and acts as the suicide substrate.

Finally, hydrogen formation in the direction of CO oxidation and formate formation in the direction of CO_2 reduction by CODH are detected. The small solvent kinetic isotope effect is observed in CO oxidation. These findings suggest metal-hydride should play a role in CODH catalysis, which might provide a new direction to design better catalysts for CO_2 reduction.

Collaborations

All protein samples, including carbon monoxide dehydrogease I and carbon monoxide dehydrogease II from *Carboxydothermus hydrogenoformans* and acetyl-CoA synthase /carbon monoxide dehydrogenase from *Moorella thermoacetica* in this thesis have been generously provided from the research group of Prof. Stephen W. Ragsdale in the University of Michigan, Ann Arbor, Michigan. Samples were purified by Dr Mehmet Can and Dr Elizabeth Pierce. The NMR experiment was carried out by Dr Nick Rees from the University of Oxford.

Acknowledgements

Well, finally, it is time to write the most important pages in my thesis and acknowledge people who ever helped my DPhil life in Oxford. First, many thanks to my "unconventional-and-out-of-blue-guru" supervisor, Fraser Armstrong. I learned a lot from him about how to pick up important scientific questions and sell your work; or more realistically speaking, how to enjoy science without caring about the number of publications. True science will stand up in the end.

I also want to thank my two thesis examiners, Prof. Julea Butt and Prof. Edman Tsang. With their critical reviews on my thesis, let this thesis be more profound. I am also grateful to Prof. Stephen W. Ragsdale, Dr Mehmet Can and Dr Elizabeth Pierce for providing me enzyme samples.

My sincere colleagues in the FAA lab, including Alison, Tom, Suzannah, Andreas, Gopan, Non, Yatandra, Philip, Sally, Annemarie, Bonnie, Edgar, Maxie, Mike, Carina, Thomas, James, Tania, Bhavin, Lang, Yiduo, Elena, Roshni are acknowledged for their help, intellectual debates and doing silly stuff with me in these four years. Especially Thank Non, Tom, Suzannah, Andreas and Sally for proof-reading this thesis and my transfer reports.

For my friends in the Wolfson College, starting from the bikii members, boss Daniel, Henry and Myron. Especially Daniel, who patiently listened to my complaint, taught me how to repair bikes and proof-read this entire thesis. Of course, other lovely Wolfson friends, such as Shane, Rui, Renee, Avi, Matthew, Robbie, Jasmines, Neil, Vanshika, Darryl, Garland, Marcus, Kristina, Antia, Ruth, Joyce, and generous "Sir" Jerry (who is very appreciated for giving me almost free meal on weekdays.) are credited with making my monumentally

unforgivable life in Oxford. Jimmy, Yuge, Jason Huang, Gary Chang, Min-Win Chung, Eliz Huang, Porky Fan and my former housemates, Henry Lai, Crystal Liang and Maya are appreciated for their help in my Oxford life. Also thank many unsung heroes/heroines who ever helped me in Oxford for these years.

Finally, I would like to thank my parents, grandparents and sister. Without their financial support and unstoppable encouragement, I could not finish this thesis.

Abbreviations and symbols

MES	2-(N-morpholino)ethanesulfonic acid
SDS	sodium dodecyl sulfate
MWCT	multi-walled carbon nanotubes
Py	1-pyrenebutyric acid (Py)
EDC	ethyl-3-(3-dimethylaminopropyl) carbodiimide
NHSS	N-hydroxy sulfosuccinimide
DMF	dimethyl formamide
Acetyl-CoA	acetyl-coenzyme A
CoA	coenzyme A
FAD	flavin adenine dinucleotide
CODH	carbon monoxide dehydrogenase
ACS/CODH	acetyl-CoA synthase/ carbon monoxide dehydrogenase
ACDS	acetyl-CoA decarbonylase synthase
CoFeSP	corrinoid-iron-sulfur protein
Ch	*Carboxydothemus hydrogenoformans*
Mt	*Moorella thermoacetica*
Rr	*Rhodospirillum rubrum*
Mb	*Methanosarcina barkeri*
PFE	protein film electrochemistry
PGE	pyrolytic graphite edge
EPR	electron paramagnetic resonance
ENDOR	electron nuclear double resonance
NMR	nuclear magnetic resonance
NEXAS	near edge X-ray absorption spectroscopy
GC	gas chromatography
QM/MM	quantum mechanics/molecular mechanics
CV	cyclic voltammetry
ET	electron transfer

PCET	proton-coupled electron transfer
KIE	kinetic isotope effect
SHE	standard hydrogen electrode
SCE	standard calomel electrode
F	Faraday constant
A	surface area
E^0	formal redox potential
j	the flux
k	the rate constant
n	the number of electrons
R	ideal gas constant
T	absolute temperature
α	transfer coefficient
Γ	electroactive area
i	current
ΔG	free energy
λ	reorganization energy
D	diffusion coefficient
υ	kinematic viscosity
ω	rotation rate
i_{lim}	limiting current
K_m	Michaelis constant
K_I	inhibition constant
K_d	dissociation constant

Table of contents

Chapter 1 ***Introduction***

1.1 Fundamental Chemistry of CO_2 reduction

One of the biggest challenge human beings face nowadays is meeting rising energy demands in a clean and sustainable way. The widely used energy from fossil fuels in the last 100 years has led to a large increase in the amount of carbon dioxide in the atmosphere, which has had a great influence on global climates and the ecosystem; therefore, how to convert CO_2 to carbon-based fuel is a highly important quest for scientists. From the thermodynamic point of view, CO_2 is a very stable molecule and the reduction of CO_2 is energetically unfavourable. Approximate ~ −2V is required to reduce CO_2 to radical $\cdot CO_2$ as eq 1.1. Using proton-coupled electron transfer (PCET) to yield reduced carbon compounds can greatly increase the redox potential between −0.61 V (formate) and −0.23 V (methane) as eq 1.2-6. However, multiple proton and electron transfers invoke a higher kinetic energy barrier since a proton is about 1836 times heavier than an electron and it is difficult to occur in synchronous proton-coupled electron transfer to avoid the high kinetic energy barrier. Therefore, the process whereby only two protons and electrons are involved in reduction of CO_2 to CO or formate (eq 1.2 and eq 1.3) seems to be the better choice for CO_2 fixation. Noticeably, CO as the part of syngas, can be used to generate liquid hydrocarbon with H_2 *via* the Fisher-Tropsch process.[1]

$$CO_2 + e^- \longrightarrow CO_2^{\bullet -} \qquad E= -1.90V \qquad (1.1)$$

$$CO_2 + 2H^+ + 2e^- \longrightarrow CO + H_2O \qquad E= -0.53V \qquad (1.2)$$

$$CO_2 + 2H^+ + 2e^- \longrightarrow HCO_2H \qquad E= -0.61V \qquad (1.3)$$

$$CO_2 + 4H^+ + 4e^- \longrightarrow HCHO + H_2O \qquad E= -0.48V \qquad (1.4)$$

$$CO_2 + 6H^+ + 6e^- \longrightarrow CH_3OH + H_2O \qquad E= -0.38V \qquad (1.5)$$

$$CO_2 + 8H^+ + 8e^- \longrightarrow CH_4 + 2H_2O \qquad E= -0.24V \qquad (1.6)$$

1.2 Carbon monoxide dehydrogenase in microorganisms

In biological systems, some microorganisms use CO as their carbon and energy source. The key enzyme participating in this reaction (the reverse reaction of eq 1.2) is called carbon monoxide dehydrogenase (CODH). Two types of CODH are found depending on the whether the organism is an aerobe or anaerobe. Some aerobic and chemolithoautotrophic organisms, such as *Oligotropha carboxidovorans*,[2] use flavin adenine dinucleotide (FAD) and molybdopterin cytosine dinucleotide with a copper atom as cofactors in CODH,[3] whereas other anaerobics, such as *Moorella thermoacetica* (*Mt*)[4] and *Carboxydothermus hydrogenoformans* (*Ch*)[5] use a unique Ni-Fe cluster and traditional iron-sulfur clusters as cofactors.[6] It has been shown that anaerobic Ni-Fe containing CODH can catalyze the interconversion between CO oxidation and CO_2 reduction reversibly with minimal overpotential.[7,8] Therefore, studying the mechanism of CODH may ultimately allow one to design better catalysts for the difficult CO_2 reduction reaction.

In some Ni-Fe containing CODH microorganisms, CODH couples to acetyl-CoA synthase to form a bifunctional enzyme which synthesizes acetyl-CoA as eq 1.7b.[9] For example, in acetogenic bacteria, acetyl-CoA synthase (ACS)[10] combines with CODH to synthesize acetyl-CoA through CO_2 reduction catalyzed by CODH (eq 1.7a), whereas in methanogenic archaea, CODH coupled with acetyl-CoA decarbonylase/synthase (ACDS)[11] cleaves acetyl-CoA to CO_2 and methane.

$$CO_2 + 2H^+ + 2e^- \rightleftharpoons CO + H_2O \qquad (1.7a)$$

$$CO + [CH_3\text{-}Co(III)FeSP]^{2+} + CoASH \rightleftharpoons CH_3COSCoA + [Co(I)FeSP]^+ + H^+ \qquad (1.7b)$$

In equation 1.7b, CoFeSP is the corrinoid-iron-sulfur protein, which carries and delivers a methyl group into ACS. In the reverse reaction of eq 1.7b carried out by ACDS/CODH, tetrahydrosarcinapterin, instead of CoFeSP, is the acceptor for a methyl group from ACDS.[11]

Ni-containing CODH and ACS family can be divided into four classes in terms of the metabolic role and subunit components of the enzymes as shown in Figure 1.1.[12] Class I enzymes consist of five subunits (αβγδε) and are found in autotrophic methanogens, where acetyl-CoA is synthesized from CO_2 and H_2. The subunit components of Class II enzymes are the same as Class I. However, enzymes found in acetoclastic methanogens catalyze the decarbonylation of acetyl-CoA to CO_2, coenzyme A (CoA) and the methyl group with tetrahydrosarcinapterin.

In comparison with multi-subunits in Class I/II, Class III enzymes divide into two different independent proteins, including an $\alpha_2\beta_2$ tetramer (ACS/CODH) and a γδ heterodimer (corrinoid-iron-sulfur protein), and are found in homoacetogens. The catalytic center in tetramer ACS/CODH is the same as Class I for synthesizing acetyl-CoA. Class IV enzymes are the only monofunctional α_2 dimer of CODH, which involve the conversion of CO to CO_2 in the anaerobic CO-dependent energy metabolism of bacteria and archaea. In this thesis, monofunctional CODHs (Class IV) from *Carboxydothermus hydrogenoformans* and bifunctional CODH/ACS (Class III) from *Moorella thermoacetica* are studied.

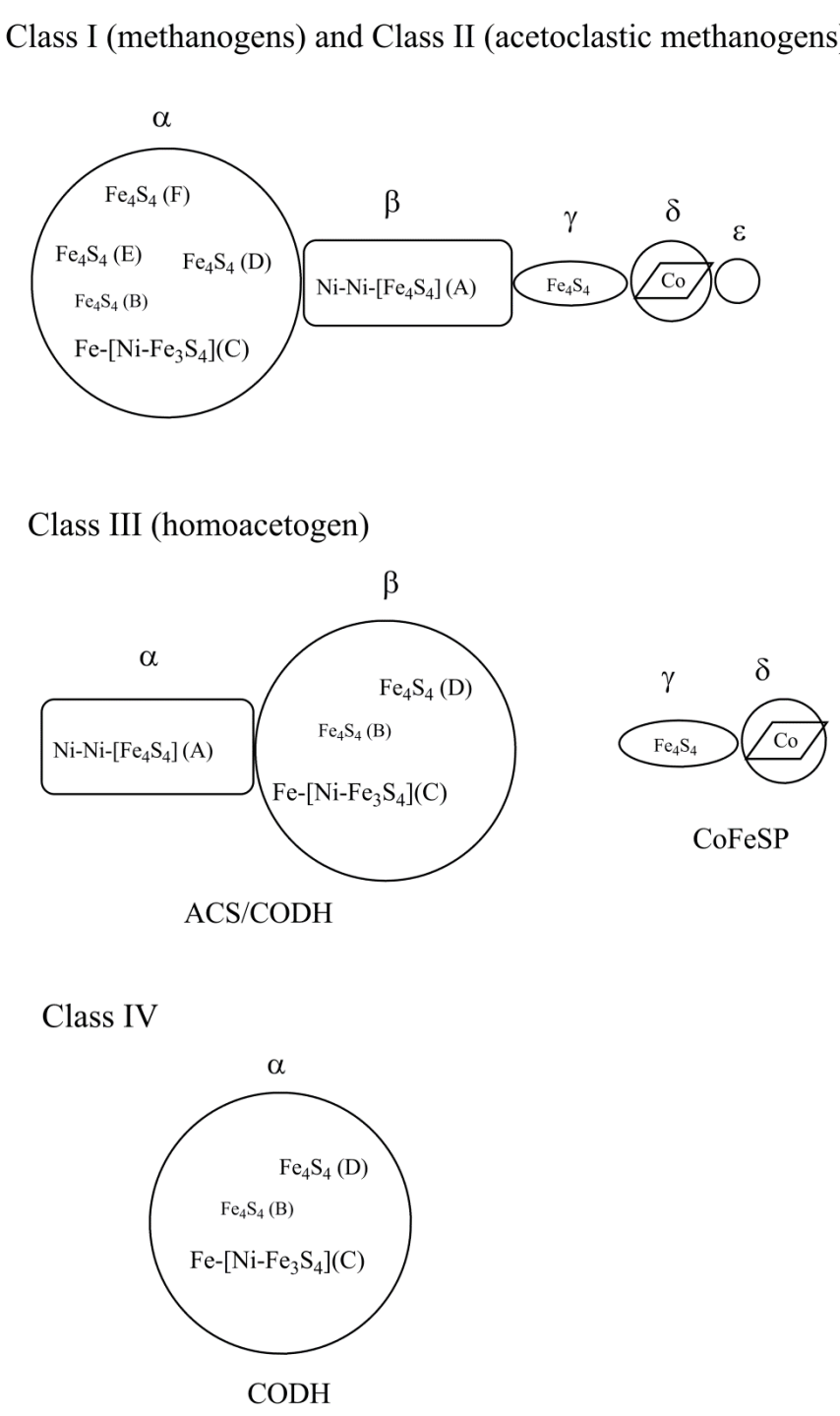

Figure 1.1 Four different classes of Ni-containing CODH are classified by the different constitution of their subunits. The meaning of the letters in brackets is explained in the section 1.3 and 1.4.

Genomic sequencing of *Carboxydothermus hydrogenoformans* (Z-2901),[13] suggests that this organism, a thermophile, expresses at least five different CODHs. CODH I_{Ch} is believed to be involved in energy conversion in which CODH I_{Ch} extracts electrons from CO oxidation and then delivers these electrons to hydrogenase for hydrogen evolution. The proposal is based on the similarity of its genomic clusters with the well-studied CODH-hydrogenase complex from *Rhodospirillum rubrum*[14] and biochemical studies.[15] Although several different CODH II_{Ch} structures from *Carboxydothermus hydrogenoformans* have been solved,[6,16,17] its biological role remains unclear. Meyer and co-workers first purified CODH I_{Ch} (125 kDa) and CODH II_{Ch} (129 kDa) and suggested both are homodimer and use a Ni-Fe-S cluster as the active site and $[Fe_4S_4]$ clusters as the electron relay centers to catalyze CO/CO_2 conversion.[5] In addition, they found CODH II_{Ch} can reduce $NADP^+$ to NADPH by two electrons from CO oxidation. The sequence identity and similarity between these two enzymes are 58.3% and 73.9% respectively. CODH III_{Ch} combines ACS to perform acetyl-CoA synthesis[10] and CODH IV_{Ch} is suggested to be associated with oxidative stress based on the genomic analysis.[13] The biological role of CODH V_{Ch} remains unclear.

1.3 Structure and mechanism of monofunctional CODH

Structural features and different active sites of CODH II from *C. hydrogenoformans* are shown in Figure 1.2 and Figure 1.3. Crystal structures of the monofunctional CODHs from *Rhodospirillum rubrum*(*Rr*)[18] and *C. hydrogenoformans*[6] show that the enzymes are homodimeric. Each subunit contains a buried active site known as the C-cluster which features a $[NiFe_3S_4]$ cubane-like center with a fourth, 'dangling' Fe atom linked to the

$[Fe_3S_4]$ fragment *via* one sulfido ligand ('dangling' emphasizes the part-external position of this Fe relative to the main cluster and it is used in preference to the less-informative terms 'ferrous center II or 'unique Fe' in the literature). There has been controversy over whether a fifth sulfido ligand, bridging the dangling Fe atom and the Ni atom, is present in the active enzyme.[19] (Figure 1.3d) Electron transfers between the C-cluster and the protein surface are mediated by two $[Fe_4S_4]$ clusters, the B-cluster, which has a typical EPR signature of a $[Fe_4S_4]^{1+}$ cluster ($g_{av} < 2$), and the surface-exposed D-cluster that is coordinated equally by both subunits. It is thought that electrons are transferred from ferredoxin to the D-cluster and pass through the B-cluster to the C-cluster, which catalyzes the reduction of CO_2 to CO.

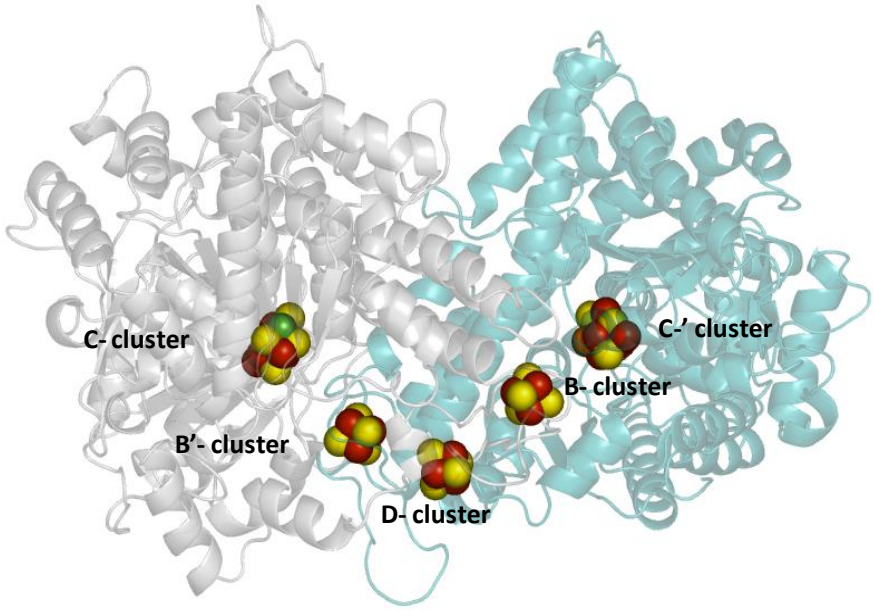

Figure 1.2 The CODH II structure from *Carboxydothermus hydrogenoformans.* The distance between two metal cofactors is about 11 Å .

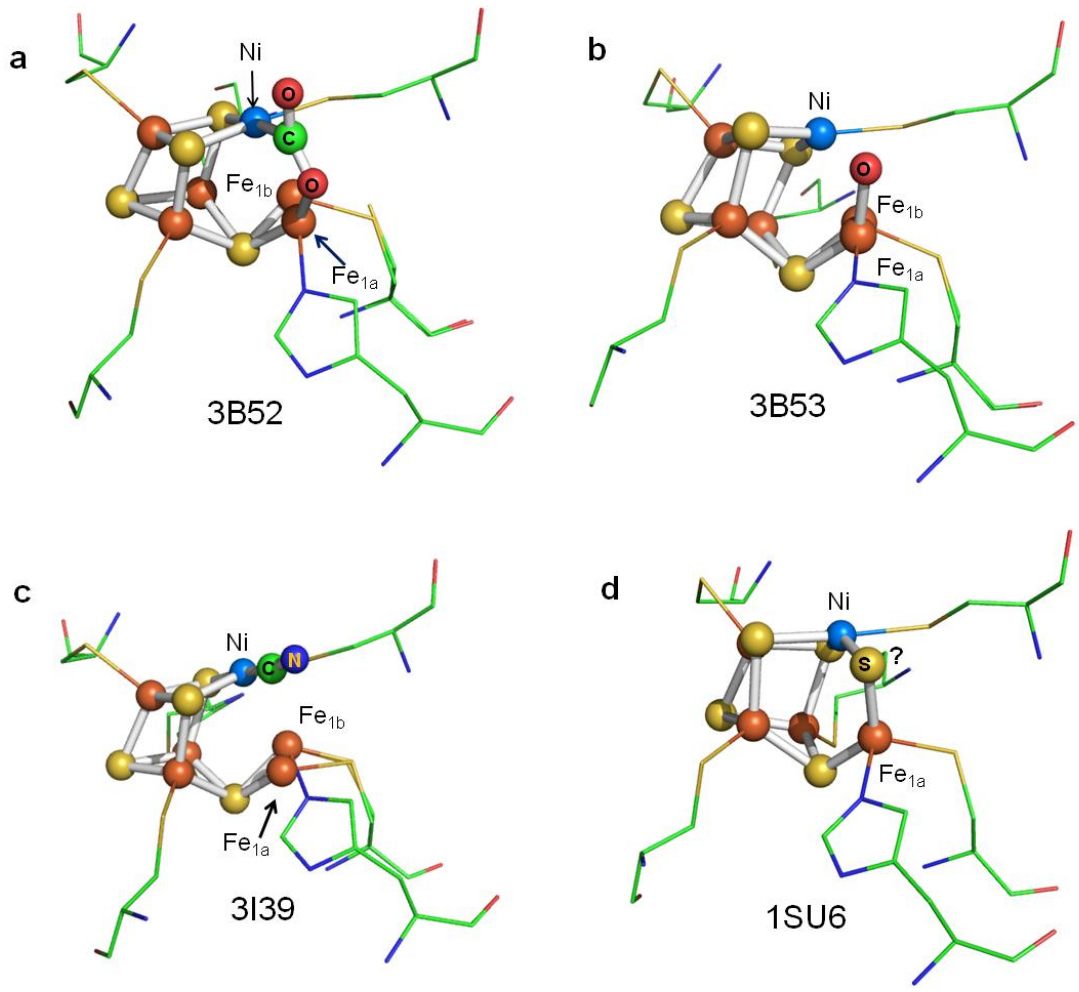

Figure 1.3 Different structures of the active sites of CODH II$_{Ch}$ crystal structures (a) –600mV with CO_2,[6] (b) –320mV,[6] (c) –320mV with cyanide[16] and (d) CO-reduced CODH.[17] Two positions are found for the dangling iron atom in the crystal structure, which is labelled Fe_{1a} and Fe_{1b} respectively. The functional role of the bridge sulfide between the dangling Fe atom and Ni atom (d) is controversial. The pdb codes are shown in each case.

This basic mechanistic model for CO_2/CO interconversion has emerged from crystallography, various kinetic and spectroscopic techniques, and theoretical calculations (Figure 1.4). A particularly significant result was reported by Jeoung and Dobbek[6] who, by incubating crystals of CODH II_{Ch} with $NaHCO_3$ under reducing conditions (–0.6 V) revealed an 'intermediate' state in which CO_2 is bound through the C-atom to the Ni atom (at 1.96 Å) to complete the square-planar coordination geometry that is quite typical of Ni(II). One of the O-atoms of the bound CO_2 is coordinated to the dangling Fe at a distance of 2.05 Å (Figure 1.3a). This result supported a working mechanistic hypothesis based on simple chemical principles – that the role of the dangling Fe atom is to abstract (as hydroxide) an O-atom from CO_2, via a proton-coupled two-electron reaction, leaving CO bound to Ni: conversely, the reverse reaction involves nucleophilic attack by the Fe-bound hydroxide on the Ni-bound carbonyl-C atom.

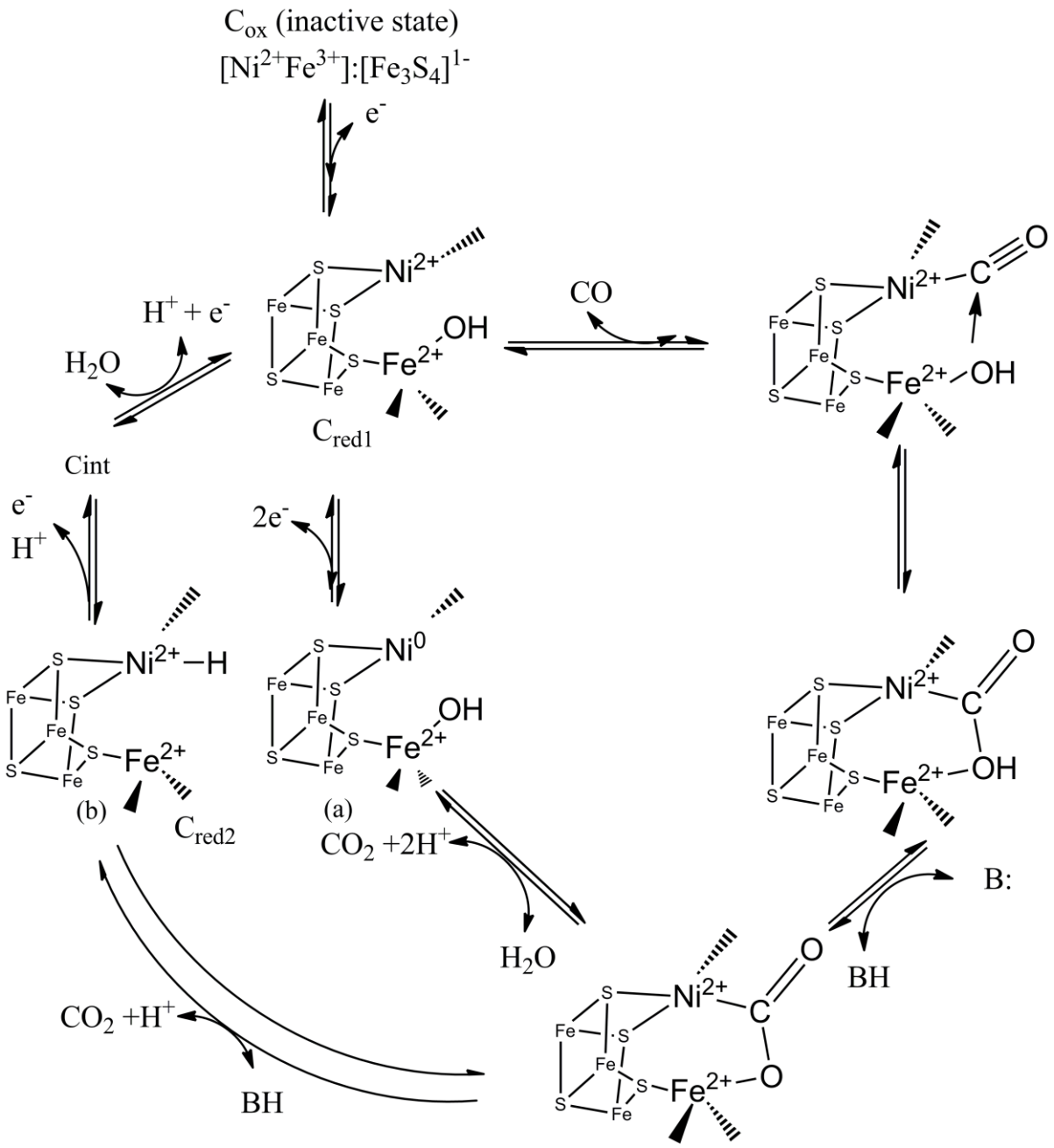

Figure 1.4 Two possible mechanisms of CODH proposed by (a) Dobbek[6] and Lindahl,[20] a Ni (0) state for the C_{red2} state and (b) Fontecilli-Camps,[21] a Ni(II)-H state for the C_{red2} state. More detailed studies are described in Chapter 7. B refers to the amino acid which accepts proton, possibly His or Lys.

The redox transformations have been studied by EPR-monitored titrations, which is summarized in Figure 1.5.[7] The inactive oxidized state C_{ox} is EPR silent: as studied with the CODH/ACS complex from *Moorella thermoacetica*, C_{ox} is reduced by one electron to the active state known as C_{red1} which exhibits a characteristic EPR signal with g_{av}~1.82 (*g* values of 2.01, 1.81, 1.65). The reduction potential for this reaction is approximately −220 mV in $CODH/ACS_{Mt}$ [7] and –110 mV in $CODH_{Rr}$.[22] In $CODH/ACS_{Mt}$, the C_{red1} state rapidly reacts with CO (the rate constant at 5 ^{o}C is 400 s^{-1} - equating to approximately 1.7 x 10^{4} s^{-1} at the physiological growth temperature of *55* ^{o}C)[23] to give CO_2 (which is released) and C_{red2}, which exhibits an EPR signal with g_{av}~1.86 (*g* values of 1.97, 1.87, 1.75). The reduction potential for the two-electron interconversion between C_{red1} and C_{red2} in $CODH/ACS_{Mt}$ is approximately –520 mV for $CODH_{Mt}$[7] and –540 mV for the CODH/ACS from *Methanosarcina thermophila*[24] at pH 7, which is very close to the formal reduction potential for the CO_2/CO couple.[8] The half-cycle regeneration of C_{red1} or C_{red2} by long-range electron transfers requires at least transient participation of an EPR-silent intermediate state C_{int}.[25] The electron distribution in the C-cluster in these different oxidation levels is still unresolved. Based on the large ^{57}Fe- and minimal ^{61}Ni-hyperfine values, most of the unpaired spin density is clearly localized on Fe in the both C_{red1} and C_{red2} states.[26] The similar EPR spectra for the C-cluster (g_{av} <2) further suggest that a $[Fe_3S_4]^{1-}$ fragment is present in both C_{red1} and C_{red2}; therefore, the two-electron transition might involve Ni(II,0) or participation of a Ni(II)-hydride,[21](Figure 1.4) the latter possibility also accounting for the instability of C_{int}.

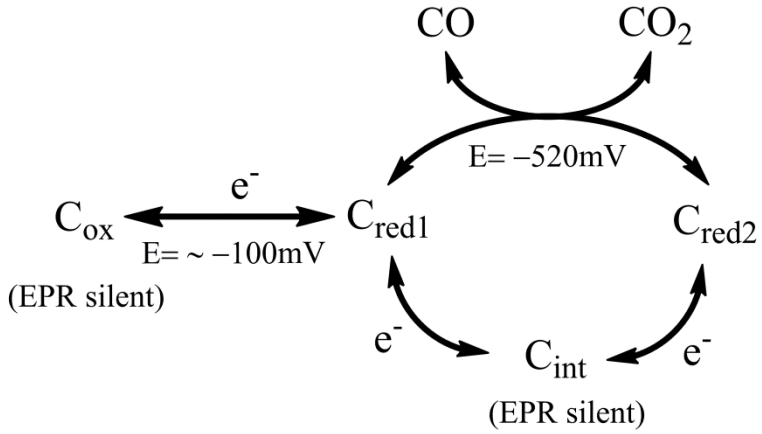

Figure 1.5 The catalytic mechanism of CODH based on EPR studies

1.4 Structure and mechanism of bifunctional acetyl-CoA synthase/carbon monoxide dehydrogenase (ACS/CODH)

Several X-ray crystal structures of ACS/CODH, including ACS/CODH[27,28] from *Moorella thermoacetica* (as shown in Figure 1.6), CODH[6] and ACS[10] respectively from *Carboxydothermus hydrogenoformans* have been solved. These structures clearly show several [Fe_4S_4] clusters are involved in electron transfer (the B-cluster and D-cluster as monofunctional CODH) and two unique metal clusters, in which the C-cluster, [$NiFe_4S_4$] in ACS/CODH is highly similar to the C-cluster in monofunctional CODH and the A-cluster, [Ni-Ni-Fe_4S_4] in ACS synthesizes acetyl-CoA. The A-cluster consists of two Ni atoms in which the distal Ni atom is bridged by two thiolates and the proximal Ni atom bridges with the [Fe_4S_4] cluster by the cysteine thiolate as shown in Figure 1.6. It is believed that only the proximal Ni atom is involved in the catalytic cycle and the distal Ni atom is redox-inactive and remains Ni (II) during the catalytic cycle.[27]

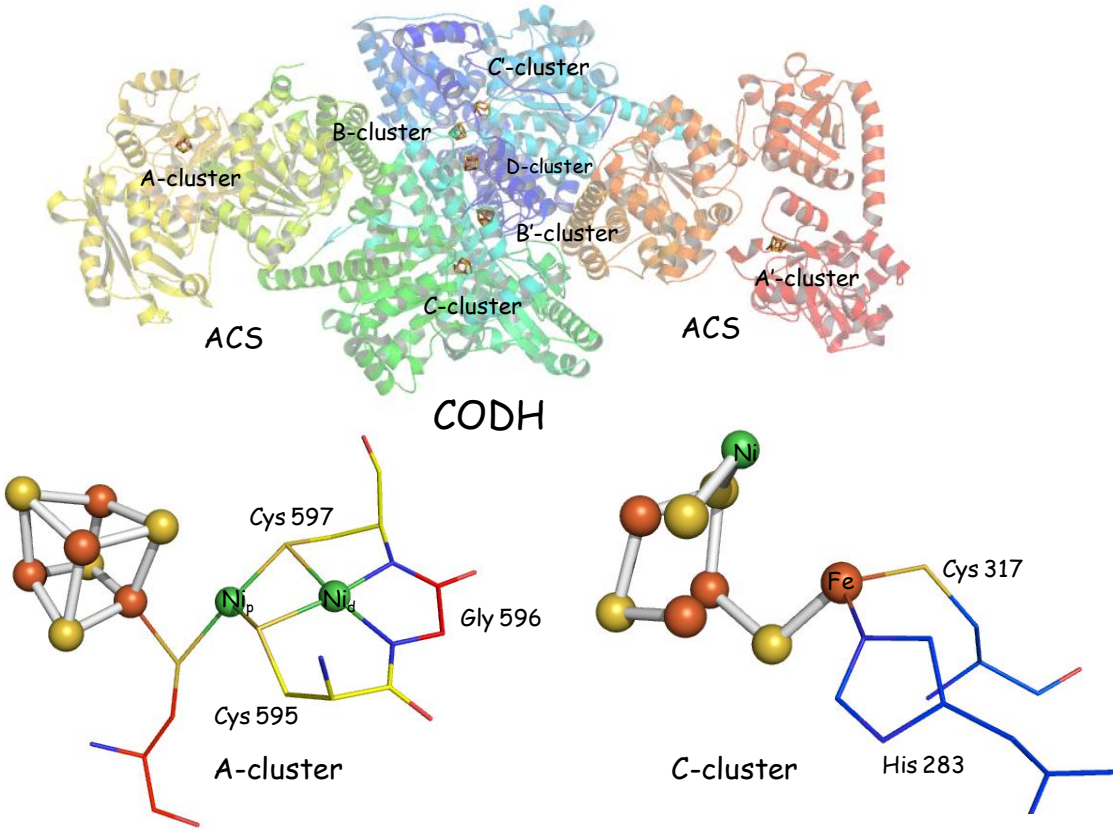

Figure 1.6 The structure of ACS/CODH (1OAO) from *Moorella thermoacetica*.[27] ACS/CODH is a $\alpha_2\beta_2$ tetrameric structure in which the A-cluster in ACS has the proximal Ni (Ni_p) ion which links to the $[Fe_4S_4]$ cluster and is the redox-active site and the C-cluster in CODH contains the dangling iron atom (Fe) outside the nickel-iron-sulfur cluster as the structures of the C-cluster from monofunctional CODH. The B and C clusters are traditional $[Fe_4S_4]$ clusters.

ACS/CODH is a $\alpha_2\beta_2$ heterotetramer (Figure 1.6) in which ACS (α-subunit) condenses CoA, CO from CO_2 reduction catalyzed by CODH (β-subunit) and a methyl group from

CoFeSP into acetyl-CoA and CODH catalyzes interconversion between CO and CO_2.[28] The Xenon–treated ACS/CODH structure exhibits a 70 Å long gas channel between two subunits[29] and no CO product from CO_2 reduction by CODH is observed during the acetyl-CoA synthesis by ACS/CODH.[30] These pieces of evidence indicate the intermediate CO product from CO_2 reduction diffuses through the channel without escaping from the interior enzyme during the acetyl-CoA synthesis.

Different conformations of the gas channel inside ACS/CODH during acetyl-CoA synthesis have been proposed as shown in Figure 1.7. Two different conformations of the β subunit are observed in a single dimer $\alpha_2\beta_2$ crystal structure from *Moorella thermoacetica*.[27] In the closed conformation of the α-subunit (ACS synthase), the less solvent exposed area of the A-cluster are observed and the putative gas channel between the C-cluster and A-cluster is open. Further Xenon-treated crystal structures prove the existence of the gas channel between the A-cluster and C-cluster.[29] In comparison, the open conformation of the α-subunit has the greater solvent accessibility for the A-cluster, which can react with a methyl group from CoFeSP. Meanwhile, the gas channel appears to be blocked by the N-terminal domain from the α-subunit. However, at least two extra discrete conformations are necessary. One discrete conformation is required for condensation between the methyl group and CO to form the acetyl group in the conformation of the less solvent exposed environment. If not, water could easily react with the acetyl-group and yield the acetate rather than the acetyl-CoA.[29] Another important conformation should be associated with a final stage of acetyl-CoA formation between CoA and the A-cluster with the acetyl group.

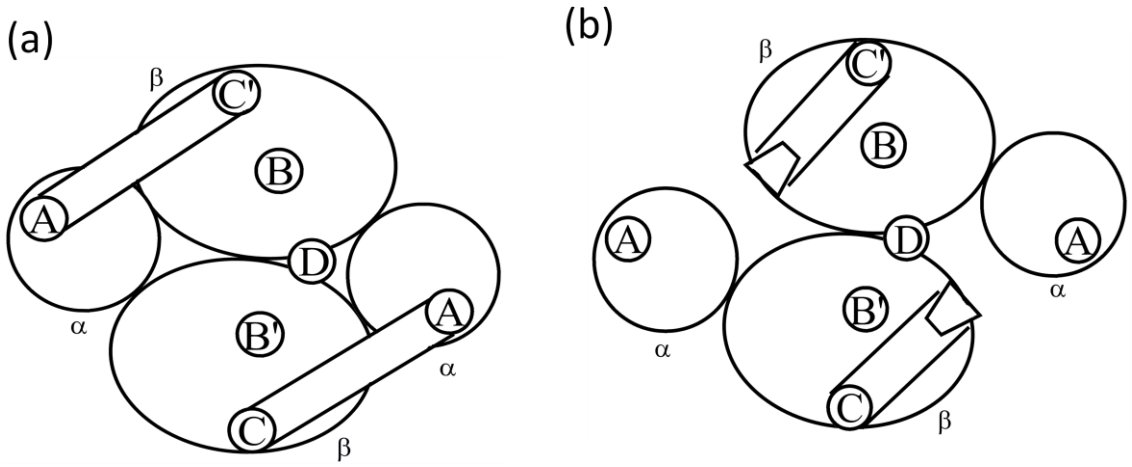

Figure 1.7 Cartoon figures show two different conformation structures based on X-ray crystal structures of ACS/CODH from *M. thermoacetica*.[27] (a) closed structure with open gas channel, which can deliver CO product from the C-cluster to the A-cluster (b) open structure with closed gas channel, which may involve the reaction between the A-cluster and a methyl group from CoFeSP.

1.5 The scope of thesis

Protein film electrochemistry (PFE) refers to a suite of techniques that address enzyme molecules directly attached onto an electrode surface, allowing catalytic activity to be recorded (as current) as a continuous function of electrode potential and/or time.[31] The rates and strengths of binding of an inhibitor are thus addressable as a precise function of potential during steady-state catalysis, and this allows the particular redox level of the enzyme that is being targeted to be identified. Importantly, information on enzyme activity is easily obtained at potentials well below those commonly accessed by chemical mediators and titrants, which is essential when studying an enzyme is able to catalyze CO_2 reduction which requires potentials more negative than −0.5 V. The fact that the enzyme is immobilized also allows

inhibitors to be added and then removed, a procedure that is impractical in solution kinetics. Many enzymes, including CODH, behave as reversible electrocatalysts and are inspirational for energy technologies such as solar fuel conversion.[8,32-34]

Based on previous PFE results which show rapidly and efficiently electrocatalytic CO and CO_2 interconversions by CODH I_{Ch} on the PGE electrode,[8] in this thesis, PFE is further used to establish and analyze the strong potential dependence of the inhibition of enzymatic CO oxidation and CO_2 reduction by cyanide and cyanate respectively, which mimic CO and CO_2 substrate, and sulfide which is used to address the controversy surrounding its role in CODH. The results, obtained for CODH I_{Ch} and CODH II_{Ch} from *Carboxydothermus hydrogenoformans*, reveal very clearly how each inhibitor targets different states of the enzyme, show how rapidly they bind or leave the active site as the redox level is changed and suggest the possible role of CODH I_{Ch} and CODH II_{Ch} in the microorganism. The findings provide a wide, continuous potential landscape for structural and spectroscopic research carried out over three decades, and explain and unify important aspects of this class of enzyme. Further comparison between monofunctional CODH and bifunctional ACS/CODH shows ACS plays an important role in modulating CODH performance. The electrocatalysis of the reduction of nitrous oxide (N_2O) by CODH is observed and where and how oxygen damages *anaerobic* CODH is reported in the first time in this thesis. These findings could open a new direction to study the mechanism of CODH. Finally, a Ni-H intermediate state in the catalytic cycle is suggested, depending on the detection of the small amount of hydrogen in the direction of CO oxidation and formate in the direction of CO_2 reduction during CODH catalysis and the observation of small solvent kinetic isotope effect value in CO oxidation.

Chapter 2 *Electrochemical theory in protein film electrochemistry*

2.1 Abstract

Protein Film Electrochemistry (PFE) is the main tool for studying carbon monoxide dehydrogenase throughout this thesis. This chapter describes some fundamental concepts in PFE, from the basic and important concept of the Butler-Volmer model to more complex processes involving enzyme catalysis, intramolecular electron transfer inside the enzyme, interfacial electron transfer between electrode and enzymes and mass transport in PFE. Finally, some equations for data analysis and experimental techniques, such as cyclic voltammetry and chronoamperometry are introduced briefly.

2.2 Background of protein film electrochemistry

Protein Film Electrochemistry (PFE) was developed in late seventies. The Kuwana group[35] and Hill group[36] respectively showed the quasi-reversible cyclic voltammogram from cytochrome c which was directly attached onto electrodes. Following this achievement, other redox proteins, such as ferredoxin or blue copper protein on different electrodes with/without surface modification were also reported.[37] Following these achievements, the electrocatalytic current (enzymatic catalysis) from enzymes, such as cytochrome c peroxidase[37] and succinate dehydrogenase (complex II)[38] directly adsorbed on the pyrolytic graphite edge (PGE) electrode are observed.

In comparison with spectroscopic potentiometry-titration in redox proteins/enzymes, there are two major advantages to PFE. Firstly, in the potentiometry-titration, the reaction is normally performed at the (steady-state) equilibrium condition without substrates. However, the catalytic potential is not necessarily the same as the value of the formal potential (Nernst potential at equilibrium) since enzymatic catalysis occurs in the presence of substrate transformation. Needless to say, the electrode can provide a wide and continuous range of potentials, which yields valuable kinetic and thermodynamic information that cannot be easily achieved with conventional methods.

Secondly, PFE can *instantly* provide information about the catalytic condition of enzymes since the electrocatalytic current is directly proportional to the catalytic turnover rate. It is feasible to observe different redox states which relate to inhibition, inactivation or activation processes and the reversible process in the case of reversible catalysis. It is difficult to conduct these kinds of experiments in the conventional solution activity assay.

In terms of operational advantage, PFE normally needs a relatively small amount of enzyme samples, about pmole/cm^2 as opposed to conventional spectroscopy, such as EPR, UV-visible and IR (~ μM). It is feasible to change different solutions which might involve different pH values, isotope effect, inhibitor and substrate concentration in the electrochemical cell or adjust temperatures on the same protein film for obtaining kinetic information because proteins are attached on the electrode surface. If the substrate is a gas, such as hydrogenase or carbon monoxide dehydrogenase, it is easy to replace substrates in the solution by purging with inert gas.

However, not all redox proteins/enzymes are able to attach onto the electrodes. In addition, the stability of protein films can be a problem and hinder data analysis. In the PGE case, stability can be increased by adding polyamines, such as polymyxin or neomycin,[39] surface modification[40] or covalent bond linkage between enzymes and PGE surface.[41] Another disadvantage of PFE is difficult to obtain any structural or chemical information about intermediates in the enzyme without complementary evidence from spectroscopic techniques. Therefore, it is important to use these tools together to obtain a more complete picture. For example, A technique, called spectroelectrochemistry, has been developed to record signals from spectroscopy and PFE simultaneously, which can reveal structural or electronic information of the specific state which is controlled by a precise applied potential.

2.3 Pyrolytic graphite edge (PGE) electrode

In comparison with most electrodes, such as the gold electrode, which are normally required for surface modification or even site-directed mutagenesis in the protein to enable protein adsorption by covalent-bond linkage, the adsorption of protein on the pyrolytic

graphite edge (PGE) electrode is much easier via hydrophobic interactions or electrostatic interactions without further surface modification.[40]

The structure of highly ordered pyrolytic graphite materials can be divided into two planes, the basal plane and the between-layer-and-layer edge plane (Figure 2.1). It is generally proposed that the edge plane has much faster electron transfer kinetics than the basal plane which is normally regarded as being inert to electron transfer. However, a very recent study reveals that the *fresh* basal plane should also have fast electron transfer kinetics and the sluggish electron transfer kinetics should be ascribed to the surface deterioration from the environment or ongoing experiments.[42] The PGE electrode is intensively used throughout this thesis and a mixture of polymyxin and enzyme is used to increase film stability on the PGE electrode.

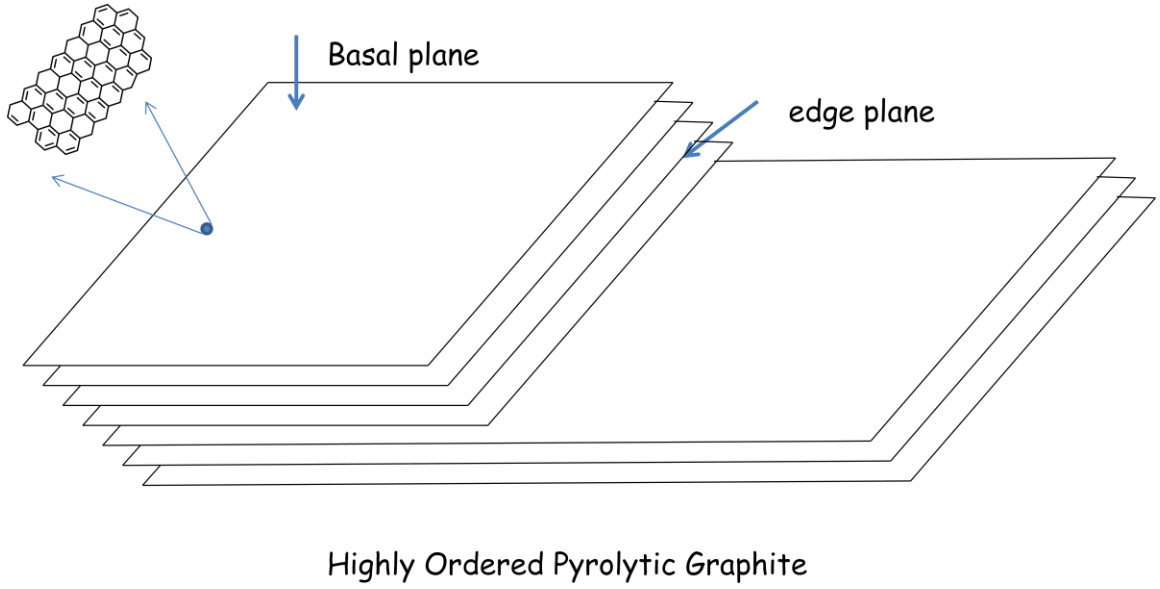

Figure 2.1 The structure of highly ordered pyrolytic graphite

2.4 Basic electrode kinetics -Faraday's Law of Electrolysis and Butler-Volmer model

When electrolysis (or a redox reaction) occurs on the electrode, the current (*i*) can be related to the flux of reactant as written in eq 2.1 according to Faraday's Law of Electrolysis.

$$i = nFAj \qquad j = k(n)[reactant]_0^n \qquad \text{Equation 2.1}$$

where *n* is the number of electrons involving electrolysis, *F* is the Faraday constant, *A* is the electrode surface area and *j* is the flux for measuring the heterogeneous rate between the electrode and reactant which undertakes electrolysis. *k(n)* is the heterogeneous reaction rate constant, which normally is the first order in a heterogeneous reaction. [*reactant*]$_0$ refers to the concentration of the reactant near the electrode since the bulk concentration of the reactant is higher when a redox reaction only occurs near the electrode.

Based on the Butler-Volmer model, we can obtain an electron transfer rate constant on the electrode surface for one-electron redox couple, such as the oxidation reaction (eq 2.2a) and reduction reaction (eq 2.2b) respectively.

$$k_O = k^0 \, exp\left[\frac{-(1-\alpha)F(E-E^0)}{RT}\right] \quad equation\ 2.2a$$

$$k_R = k^0 \, exp\left[\frac{-\alpha F(E-E^0)}{RT}\right] \qquad equation\ 2.2b$$

where k_O and k_R are the oxidative rate constant and reductive rate constant respectively, k^0 is a standard rate constant, E^0 is the formal redox potential, *R* is the ideal gas constant, *T* is the absolute temperature and α is a transfer coefficient which is normally taken as 0.5 assuming that a symmetrical reaction occurs.

When incorporating eq 2.2 into eq 2.1 and assuming the redox reaction is at equilibrium, the net current from the oxidative current and reductive current is zero. The final equation (eq 2.3) is the same as the Nernst equation which describes the relation between the potential and concentration of the redox couple at equilibrium.

$$E = E^0 + \frac{RT}{F} ln \frac{[Ox]_0}{[Red]_0} \quad equation\ 2.3$$

When electroactive enzymes are adsorbed on the electrode surface, such as CODH studied in this thesis, several factors in PFE need to be considered as illustrated in Figure 2.2.

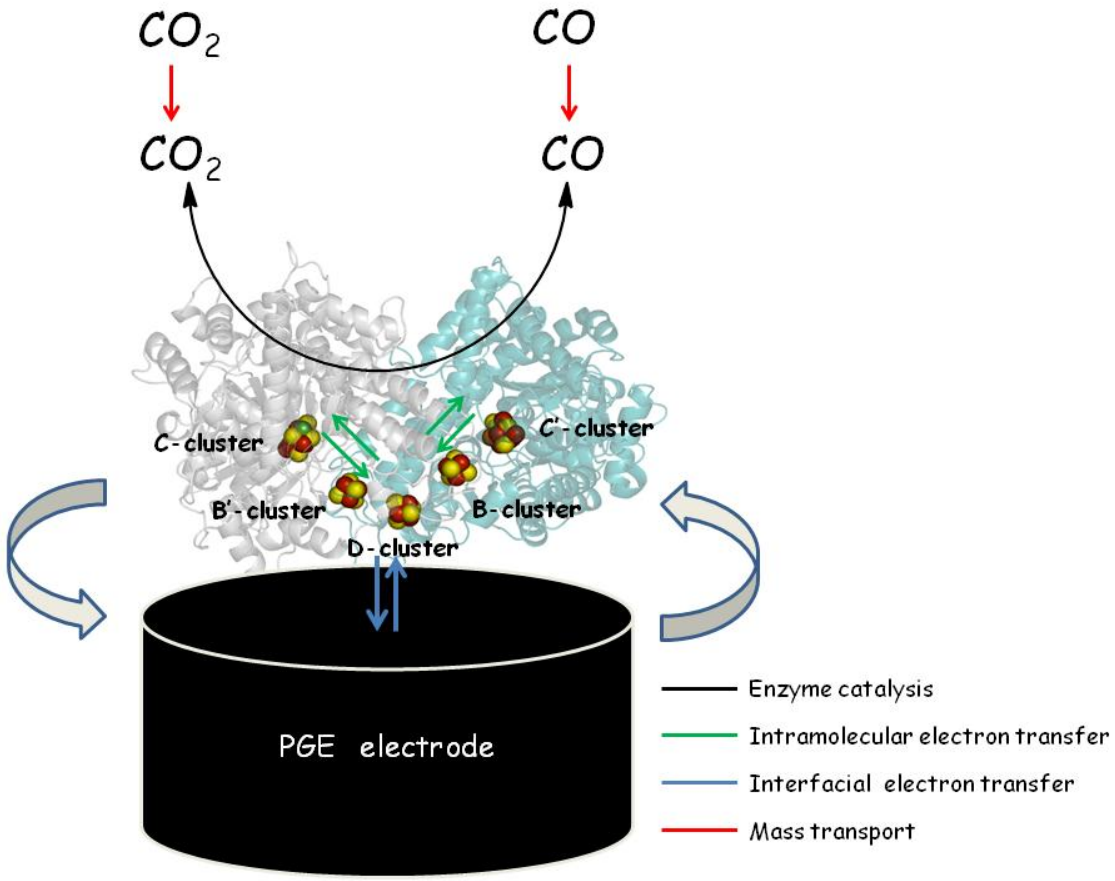

Figure 2.2 An illustration of the four factors which contribute to the electrocatalytic current from enzymatic electrocatalysis on electrode in protein film electrochemistry

Four factors can contribute to the apparent current: enzyme catalysis, intramolecular electron transfer (ET), interfacial ET and substrate mass transport. If all factors could be simply regarded as a series circuit, the apparent current can be expressed as eq 2.4.

$$\frac{1}{i} = \frac{1}{i_{cat}} + \frac{1}{i_{interfacial-ET}} + \frac{1}{i_{intra-ET}} + \frac{1}{i_{mt}} \quad equation\ 2.4$$

Obviously, interfacial ET ($i_{\text{interfacial-ET}}$) and mass transport ($i_{\text{mt}}$) should be avoided because investigation of the enzymatic mechanism is the main purpose in PFE. In this thesis, intramolecular ET ($i_{\text{intramolecular ET}}$) between electron relay centers (the B-cluster and D-cluster) in CODH are not particularly studied and the main research will focus on the inherent property of enzyme catalysis (i_{cat}).

2.5 Enzyme catalysis

First, enzyme catalysis (i_{cat}) is discussed. A simple kinetic model for enzymatic catalysis is shown in Figure 2.3. In this model, the oxidized state (O), intermediate state (I) and reduced state (R) are different redox state in the active site. The substrate (S) only reacts with the reduced state (R) in the enzyme, which catalyzes substrate (S) to product (P) irreversible with a turnover frequency, k_2. More complex models and detailed explanations, for example, showing substrate binding to different redox states and electron transfer reactions coupling to chemical reaction (EC reaction), can be found in these papers.[41,43-45]

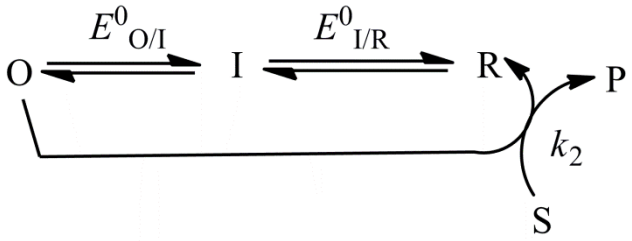

Figure 2.3 The mechanistic model for enzymatic catalysis on the electrode is used in this chapter. O (oxidized state), I (intermediate state) and R (reduced state) are different redox state in the active site. E^0 is the redox potential between two different redox states. S is the substrate and P is the product. The turnover frequency for the enzyme is k_2.

2.5.1 Non-turnover rate

First, the non-turnover signal from enzyme is discussed. For a monolayer of electroactive molecules adsorbed on an electrode surface, the relation between the non-turnover current and potential can be described as eq 2.5 at equilibrium (The derivation of eq 2.5 can be found in these references.[46,47])

$$i(E^0) = \frac{n^2F^2A\Gamma\nu}{RT}\frac{exp[nf(E-E^o)]}{(1+exp[nf(E-E^o)])^2} \qquad equation\ 2.5$$

where Γ is the electroactive area, ν (=dE/dt) is the scan rate, f=F/RT and the rest of terms are defined as in eq 2.1 and 2.2.

When proteins absorb on the electrode, the redox potential comes from redox-active metal centers buried inside a protein and it can be obtained by cyclic voltammetry (which records current as a function of applied potential. More details will be discussed later in section 2.8). The electroactive protein concentration (Γ) can be obtained by equation 2.5. Several examples, such as iron-sulfur cluster protein[39], azuin[48] and even enzyme, hydrogenase[49] have been reported. If there is only the one-electron redox couple, the voltammogram reveals a symmetrical peak for the oxidation and reduction as shown in Figure 2.4.

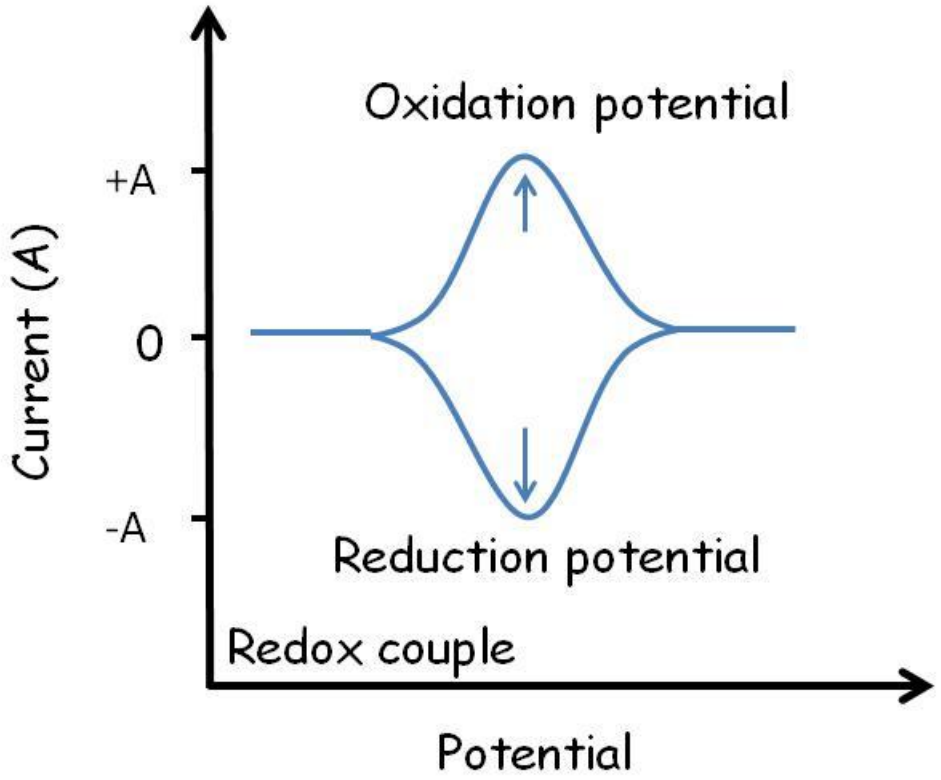

Figure 2.4 Illustration of the non-turnover signal of redox proteins/enzymes adsorbed on the electrode

However, some enzymes (proteins) contain more than two redox couples. For example, the model in Figure 2.3 has two redox couples. The addition of the second electron could be the more favourable ($E^0_{O/I} < E^0_{I/R}$) or less favourable reaction ($E^0_{O/I} > E^0_{I/R}$) than the first ET. This phenomenon is called cooperativity and affects the shape of voltammograms. The apparent value of n (obtained from experiments) can indicate the extent of cooperativity. In theory, two peaks merge together in full cooperation (n=2) in the voltammogram and it is narrower and taller than the standard peak from a separate single-electron in the non-cooperation manner (n=1). More detailed discussion about the cooperative phenomenon

between the number of electrons, the relation between cooperativity and voltammogram shapes can be found in the reviews paper by Leger.[41]

2.5.2 Catalytic current in enzymes (Turnover rate)

When substrates enter the active site, enzyme catalysis occurs. Based on the Butler-Volmer model in the steady-state condition, the relation between the electrocatalytic current and potential can be described by eq 2.6a for the model in Figure 2.3 without limitation by mass transport or interfacial electron transfer and the shape of a voltammogram is sigmoidal. (Figure 2.4)

$$i = \frac{i_{lim}}{1 + \exp\left[f\left(E^0_{O/I} - E\right) + \exp\left[nf\left(E^0_{O/R} - E\right)\right]\right.} \quad equation\ 2.6a$$

$$i_{lim} = nFAk_{cat}\,\Gamma \quad \text{equation 2.6b}$$

where i_{lim} refers to the maximum current when enzymes are saturated with substrates (K_{m} << [S])

When enzymes are saturated (K_{m} << [S]) by substrate concentration, the electrocatalytic current is not potential-dependent anymore and follows eq 2.6b. The value k_{cat} can simply be obtained by eq 2.6b if the value Γ can be obtained by the non-turnover signals (eq 2.5). In some cases, such as CODH, the electrocatalytic current starts to drop when the potential continues to increase beyond the potential region in which i_{lim} occurs (Figure 2.5). This suggests that the enzyme forms another inactive redox state in this potential region.

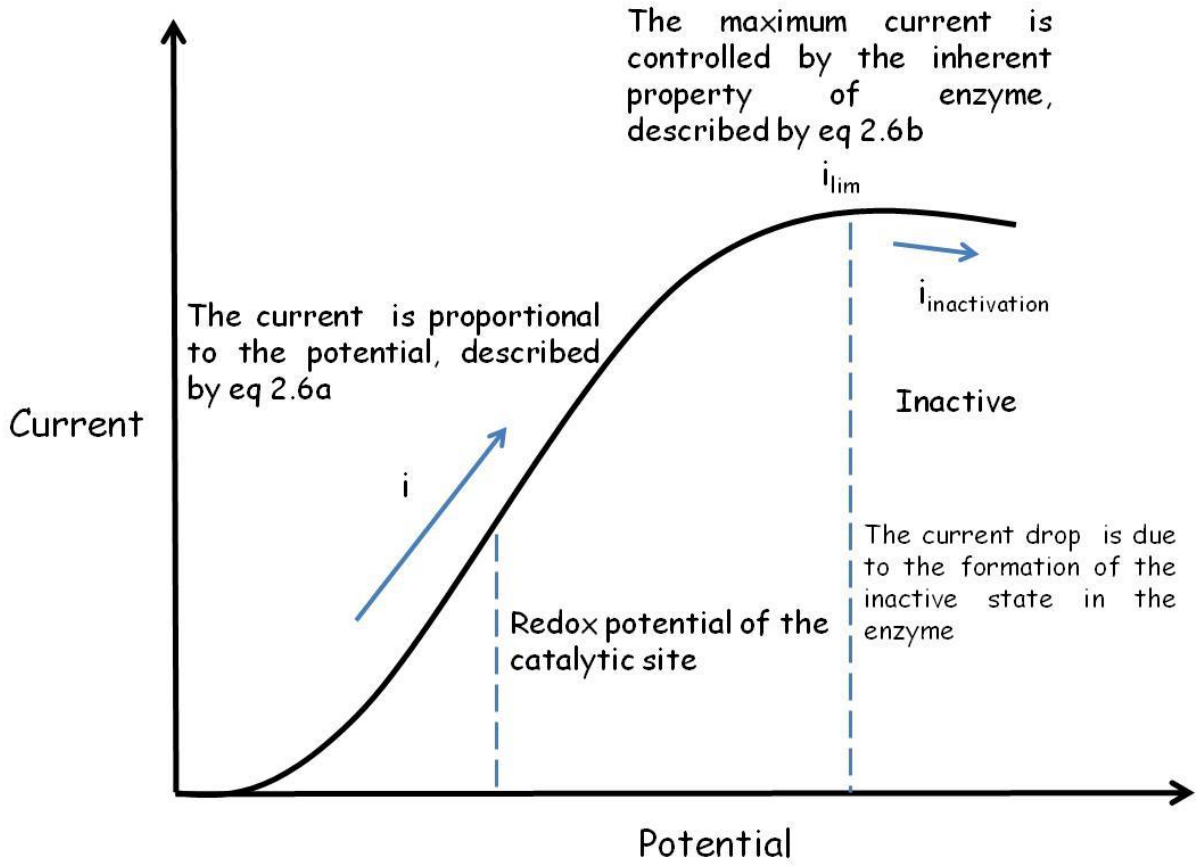

Figure 2.5 The relation between current and potential in the catalytic enzyme on the electrode and information can be obtained from the voltammogram.

2.5.3 Intramolecular electron transfer between electron relay centers

The ET rate between electron relay centers plays another important role in controlling enzyme catalysis. The ET rate between a donor and an acceptor in proteins could be estimated by eq 2.7 in the downhill ET reaction. [50,51]

$$log_{10}k_{ET} = 13 - 0.6(r - 3.6) - \frac{3.1(\Delta G + \lambda)^2}{\lambda} \qquad \text{equation 2.7}$$

where r is the distance between a donor and an acceptor, ΔG is the free energy between a donor and an acceptor and λ is the reorganization energy.

In CODH, the distance between electron relay centers (between the B'-cluster and the D-cluster) or the electron relay center (B'-cluster) and active site (C-cluster) is about 10 Å (Chapter 1).[52] The difference in redox potential between the C-cluster and B'-cluster (electron relay center) is about 200 mV[20] but the redox potential of the D-cluster is still unclear. For intramolecular ET in protein, the reorganization energy can be roughly estimated as 0.7 eV.[51] Therefore, according to eq 2.7, the ET rate between the C-cluster and B'-cluster is about 10^8 s^{-1}, which is much faster than the turnover rate (k_{cat}) (10^5 s^{-1}).[5] The reaction of substrate turnover is the rate-determining step in CODH catalysis.

The kinetic model involving intramolecular electron transfer is more complex. For example, in comparison with eq 2.6 only describing the relation between the electrocatalytic current and potential in enzyme catalysis, k_{cat} now includes the rate constants, k_2 (substrate turnover rate) and k_{ET} (intramolecular ET rate) (eq 2.8) and the potential is replaced by the apparent reduction potential which is controlled by the kinetics of slow intramolecular ET instead of only the catalytic center. More detailed information can be found in these papers.[41,43]

$$\frac{1}{k_{cat}} = \frac{1}{k_2} + \frac{1}{k_{ET1}} + \frac{1}{k_{ET2}} + \cdots \qquad equation\ 2.8$$

2.6 Interfacial electron transfer

When interfacial ET is slower than the turnover current, the relation between current and potential can be described by eq 2.9. Term a and term b represent enzyme catalysis and interfacial ET respectively. If the interfacial ET (term b) is the rate-determining step, the explanation for the inherent property of enzyme catalysis may not be correct.

$$\frac{i_{lim}}{i} = a + b \qquad equation\ 2.9a$$

$$a = 1 + \exp\left[f\left(E^0_{\frac{O}{I}} - E\right)\right] + \exp\left[nf\left(E^0_{\frac{I}{R}} - E\right)\right] \quad equation\ 2.9b$$

$$b = \frac{k_2}{k_0^{O/I}} \exp\left[\frac{f}{n}\left(E^0_{O/I} - E\right)\right] \left(1 + \exp\left[\left(E^0_{I/R} - E\right)\right]\right.$$

$$\left. + \frac{k_2}{k_0^{I/R}} \exp\left[\frac{f}{n}\left(E^0_{I/R} - E\right)\right]\right. \quad equation\ 2.9c$$

$$I_{lim} = nFAk_{cat}\,\Gamma \quad \text{equation 2.9d}$$

where $k_0^{O/I}$ and $k_0^{I/R}$ refer to the interfacial ET rate constants

2.7 Mass transport

The other important factor leading to misinterpretation of the inherent property of enzyme catalysis is diffusion-controlled mass transport. This contribution can be relieved by rotating the electrode at high rates. The relation between the current and rotation rate can be described by the Koutecky-Levich equation (equation 2.10).

$$\frac{1}{i_{\lim(\omega)}} = \frac{1}{i_{\lim}} + \frac{1}{0.62nFAD^{2/3}\nu^{-1/6}\omega^{1/2}[S]} \quad equation\ 2.10$$

where D is the diffusion coefficient of the substrate, υ is the kinematic viscosity of the solvent, ω is the rotation rate, $i_{\lim}(\omega)$ is the limiting current at a certain rotation rate and i_{lim} is the maximum limiting current achieved at the infinite rotation rate. The remaining terms are as previously defined. The reciprocal of the 3rd term in equation 2.10 gives rise to the Levich equation in which the current is controlled hydrodynamically by a planar rotating electrode at a certain rotation rate.

When the rotation rate increases, the limiting current gets closer to $i_{\lim}$ (the ideal value) and the diffusion-controlled mass transport limitation are removed. However, in this thesis, rotation rates are chosen when the current and shape no longer have apparent changes with further increase of rotation rates. In addition, mass transport can also be relieved by using a microelectrode (<1μm diameter) or the low coverage of enzymes on the electrode.

2.8 Cyclic voltammetry and Chronoamperometry

Voltammetry is an electrochemical technique in which the current is a function of applied potential. Cyclic voltammetry (CV) reveals the reversibility of electrochemical reactions by *cyclic* sweep of potential which consists of the oxidative sweep direction and reductive sweep direction. Most of the equations in this chapter present the relation between the current and potential. Therefore, cyclic voltammetry is a very powerful tool for exploring enzyme catalysis in PFE.

In a slow scan rate, the reaction reaches a steady state and can be treated as Nernst equilibrium. Equation 2.11, the Heyrovsky-Ilkovich equation,[41] can be used to obtain the number of electrons involved in the catalytic cycle and analyze the cooperative behaviour of the reaction.

$$i = \frac{i_{lim}}{1 + \exp\left[\pm n_{cat} f(E_{cat} - E)\right]} \quad equation\ 2.11$$

Chronoamperometry is an electrochemical technique in which the current is a function of time at a constant potential. As opposed to CV, it is possible to observe an instant change in current and obtain kinetic information at a constant potential as shown in Figure 2.6. The kinetic rate constant can be obtained by fitting the current against time.

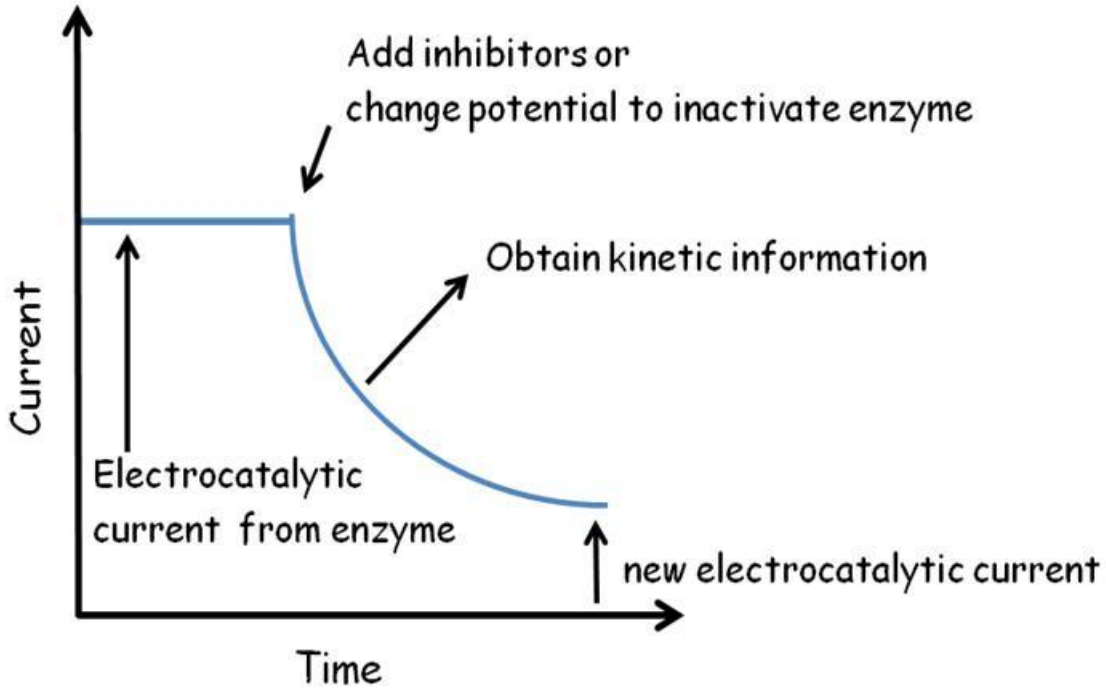

Figure 2.6 Illustration and explanation of chronoamperometry in the PFE experiment.

In addition, the Michaelis-Menten equation in the competitive inhibition can be rewritten as eq 2.12 since the electrocatalytic current is directly proportional to the turnover rate (eq 2.6)

$$i = \frac{i_{lim}[S]}{[s] + K_m \times (1 + \frac{[I]}{K_I})} \qquad equation\ 2.12a$$

$$\frac{1}{i} = \frac{K_m}{i_{lim}[s]} \times \left(1 + \frac{[I]}{K_I}\right) + \frac{1}{i_{lim}}\ equation\ 2.12b$$

where K_I is the inhibition constant, K_m is the Michaelis constant, and [I] is the concentration of inhibitor.

Therefore, it is possible to use eq 2.12 to obtain K_I and K_m values by chronoamperometry or CV.

Chapter 3 *A unified electrocatalytic description of the action of inhibitors of carbon monoxide dehydrogenase I*

3.1 Abstract

Several small molecules and ions, notably carbon monoxide, cyanide, cyanate and hydrogen sulfide are potent inhibitors of Ni-containing carbon monoxide dehydrogenases (Ni-CODH) that catalyze very rapid, efficient redox interconversions of CO_2 and CO. Protein film electrochemistry, which probes the dependence of steady-state catalytic rate over a wide potential range, reveals how these inhibitors target particular oxidation levels of Ni-CODH relating to intermediates (C_{ox}, C_{red1} and C_{red2}) that have been established for the active site. The following properties are thus established: (1) CO inhibits CO_2 reduction (CO is a product inhibitor) at all potentials more negative than –0.5 V, at which CO_2 is reduced; (2) cyanide totally inhibits CO oxidation but its effect on CO_2 reduction is limited to a narrow potential region (between –0.5V and –0.6V) below which CO_2 reduction activity is restored; (3) cyanate is a strong inhibitor of CO_2 reduction but inhibits CO oxidation only within a narrow potential range just above the CO_2/CO thermodynamic potential; (4) hydrogen sulfide (H_2S/HS^-) inhibits CO oxidation but not CO_2 reduction – the complex on/off characteristics are consistent with it binding at the same oxidation level as C_{ox} and forming a modified version of this inactive state rather than reacting directly with C_{red1}. The results provide a new perspective on the properties of different catalytic intermediates of Ni-CODH - uniting and clarifying many previous investigations.

3.2 Introduction

In biology, the rapid and direct redox interconversion of CO and CO_2 as shown in eq 3.1, a reaction of enormous technological importance, is catalyzed by metalloenzymes called carbon monoxide dehydrogenases (CODHs).[19,53]

$$CO + H_2O \leftrightarrow CO_2 + 2H^+ + 2e^- \qquad (3.1)$$

The enzymes found in anaerobic organisms contain Ni and are referred to as Ni-CODHs. Five Ni-CODHs expressed from the thermophilic bacterium *Carboxydothermus hydrogenoformans* (*Ch*) which can grow chemolithoautotrophically on CO as sole carbon and energy source [53,54], have been suggested based on analysis of the genome.[13] Two of these enzymes, CODH I_{Ch} and CODH II_{Ch}, have been reported for CO oxidation with turnover frequencies as high as 30,000 s^{-1} at pH 8, 70 °C by conventional kinetic assays and both of which are monofunctional (i.e. they catalyze only the CO/CO_2 interconversion) and have similar spectroscopic properties.[5]

Several small molecules such as cyanide (CN^-), cyanate (NCO^-) and sulfide (introduced as H_2S or HS^-) are known to be inhibitors of CODH.[17,55-59] Although reactions of these inhibitors with CODH isozymes have been investigated by kinetic methods, spectroscopy and crystallography, it is still unclear how they *selectively* target discrete species in the catalytic cycle (e.g. C_{ox}, C_{red1}, C_{red2}) and the previous studies mainly suggest these inhibitors target C_{red1} rather than C_{red2} (scheme 3.1). Cyanide, an electronic and structural mimic of CO, is a slow-binding competitive inhibitor of CO oxidation[56,58,60,61] and this is consistent with the observation that its binding affects the EPR spectrum of C_{red1} but not C_{red2}.[60] It thus follows that NCO^-, which structurally and electronically resembles CO_2, should bind preferentially to

C_{red2}. The EPR experiments carried out on the CODH/ACS_{Mt} complex from *Moorella thermoacetica* are not easily interpreted in this context, because they showed that NCO^- binding causes major changes to the EPR spectrum ($g_{av} > 2$) under conditions that favor C_{red1}.[55] Less intuitive is any prediction of the state(s) that an exogenous sulfido species should target, and there remains some controversy. An additional sulfur atom is found in certain crystal structures of Ni-CODHs as a bridging ligand between the Ni atom and the dangling Fe atom[17,56] , yet reported effects of exogenous sulfide vary between it being an inhibitor[57] and an activator.[17,56]

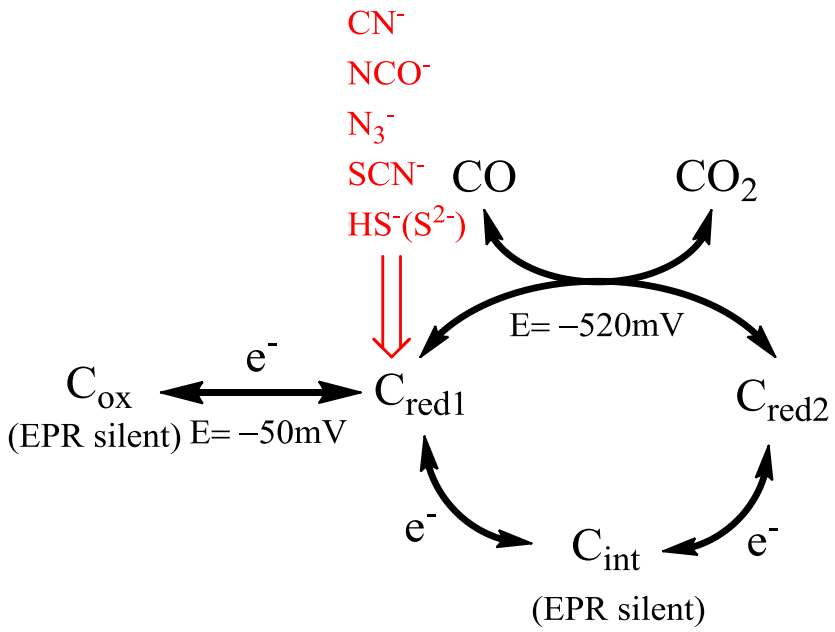

Scheme 3.1 The target state of CODH by inhibitors (red colours) in the catalytic cycle from previous studies.

In this chapter, the use of PFE is able to establish and analyze the strong potential dependence of the inhibition of enzymatic CO oxidation and CO_2 reduction by cyanide,

cyanate and sulfide. The experiments focus mainly on one technique, cyclic voltammetry, which provides immediate qualitative information in both time and potential dimensions. The results, obtained for CODH I_{Ch} from *Carboxydothermus hydrogenoformans*, reveal very clearly how each inhibitor targets different states of the enzyme and show how rapidly they bind or leave the active site as the redox level is changed. Selective binding of cyanate to C_{red2} is confirmed by EPR spectroscopy.[62] The findings provide a wide, continuous potential landscape for structural and spectroscopic research carried out over three decades, and explain and unify important aspects of this class of enzyme.

3.3 Material and Methods

Isolation and purification of CODH I_{Ch} from *Carboxydothermus hydrogenoformans* were carried out as previously described.[63] All chemicals were of analytical or equivalent grade. The gases, carbon monoxide, carbon dioxide and argon were purchased from BOC. Potassium cyanide and potassium thiocyanate were obtained from Fluka, and sodium sulfide and potassium cyanate were purchased from Sigma-Aldrich. 2-(*N*-morpholino) ethanesulfonic acid (MES) (Sigma-Aldrich) was used as buffer or electrolyte solution and NaOH (Sigma-Aldrich) was used to adjust the pH value. All electrochemical experiments were undertaken in a glovebox (Vacuum Atmospheres, O_2 < 5ppm). An all-glass electrochemical cell was used for all experiments. The experimental conditions, such as pH values, temperatures and parameters for electrochemical experiments are described in each figure legend.

The cell was fitted with an inlet and an outlet (vented to flue) for gases, a port for injection of solutions, a Luggin side arm that housed the saturated calomel electrode (SCE) reference, a Pt counter electrode, and a housing into which the electrode rotator fitted snuggly and formed a gas-tight seal. The whole setup for electrochemical experiments is illustrated in Figure 3.1.

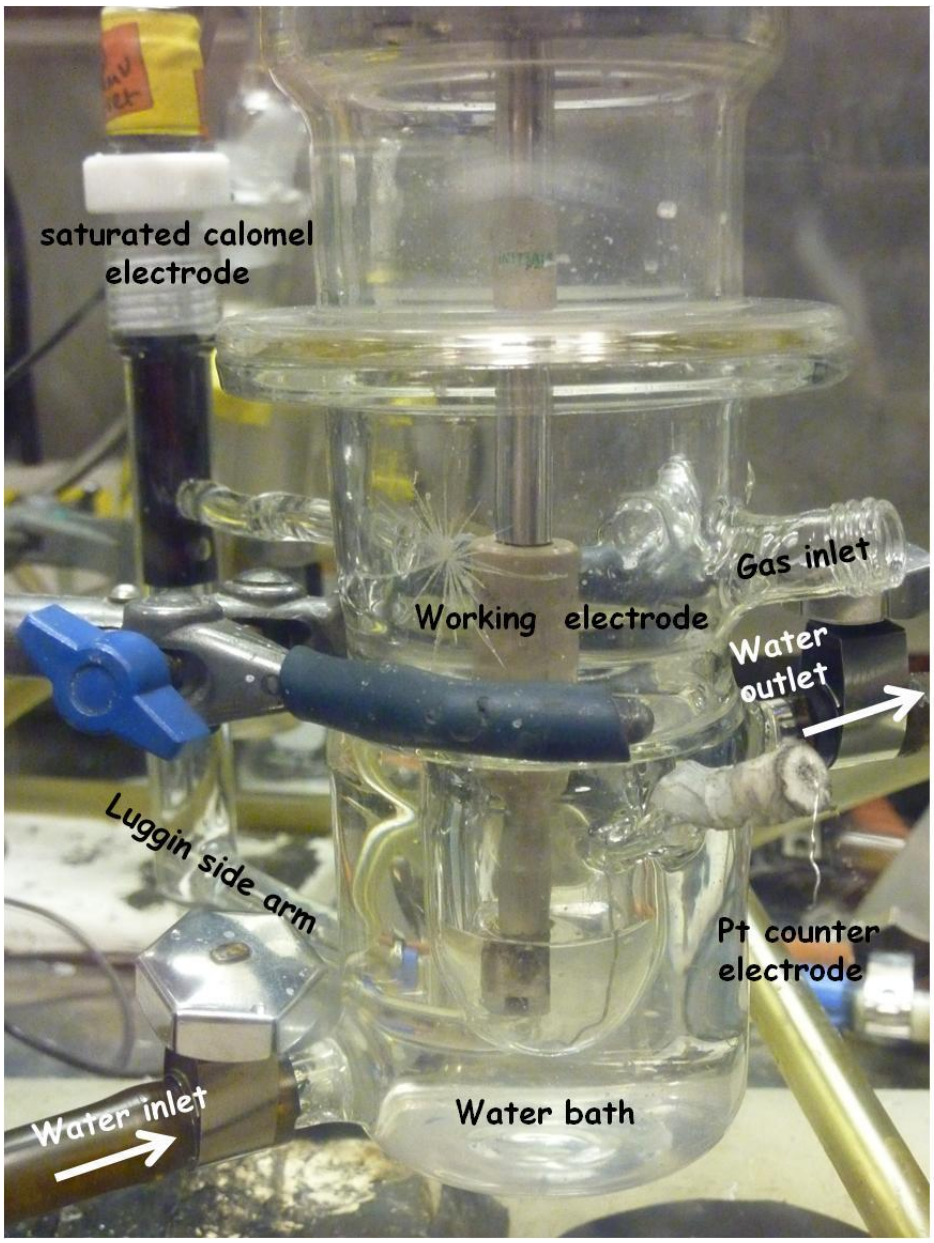

Figure 3.1 The picture of the electrochemical cell which is used in the PFE experiment.

The pyrolytic graphite 'edge' (PGE) electrode (diameter 2 mm) was constructed as described below. The pyrolytic graphite edge (PGE) was purchased from Momentive performance. A piece of PGE was sliced into the shape of a rod with 0.02 cm^2 surface area as the electrode by PTCL workshop in the Department of Chemistry, University of Oxford. The rod-shaped electrode and electrode casing were roughly polished with the sandpaper (p400 or p800) to make surface smooth. The electrode casing and rod-shaped PGE electrode were sonicated in ethanol and DI water respectively for 15 minutes to remove debris. A conducting epoxy (1:1 mixture of silver loaded epoxy adhesive and hardener (RA, 186-3616)) was evenly spread on the end of the rode-shaped PGE electrode. The rod-shaped PGE with conducting epoxy on the end was inserted into the channel in the electrode casing and then placed for an hour.

Wrap a tape around the electrode casing with rod-shaped PGE inside. Pouring insulting epoxy resin mixtures (which is composed of three parts of resin Araldite CY1300GB (Robnor Resin) and one part of hardener Arador HY1300 GB (Robnor Resin) by weight) into the cylinder-shaped wall made by a tape on the top of the electrode casing. Epoxy Resin forms solid and covers the PGE rod after placing the electrode on the top of the oven overnight. The finished PGE electrode inside the electrode casing normally has less than 10 Ω resistance.

Before each electrochemical experiment, the PGE electrode was polished using 5μm sandpaper and sonicated to remove debris. Approximately 2μL of enzyme solution (16mg/mL) was discharged from a pipette onto the PGE surface. To improve the stability of the enzyme film on the electrode, polymyxin (Duchefa Biochemie) (dissolved in the MES water for final concentration of 0.12 M) was added to the coating solution in a 3:1 ratio over enzyme.

Instability (we refer to this as film loss) was usually only a problem when conducting experiments over several hours at 25 ^{o}C.

All potentials are quoted versus the standard hydrogen electrode (SHE) using the scaling correction E(SHE) = E(SCE) + 241 mV at 25 ºC. Voltammetry and chronoamperometry were performed with an Autolab PGSTAT10 or PGSTAT20 electrochemical analyzer. The rotation rate (ω) of the electrode was usually set at 3500 rpm, above which the current was always independent of ω. Unless otherwise stated, experiments were carried out using 0.2 M MES buffer (pH=7.0) as buffer-electrolyte at 25ºC, the high concentration of MES being necessary to minimize changes in pH due to reaction with CO_2. Gas mixtures were introduced into the cell headspace without bubbling – the electrode rotation being sufficient to facilitate equilibrium between headspace and solution. The gas flow rate and the composition of gas entering the cell headspace were controlled by mass flow controllers (Sierra). The gas concentration in the buffer is estimated based on the Henry constant. (k (CO_2)= 3.4×10^{-2} M·atm^{-1} and k (CO)= 9.5×10^{-2} M·atm^{-1} at 25ºC). The K_m values and K_I values were obtained from chronoamperometric experiments using the Lineweaver-burk plot for data analysis (eq 2.12b). Some protein films desorb from the PGE electrode during the experiment. The film loss correction is employed to obtain the real concentration of enzymes on the electrode surface. Some results of chronoamperometry with film loss, which is observed as the decline of electrocatalytic current with time, are corrected by film loss rate. The method for obtaining the film loss rate is as follows [41]: the film loss rate can be estimated by fitting the exponential decay to the electrocatalytic current before injecting any inhibitors. The film loss rate is obtained from the fitting of the exponential equation, which is used to

obtain the real electrocatalytic current contributed from active enzymes still adsorbed on the electrode.

3.4 Results

3.4.1 Carbon monoxide as a product inhibitor

Cyclic voltammograms to probe product inhibition by CO during the reduction of 40 % CO_2 are displayed in Figure 3.2. The enzyme is adsorbed on the rough PGE surface in such a way that electronic contact is made between the electrode and the active site, via the Fe-S clusters that extend to the protein surface. In a cyclic voltammogram the electrode potential is varied in a cyclic manner back and forth between two limits. The potential variation induces a flow of current that depends on the equilibrium potential set by the Nernst equation (i.e. the standard potential adjusted by the logarithmic activities of oxidized and reduced forms) and by the corresponding rates of catalytic electron transfer in each direction. Catalytic reduction of CO_2 appears as a negative current that begins at electrode potentials more negative than –0.5 V whereas oxidation appears as a positive current that begins above –0.5 V. The current is directly related to steady-state enzyme activity. Absolute activity is usually difficult to calculate because it requires knowledge of the electroactive coverage of the enzyme, which is usually too low to measure reliably, but the voltammetry gives excellent information on the *relative* rates of catalysis in either direction. As the potential is varied, inhibitors may become bound or released, thereby altering the current in particular regions of the voltammogram. The kinetics of inhibitor binding and release can be studied by carrying out experiments at different scan rates, or by introducing an inhibitor at certain fixed potential and monitoring the current as a function of time. The reason for performing *cyclic* voltammetry as opposed to simply using single linear sweeps of potential is that processes that are not at steady state become visible; importantly, interconversions that are slow compared to the potential scan rate appear

as hysteresis, in contrast to the strict overlay in either direction that would occur if all processes conform to steady-state kinetics.

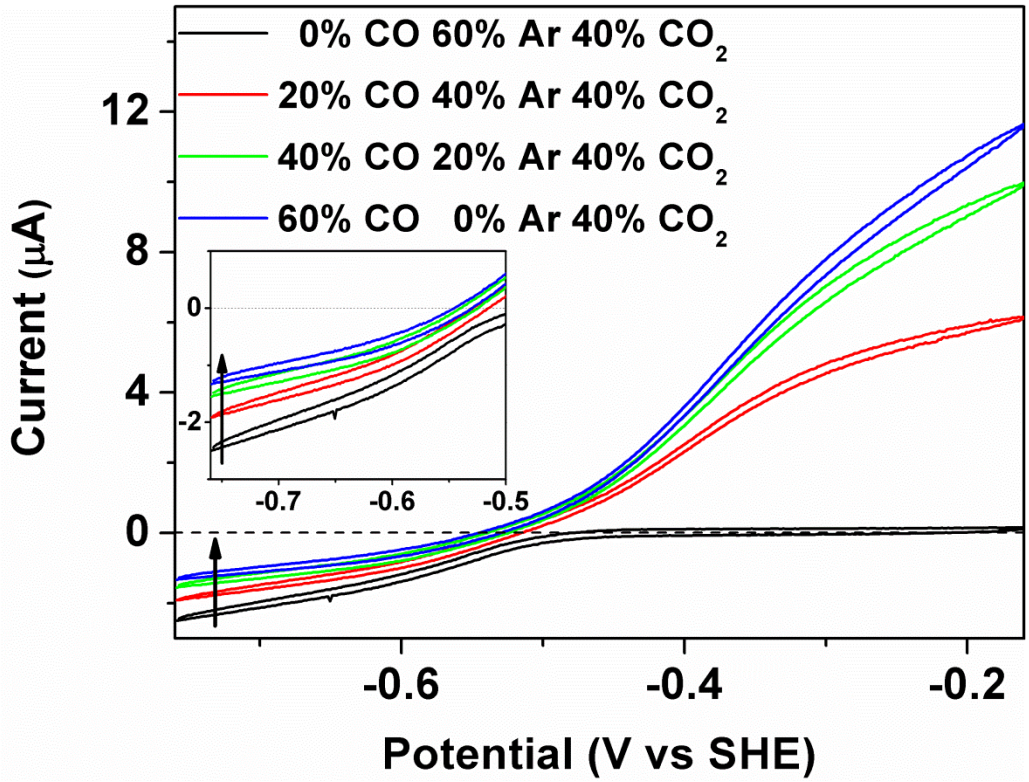

Figure 3.2 Inhibition of CODH I_{Ch} by CO. Different partial pressures of CO were introduced into the electrochemical cell to measure product inhibition. As the CO concentration increases, the electrocatalytic current for CO_2 reduction decreases. The inset enlarges the region in which CO_2 reduction occurs. Experimental conditions: 25℃, 0.2 M MES buffer (pH=7.0), rotation rate 3500 rpm and scan rate 10mV s^{-1}.

In Figure 3.2, cyclic voltammetry was conducted between limiting potentials of −760 mV and −160 mV, at different levels of CO, using Ar to maintain the total gas balance. As the CO concentration in the headspace is increased the current due to electrocatalytic CO_2 reduction decreases. The attenuation of current is due to product inhibition: as expected for rapid on/off processes the voltammograms conform to a steady-state condition throughout the cycle with no hysteresis. In addition to the decrease in CO_2 reduction current as CO is added, the average potential at which the scans in either direction cross the zero current line becomes more negative. These two observations are connected in an important way because the decrease in zero-current potential, a thermodynamic effect – shows that the driving force has decreased and this could alone explain the lower CO_2 reduction activity; however even after taking this factor into consideration by adjusting the horizontal position of the voltammogram, the rate of CO_2 reduction is clearly retarded if CO is present.

Lineweaver-Burk plots (eq 2.12 in Chapter 2) using chronoamperometric data were used to obtain the apparent K_I value for CO at two different electrode potentials, −560 mV and −760 mV at pH 7 (an experiment at −760 mV is shown in Figure 3.3). Data are shown in Table 3.1. A 7-fold higher inhibition constant is obtained at the more negative potential (K_I values 348μM vs 46 μM) showing clearly that CO has a much lower affinity for the more reduced state of the active site.

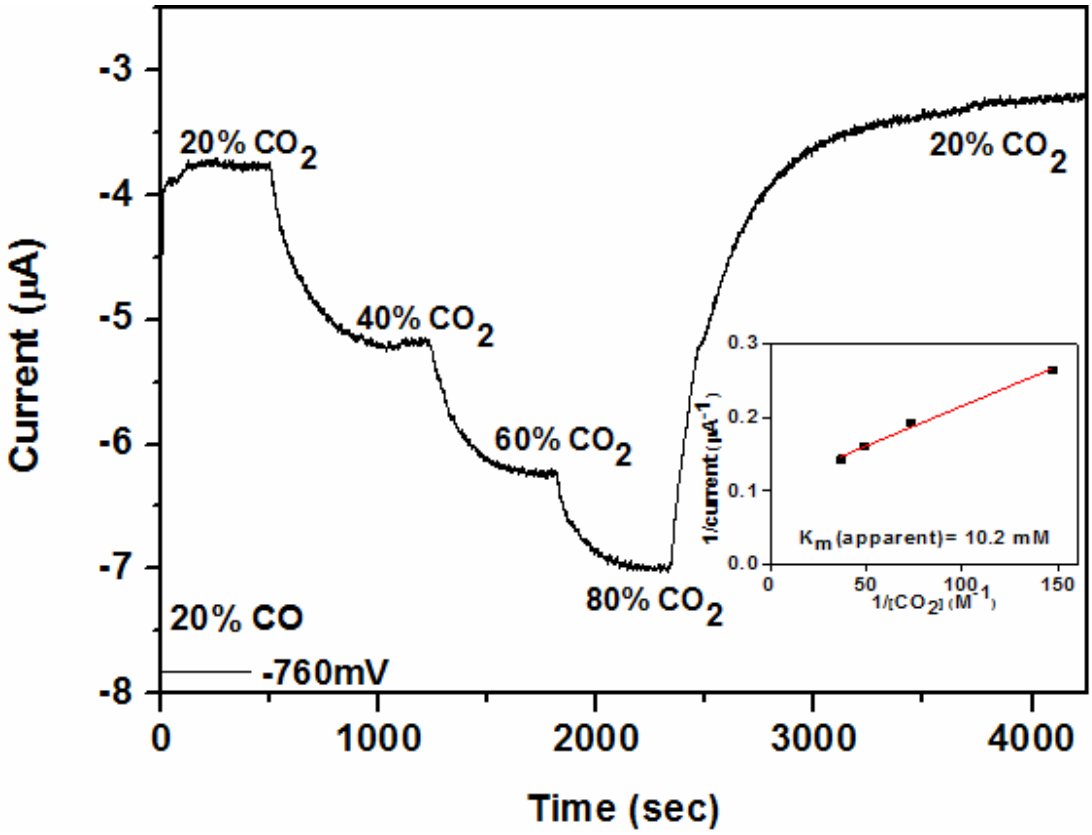

Figure 3.3 CO product inhibition at –760 mV. The proportion of CO concentration was constant 20% in the experiment. The percentage number in the figure indicates the percentage of CO_2 was used in the total gas atmosphere. Argon was used to control the total gas balance. The inset figure shows the result of the Lineweaver-burk plot.

Table 3.1 The K_m value for CO_2 and K_I value for CO product inhibition from CODH I

	-560mV	**-760mV**
K_m (CO_2)	8.06±2.07mM	7.08±0.70mM
K_I (CO)	46μM	348μM

3.4.2 Cyanide- as an inhibitor of CO oxidation

Cyanide is a well-studied inhibitor of CODH.[56,58,61,63-65] According to EPR studies,[20,56,58,59] an EPR signal with g_{av} = 1.72 (g-values of 1.87, 1.78, 1.55) is observed when CN^- is added to the C_{red1} state of the CODH/ACS_{Mt}. Figure 3.4 shows catalytic cyclic voltammograms obtained before and after injection of KCN to a final concentration of 1 mM into the electrochemical cell under 100% CO_2. The cycles were initiated at –0.74 V and the scan rate was 1 mV s^{-1} – chosen to reveal hysteresis, reversibility and changes in these features as the CN^- concentration drops due to HCN evaporation. Panel (a) shows the effect of injecting CN^- at the beginning of the second cycle (also at – 0.74 V): the current due to CO_2 reduction does not immediately drop to zero, but does so over the course of several seconds as the potential is scanned in the positive direction. Toward the end of the second cycle, the current increases sharply below –0.6 V showing that the inhibitor is released rapidly as the enzyme adopts a more reduced steady-state level in the catalytic cycle. Upon commencing the third cycle, inactivation occurs at a slower rate, attributable to evaporation of HCN (pK_a, 9.21) from the cell solution; accordingly, this hysteresis was especially evident from a separate experiment (Figure 3.5) in which CN^- was injected to give a final concentration of just 0.1 mM. Panel (b) shows a similar experiment except that CN^- was injected during the latter part of the first cycle, as the potential passes down through –0.6 V. Especially evident now is the slow rate at which CN^- inhibits the enzyme (over the 50 s taken to reach –0.65 V) before it dissociates as the potential continues on to –0.74 V. The second cycle continues as expected from Panel (a).

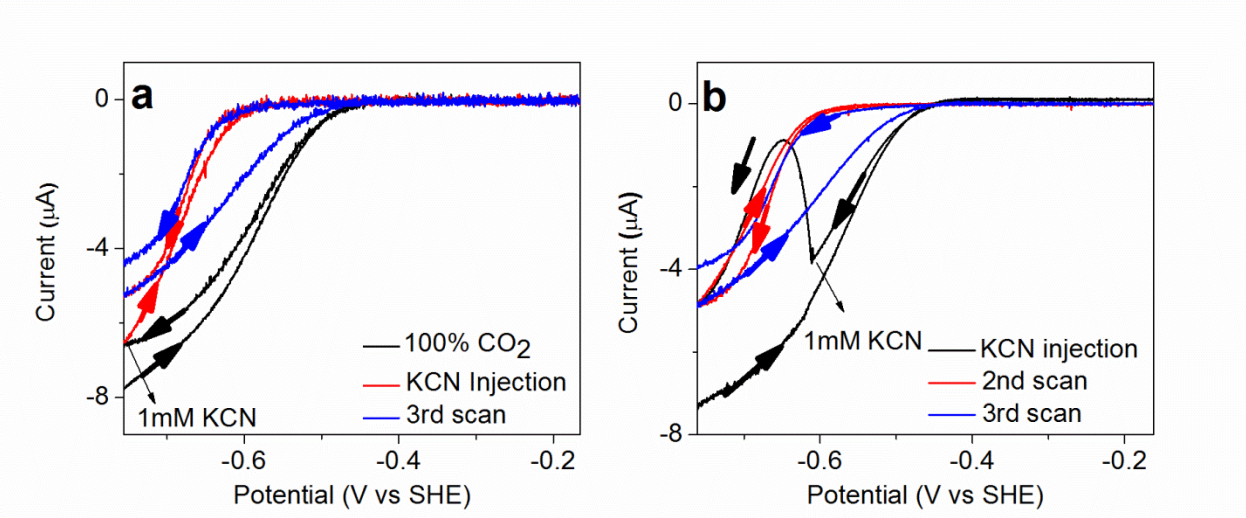

Figure 3.4 Cyclic voltammograms showing the potential and time dependence of inhibition of CODH I_{Ch} by cyanide. Experimental conditions: 25°C, 0.2 M MES buffer (pH=7.0), scan rate 1 mV s^{-1}. (a) After a complete cycle, KCN was injected into the electrochemical cell at –0.74 V to give a final concentration of 1mM. Subsequent scans reveal the release of CN^- as the potential is taken below –0.6 V and re-binding of CN^- of the return oxidative scan. (b) Same as (a) except that CN^- is injected (also to a final concentration of 1 mM) at –0.6 V, i.e near the end of the first cycle while the potential becomes more negative. This experiment clearly shows CN^- binding then dissociating from the enzyme as the potential goes below –0.65 V.

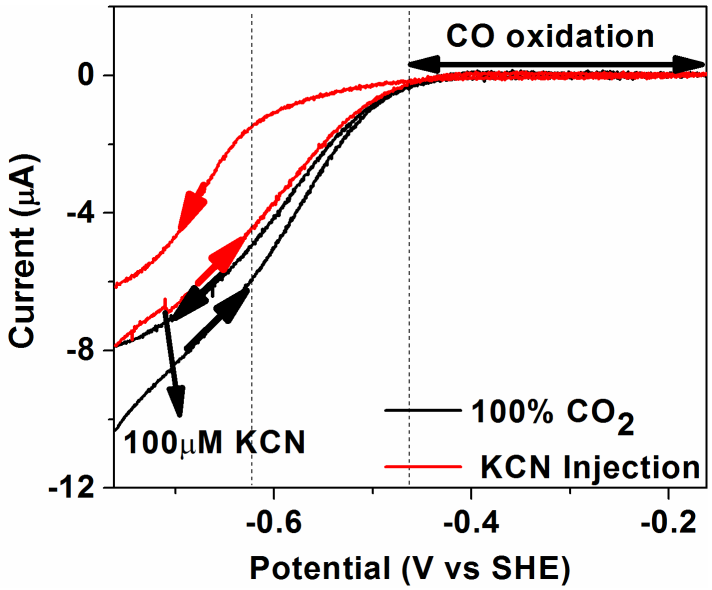

Figure 3.5 The cyclic voltammogram shows the potential and time dependence of inhibition of CODH I_{Ch} by cyanide. After a complete cycle, KCN was injected into the electrochemical cell at −0.74 V to give final concentrations of 0.1 mM. Experimental conditions: 25℃, 0.2 M MES buffer (pH=7.0) and scan rate 1 mV s^{-1}.

Further experiments confirmed that CO oxidation activity is totally abolished by cyanide regardless of the presence or absence of CO_2 (Figure 3.6).

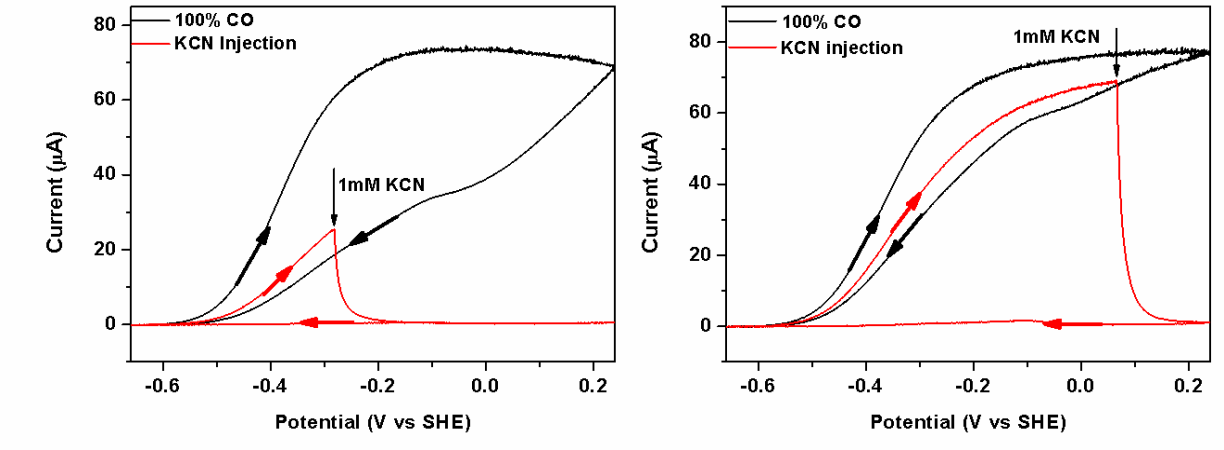

Figure 3.6 Inhibition of CODHI$_{Ch}$ by cyanide in CO oxidation No potential-dependence of inhibition by cyanide was observed under 100% CO. The experimental condition: 25℃, 0.2 M MES buffer (pH=7.0), rotation rate 3500 rpm and scan rate 1 mV s^{-1}

To establish the stoichiometry and cooperativity of the redox transition between oxidized CN^- binding and reduced CN-free states, we studied the cyclic voltammetry in the presence of CN^- under conditions designed to minimize hysteresis, i.e. at a very slow scan rate (0.4 mV s^{-1}) and a high concentration of CN^- (10mM). By plotting log [fractional inhibition] against electrode potential, we obtained a *n*-value between 1.3 and 1.6 in several experiments, where *n* represents the degree of cooperativity for a reaction involving more than one electron. An example is given in Figure 3.7, which is obtained from the red trace of Figure 3.4(a).

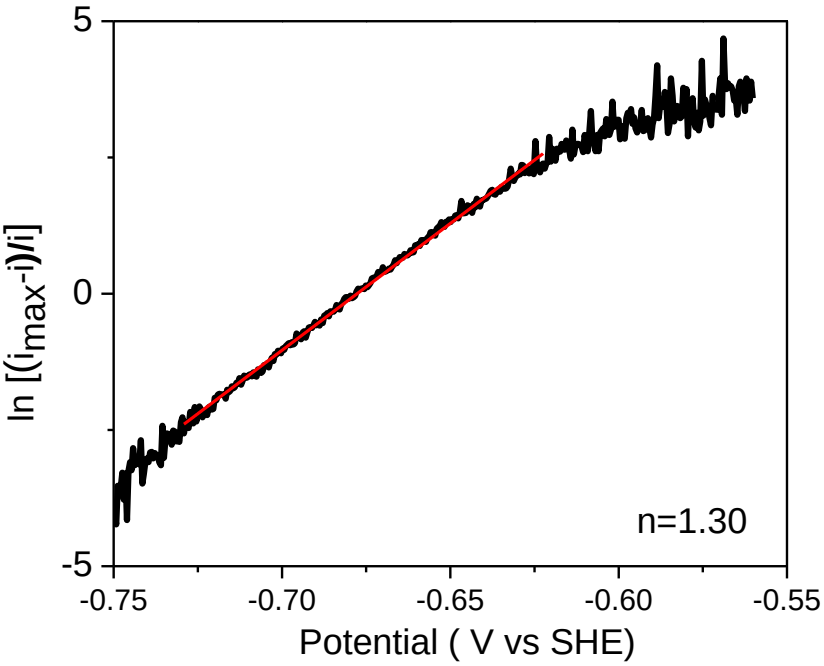

Figure 3.7 The red trace of Figure 3.4 (a) is fitted by the Heyrovsky-Ilkovich equation (eq 2.11). The value of n = 1.3 is obtained.

In the context of these experiments, 'cooperativity' means the degree to which a one-electron redox transformation results in spontaneous transfer of the second electron: a fully cooperative reaction would show n = 2.0, meaning that the one-electron intermediate is highly unstable. The significance of an n-value between 1.3 and 1.6 is that a one-electron intermediate (in this case C_{int}) is unstable. In unbiased terms this means that the release of CN^- occurs predominantly from a state that is two electrons more reduced than the state to which it binds tightly. This estimation was not trivial: first, the large differences in the rates at which

CN^- inhibits and is released, and the strong potential dependence of these rates make it difficult to attain a reversible situation, therefore a very low scan rate was required. Second, the reactivation potential for CN^- inhibited CODH starts below ~ –620 mV, which limits the range over which a sigmoidal current trace can be defined because the slope due to proton reduction from water at the PGE electrode becomes significant at ~ –1V. Third, CN^- is largely present as HCN which evaporates from the electrochemical cell at pH = 7.0. This evaporation could be minimized by halting the gas flow (CO_2) during the experiment.

3.4.3 Cyanate – an inhibitor of CO_2 reduction and marginal inhibitor of CO oxidation

As for cyanide, we studied cyanate inhibition by cyclic voltammetry, through which both CO_2 reduction and CO oxidation are observed in the same experiment, making it possible to deconvolute the effect of inhibitors in both states. As evident from Figure 3.8a, the current due to CO_2 reduction decreases to almost zero when potassium cyanate is injected to a final concentration of 6.67 mM at –0.76 V during the sweep to more positive potential. On the return cycle there is a narrow window, just above –0.6 V where CO_2 reduction is observed before full inhibition is re-established. The dissociation constant of NCO^- was estimated to be about 1.9 mM for CO_2 reduction at –760mV (Figure 3.9). Figure 3.8b shows the effect of NCO^- on CO oxidation: there is a narrow region of potential where CO oxidation appears inhibited, but above –0.4 V the effect on CO oxidation is almost insignificant (the decrease in limiting current at high potential is attributable to slow film loss). The catalytic

voltammogram recorded in the presence of 6.7 mM NCO^- is essentially the same as recorded without inhibitor except that the sigmoidal wave is shifted by about 50mV in the positive direction. The clear conclusion from these experiments is that cyanate is a potent inhibitor of CO_2 reduction and inhibits CO oxidation only within a narrow window just above the thermodynamic potential for the CO_2/CO couple. Selective binding of cyanate to C_{red2} is confirmed by EPR spectroscopy.[62]

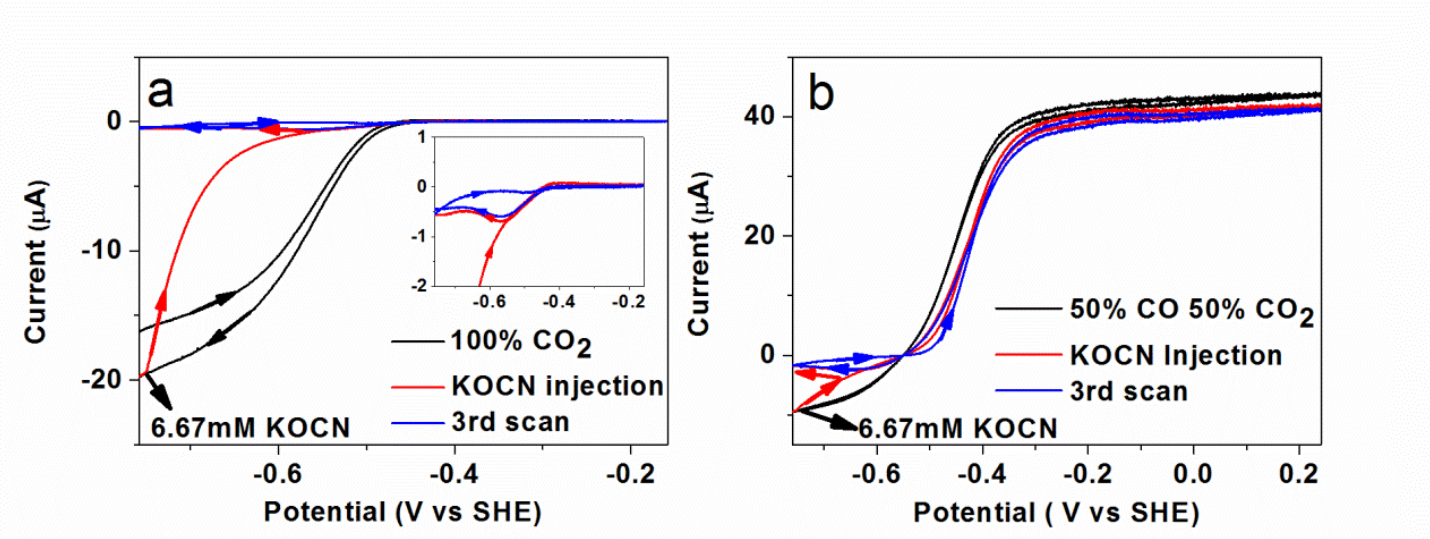

Figure 3.8 Inhibition of CODH I_{Ch} by cyanate. Potassium cyanate was injected (final concentration in the solution is 6.67 mM) into the electrochemical cell under gas atmosphere at 100% CO_2 (Figure 3.8a) and 50% CO, 50% CO_2 (Figure 3.8b). Experimental conditions: 25 °C, 0.2 M MES buffer (pH=7.0), rotation rate 3500 rpm and scan rate 1mV s^{-1}.

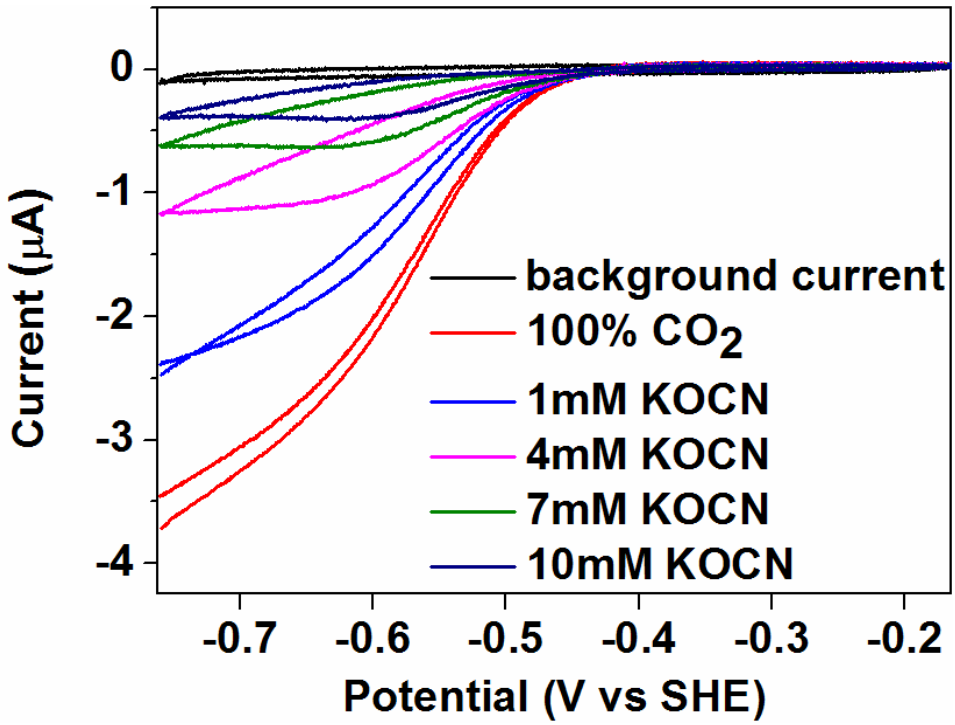

Figure 3.9 Different concentration of potassium cyanate (the final concentration is shown in the figure) was added. Experimental conditions: 25℃, 0.2 M MES buffer (pH=7.0) and rotation rate 3500 rpm.

3.4.4 Sulfide – an inhibitor of CO oxidation that binds to an oxidized inactive state

Some crystal structures of CODHs have revealed a sulfide ion bridged between the Ni atom and the dangling Fe atom and there has been some controversy as to whether this structural feature is physiologically relevant.[6,17,52,56,57] Experiments to examine the inhibition of CODH by sulfide are shown in Figure 3.10. No inhibition of catalytic CO_2 reduction was observed (Figure 3.10a), even when a relatively high concentration of buffered sodium sulfide (to a final value of 2 mM) was injected (the loss in current during a cycle is due to natural film instability). This result correlates strongly with the observation that no EPR signal changes are observed when sulfide is added to a sample in the C_{red2} state.[56,57] In contrast, sulfide inhibits CO oxidation in a complex manner, as shown in Figure 3.10 b-d. Without addition of sulfide, cyclic voltammograms at low scan rates show slow inactivation as the potential is taken above 0 V, with a partial re-activation observed between −50 and −100 mV on the return scan. The re-activation potential corresponds to values expected for the C_{ox}/C_{red1} couple based on several studies of CODH from different species. When 1mM sodium sulfide (final concentration) is injected at −400 mV (at which potential the CO electrocatalytic oxidation current is small due to the low driving force, but still very evident) there is no immediate drop in current or even the slightest change of shape of the cyclic voltammogram as the potential is increased over the next 0.3 V. This result is consistent with the report from Svetlitchnyi et al[56] who concluded that sulfide does not inhibit CO oxidation by methyl viologen. Feng and Lindahl, by contrast found that sulfide *partially* inhibited CO oxidation activity (limiting values being 30% and

60% for $CODH_{Mt}$ and $CODH_{Rr}$, respectively) when using methyl viologen as electron acceptor.

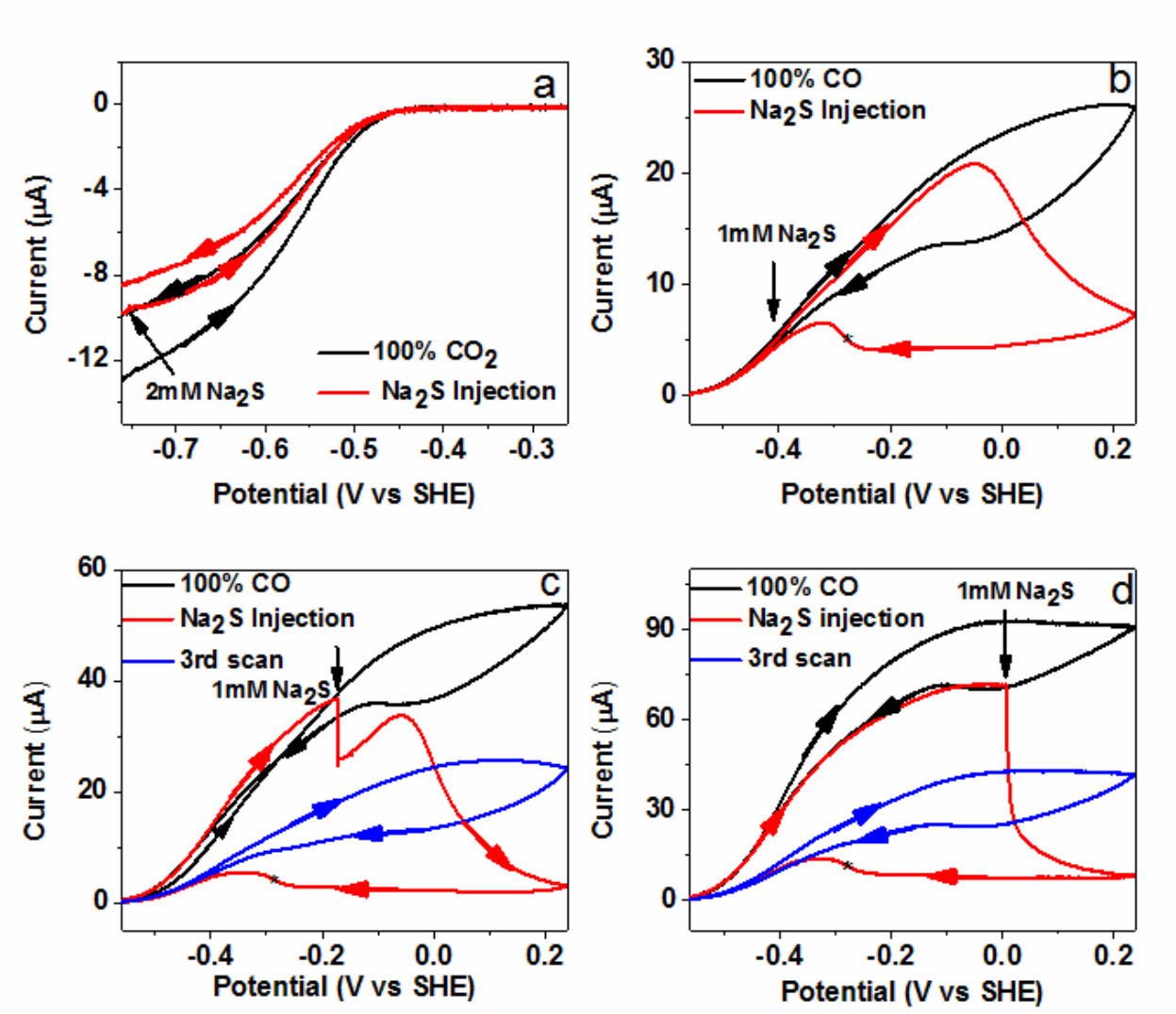

Figure 3.10 The potential control of CODH I_{Ch} inhibition by sulfide 1 mM Na_2S or 2 mM Na_2S (final concentration) was injected at different potentials. The asterisk refers to the reactivation potential. Experimental conditions: 25°C, 0.2 M MES buffer (pH=7.0), rotation rate 3500 rpm and scan rate 1 mV s^{-1}.

However, a very different and more detailed picture emerges when the potential scan is continued in a positive direction, as the current levels off and decreases rapidly above –50 mV. The enzyme remains inactive during much of the return scan to negative potential, and then reactivates at potentials below –0.25 V in a sharp transition (which remained sharp when the scan rate is increased to 10 mV s^{-1}). Experiments in which the sulfide solution is injected at more positive potentials (Figures 3.10c and 3.10d) show that inhibition occurs immediately, and the degree of inhibition increases as the potential increases, being complete at potentials above 0 V. The potential at which CODH is rapidly inactivated in the presence of sulfide coincides closely with the potential (ca. –50 to –100 mV) at which the enzyme inactivates (albeit very slowly) in the absence of sulfide. Chronoamperometric experiments showed that the reaction with sulfide is much faster than the reaction with CN^- at +0.16 V (Figure 3.11). The results therefore show that sulfide does not bind directly (or at least rapidly) to a catalytic state of CODH I_{Ch} (allowing CO oxidation to occur unaffected over a wide potential range, up to approximately –0.1 V and well above that attainable with oxidized methyl viologen) but enters via a more oxidized state, which it stabilizes. Release of the inhibiting sulfide species does not occur until a more reducing potential is applied. This potential (ca. –0.25 V) is more negative than that observed for the normal activation process (–50 to –100 mV) assigned to the reductive one-electron transformation from C_{ox} to C_{red1}. Continuing the scan down to –560 mV then scanning back to the region of CO oxidation reveals only a small amount of further recovery has occurred under highly reducing conditions (compare the currents at –400 mV). The general decrease in catalytic activity that is observed compared to experiments performed without sulfide suggests that sulfide also causes less reversible changes to the enzyme.

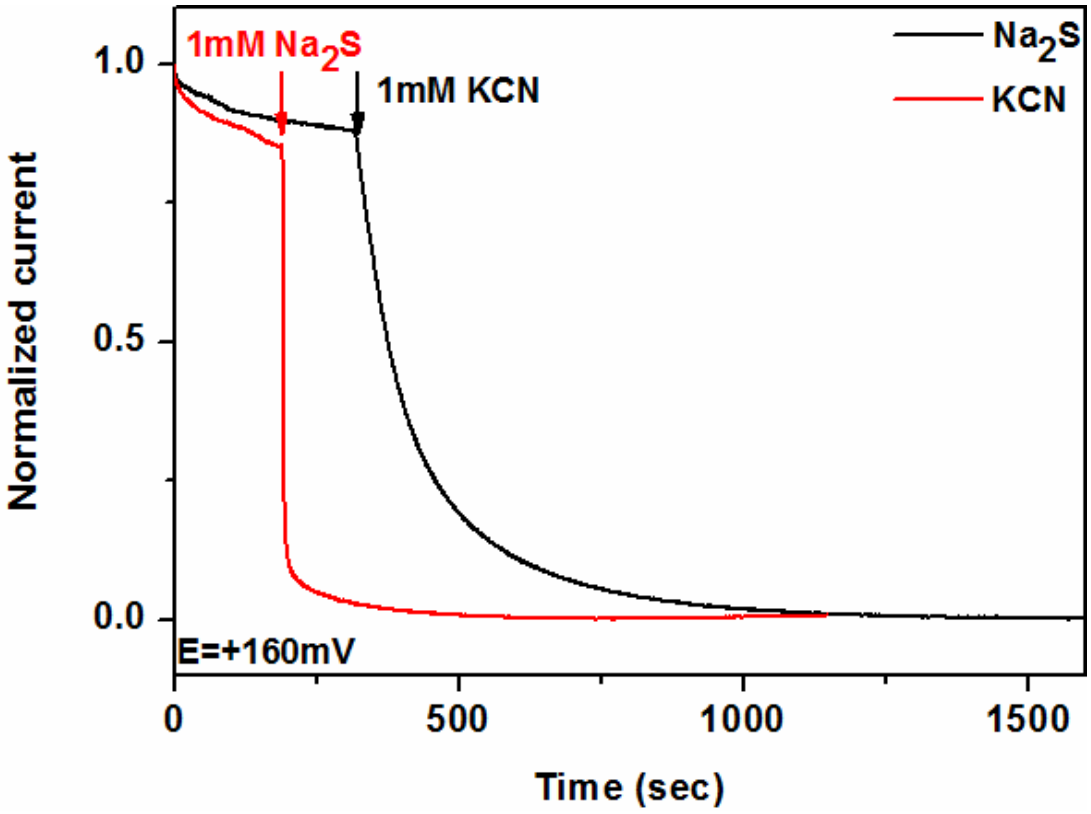

Figure 3.11 Comparison of the rates of inhibition by cyanide and sulfide. In each case, 1mM potassium cyanide or 1 mM sodium sulfide was added at +160 mV. At this potential sulfide is a good inhibitor and binds much faster than cyanide. Experimental conditions: 25℃, 0.2 M MES buffer (pH=7.0) and rotation rate 3500 rpm.

3.5 Discussion

Several small molecules and ions, carbon monoxide, cyanide, cyanate and hydrosulfide (sulfide) act as inhibitors of Ni-CODH in a redox-dependent manner, as summarized in Fig. 3.12. In this Figure, *red* indicates the potential region over which the enzyme is inhibited, *gray* indicates no binding, and *green* indicates that binding leads to turnover. The dashed arrows indicate reactions that are slow compared to those indicated by full arrows. As a guide, the reduction potentials for CO_2/CO as well as values determined by EPR titrations for the $C_{ox}/C_{red1}/C_{red2}$ interconversions are also indicated.

The results of PFE studies suggest a model for how these inhibitors intercept the catalytic cycle at different stages, as shown in scheme 3.2. We assume that all inhibitors target the active site: X-ray crystallography of the enzymes from *R. rubrum*,[18] *C. hydrogenoformans*,[6] and *M. thermoacetica* [27,66] shows that the active site consists of a distorted [Ni–3Fe–4S] cubane coordinated to a unique dangling Fe site (also called ferrous component II (FCII)). Structures of the *C. hydrogenoformans*[6] and *M. thermoacetica*[28] enzymes demonstrate binding of the substrate water molecule to the dangling iron, consistent with spectroscopic studies indicating that water binds to Fe.[67] The structure of the CO_2-bound *C. hydrogenoformans* enzyme reveals the carbon bound to Ni and one of the oxygen atoms bound to the dangling iron.[6]

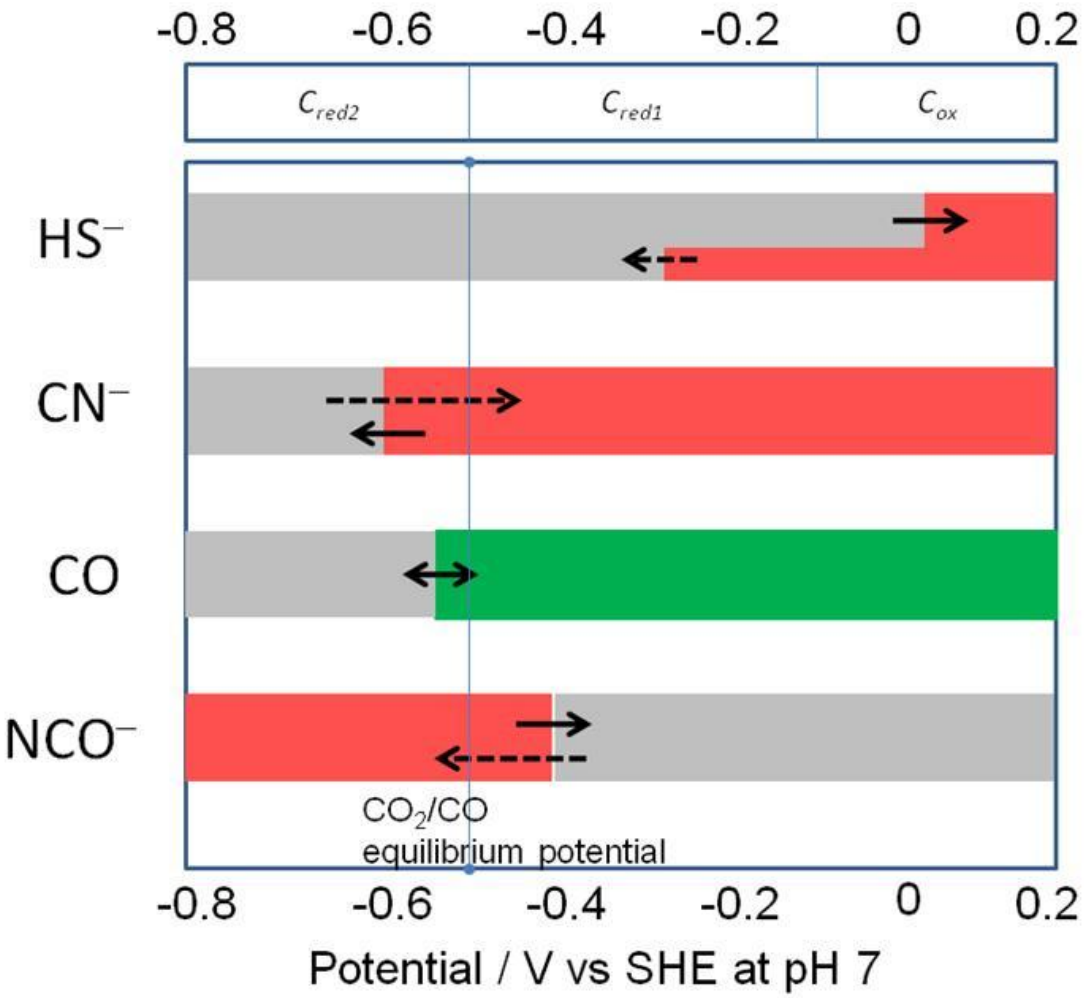

Figure 3.12 Potential dependence of binding of inhibitors to CODH I_{Ch}. *Red* refers to the potential region over which the enzyme is inhibited, *gray* indicates no binding, and *green* indicates that binding leads to turnover. The dashed arrows indicate reactions that are slow compared to those indicated by full arrows. The reduction potentials indicated at the top of the chart are guiding estimates based on values reported in the literature for C_{red1}/C_{red2}[8, 11] (close to the CO_2/CO potential at pH 7) and the observation from the voltammetry in the case of C_{ox}/C_{red1}.

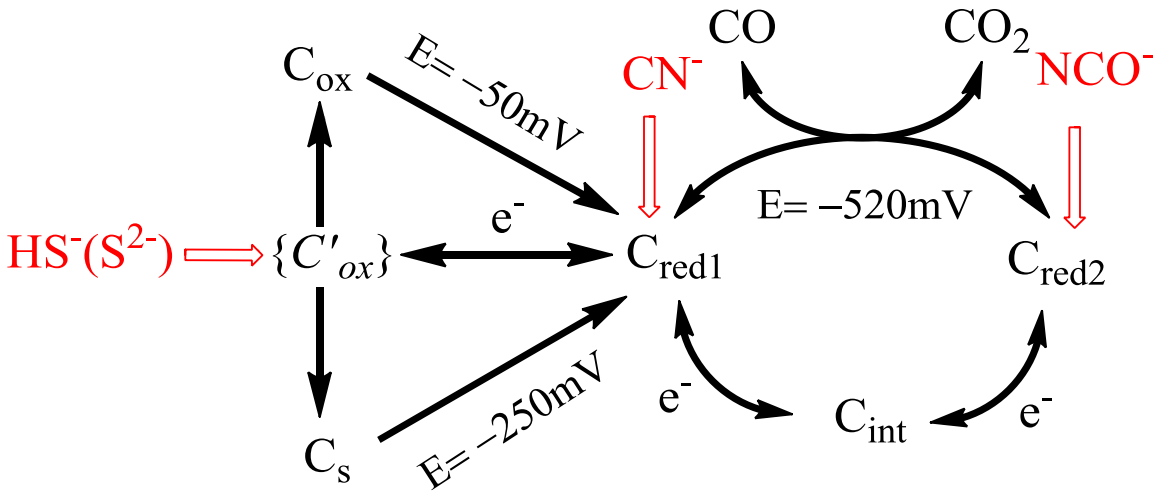

Scheme 3.2 Summary of the interceptions of the catalytic cycle of CODH I_{Ch} by small molecule inhibitors. The potentials −50 mV and −250 mV are the values observed for re-activation of enzyme with and without sulfide. The potential −520 mV is the standard potential for the CO_2/CO half cell reaction at pH 7.0.

Electrochemical results demonstrate that CO inhibits CO_2 reduction by binding as a product inhibitor to the C_{red1} state of CODH. Product inhibition is further quantified by chronoamperometry, which shows that K_I for CO increases as the potential becomes more negative. This binding stabilizes the product complex as C_{red1}-CO, impeding return to the active C_{red2} state for CO_2 reduction. In a structure of the CODH from *Methanosarcina barkeri(Mb)* , CO was shown to bind to Ni with a bent conformation, adjacent to the water-Fe complex.[68] Multiple infrared bands at 2078, 2044, 1970, 1959, and 1901 cm^{-1} were attributed to multiple CO molecules or heterogeneous modes of binding to the C-cluster.[69]

The electrochemical studies are entirely consistent with previous conclusions that CN^- targets the C_{red1} state,[56,58,60,61] and show further that it is released at very negative potentials

(the *n*-value shows that release occurs from a state that is two electrons more reduced, which must be C_{red2}) enabling CO_2 reduction to occur. The results further highlight the unusually slow rate at which CN^- binds, which results in severe hysteresis of the catalytic cyclic voltammetry. All Ni-containing CODHs are subject to potent inhibition by cyanide.[56,58-61,70,71] Binding of cyanide results in conversion of the EPR spectrum of C_{red1} to a similar spectrum with *g* values at 1.87, 1.78, and 1.55.[60] There is significant kinetic and structural evidence that CN^- binds to the Ni center of the C-cluster; although some spectroscopic studies suggest that CN^- binds to the dangling Fe.[67,72] Support for a Ni-CN complex include early studies of the *R. rubrum* enzyme, which showed that the Ni-deficient enzyme does not bind CN^-.[58,71] Similarly, crystallographic studies of the C-cluster in the *M. thermoacetica* CODH/ACS_{Mt} indicate that CN^- binds to Ni in a bent conformation reminiscent of the Ni-CO complex (above), again with an adjacent water remaining bound to the dangling Fe.[28] A conserved isoleucine residue, which is present in both the *M. barkeri* and *M. thermoacetica* structures appears to promote this bent configuration, sterically preventing formation of the expected linear Ni-CO and Ni-CN complexes. On the other hand, a linear Ni-CN complex has been observed in the crystal structure of cyanide-bound CODH II_{Ch} from *C. hydrogenoformans.*[16] These two (linear and bent) modes of cyanide binding (Figure 3.13) are consistent with steady-state kinetic studies which demonstrate that CN^- acts as a slow inhibitor,[58] thus suggesting that cyanide forms a rapid, reversible complex that undergoes a slow rearrangement to form a tight-binding complex.[16,63]

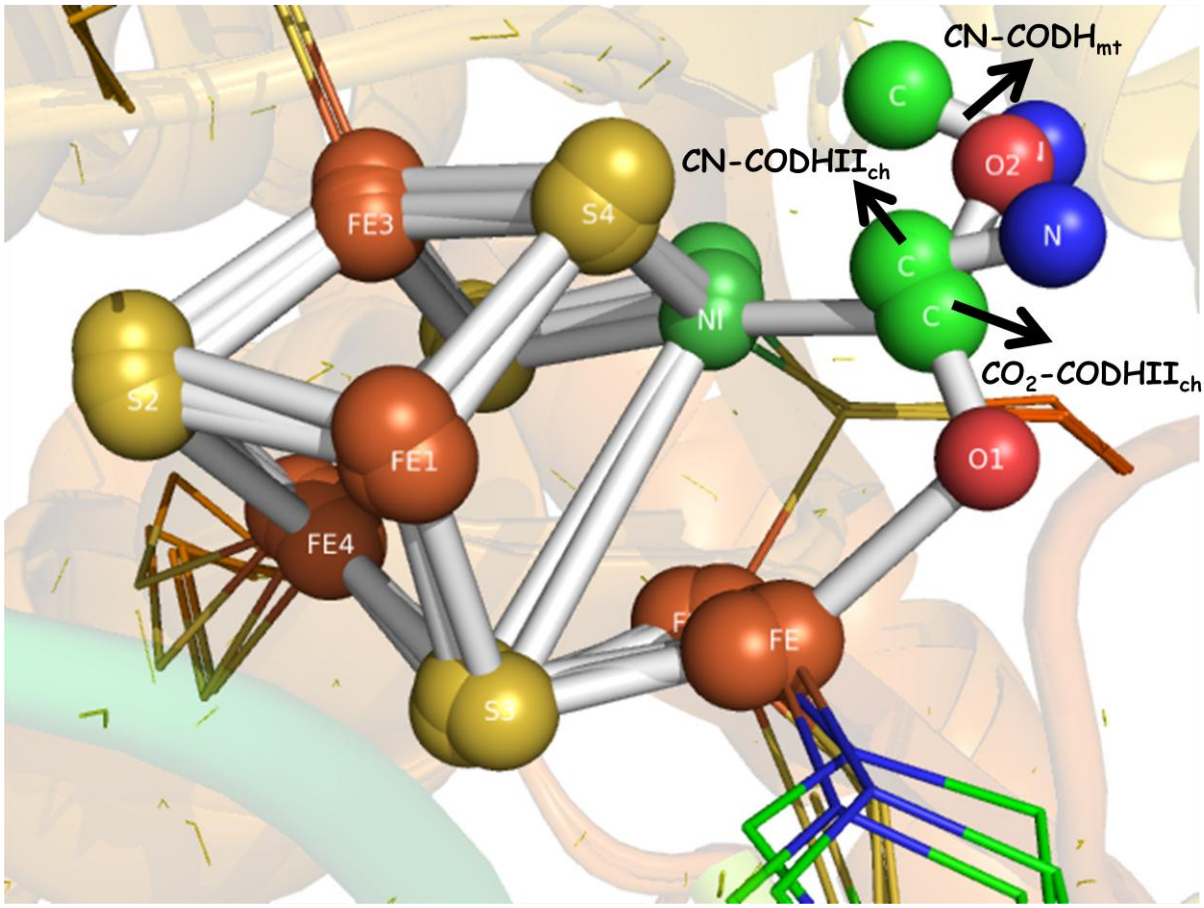

Figure 3.13 The superimposition of three crystal structures, straight-bound CN-CODH II$_{Ch}$,[16] bent-bound CN-CODH$_{Mt}$[28] and CO_2-CODH II$_{Ch}$.[17] The carbon atom of cyanide in CN-CODH II$_{Ch}$ overlaps with the carbon atom of CO_2 in CO_2-CODH II$_{Ch}$, whereas the nitrogen atom of cyanide in CN-CODH$_{Mt}$ overlaps with the oxygen atom of CO_2 in CO_2-CODH II$_{Ch}$.

Based on electrochemical studies in this chapter, cyanate (NCO^-), an analog of CO_2, binds at the C_{red2} level and is released as the potential is raised to favor C_{red1} at steady state. As with CN^- the binding of NCO^- is slow, on the timescale of several seconds for mM concentrations. Cyanate may bind in a bridging mode similar to that of CO_2, with carbon bound to Ni and one

of the oxygens bound to Fe.[6] The EPR results fully support the stabilization of C_{red2} provided by cyanate binding (which results in an enhancement of the spectrum) ;[62] equally, the lack of changes in spectral shape provide indirect evidence that the NCO^- ligand binds to the Ni site (which harbors little spin density) within the NiFeS core instead of the $[3Fe\text{-}4S]^-$ core where most of the spin density is housed. Equally, compared to CN^-, NCO^- is a much weaker donor and less likely to exert an indirect electronic effect on the $[3Fe\text{-}4S]^-$ core.

The binding of sulfide to CODH has been a source of much controversy and studies have indicated that sulfide can act either as an inhibitor[57] or an activator.[17,56] Initial structures of the *C. hydrogenoformans* CODH included a sulfide bridge between Ni and the dangling Fe in the C-cluster,[17,56] which is not observed in the enzymes from *R. rubrum* and *M. thermoacetica*. Subsequent studies of the *C. hydrogenoformans* enzyme indicated that the sulfide is absent in catalytically competent enzyme species and that its replacement leads to enzyme activation. The experiments in this chapter show that sulfide does not bind (at least rapidly) until a potential above –50 mV is applied, meaning that (at least) one electron must first be removed from the C-cluster. This potential is close to values reported for the C_{ox}/C_{red1} redox couple, which is associated with re-activation of oxidatively inactivated CODH, and corresponds also to the small re-activation peak always observed in the absence of sulfide when the electrode potential has been taken to a high value. However, the product formed in the presence of sulfide does not reactivate until a more reducing potential of –0.25 V is applied. Addition of sodium sulfide to the enzyme that had been held at a high potential for a long period (to produce a larger amount of C_{ox}) still showed re-activation at –0.1 V, demonstrating that sulfide

does not react, at least rapidly, with C_{ox} itself. Therefore sulfide (as HS^-) rapidly intercepts a state that is also oxidized above C_{red1} before the stable form(s) of C_{ox} is established.

The explanation for past confusion about sulfide ligation is therefore (at least for $CODH_{Ch}$) that two forms of C_{ox} can co-exist, one with O-atom bridge and the other (C_s in Scheme 3.2) with an S-atom bridge, the latter state being more stable and requiring a more negative potential to release the sulfide ligand. Although we cannot rule out sulfide binding to a more reduced state it is important to note that if the re-activation process instead corresponded to the reductive removal of sulfide from C_{red1} (reports vary from it being a *zero* or *partial* inhibitor of CO oxidation by the weak oxidant, methyl viologen[17, 18, 19]) it would not be possible to account for the potential of re-activation that is so clearly observed. Sulfide binding that is specific to C_{red1} must stabilize that state relative to C_{red2} and thus lower the reduction potential for the C_{red1}/C_{red2} couple, i.e. a much more negative value would be expected for re-activation, as is observed with CN^-. The stark contrast to the behavior with respect to the C_{red1} inhibitor CN^-, observed so clearly using PFE, shows that sulfide acts instead by targeting and stabilizing a higher oxidation level than C_{red1}. In a previous study of CODH by PFE we consistently noted *two* reactivation peaks at high potential,[8] although the relative sizes of each varied from one sample to another. This can now be explained if that enzyme sample contained a certain fraction of the sulfide-inactivated oxidized form. Interestingly, the structure (Figure 1.3d in Chapter 1) showing a bridging S-atom was prepared by reduction under CO, perhaps reflecting how difficult it is to control the oxidation states of centers during sample preparation for crystallography.

In summary, these PFE experiments represent the first investigations of reversible inhibitor binding to a CODH over a wide and continuous range of potentials. The results unambiguously reveal the extent of inhibition and rates of binding or release of different inhibitors as the electrode potential is varied; the electrode potential in turn controls the prevailing redox state of the enzyme during steady-state catalysis. Cyanide, which is known to bind to C_{red1}, ceases to be an inhibitor of CO_2 reduction at very negative potentials. Cyanate is established as a selective inhibitor of CO_2 reduction with only a marginal effect on CO oxidation; it therefore binds selectively to C_{red2}, as expected for a molecule that is isoelectronic with CO_2. Sulfide, which behaves entirely differently to CN^- and does not inhibit CO oxidation under a modest driving force, is established to bind only under more oxidizing conditions. Sulfide thus stabilizes an inactive oxidized state that may be analogous to C_{ox} but with a bound sulfide ligand, its binding and release being poorly reversible. The information thus obtained offers an invaluable guide for interpreting and understanding the complex and diverse observations made through spectroscopic and structural investigations.

Chapter 4 *Comparison between CODH I and CODH II from Carboxydothermus hydrogenoformans*

4.1 Abstract

Carbon monoxide dehydrogenase (CODH) is known to catalyze the reversible conversion between CO and CO_2. Several small molecules; CO (CO product inhibition), cyanide, cyanate, thiocyanate and sulfide; are added into CODH I and CODH II from *Carboxydothermus hydrogenoformans* to investigate the catalytic states *via* protein film electrochemistry. The two isozymes, which share 58.3% sequence identity and 73.9% sequence similarity, show similar features of inhibition by these molecules as follows: CO oxidation is mainly inhibited by cyanide, sulfide and thiocyanate. CO_2 reduction is inhibited by cyanate, cyanide and CO product inhibition.

The main differences between CODH I and CODH II are CO product inhibition and cyanide inhibition in which CODH II is about ten-fold stronger inhibition by CO product and cyanide. Similar features of inhibition by cyanate and sulfide between CODH I and CODH II are observed except the slightly smaller inhibition is observed in CODH II. The reversible and partial inhibition by thiocyanate occurs in the region of CO oxidation with different switch potentials, –0.18 V (for CODH I) and –0.09 V (for CODH II) and no inhibition of CO_2 is observed. The full inhibition of both CODH I and CODH II by sulfide occurs at the high oxidizing potential, −0.05 V and it is reactivated at ~ −0.25 V. These results indicate inhibition of CODH by these molecules is highly potential-dependent and also consolidate the emerging model for potential-dependent inhibition as laid out in Chapter 3.

4.2 Introduction

Carbon monoxide dehydrogenase (CODH) is known to catalyze the reversible conversion between CO oxidation and CO_2 reduction as eq 4.1.

$$CO + H_2O \rightleftharpoons CO_2 + 2H^+ + 2e^- \qquad (4.1)$$

The enzymes found in anaerobic organisms contain Ni and are referred to as Ni-CODHs. Important examples are provided by the thermophilic bacterium *Carboxydothermus hydrogenoformans* (*Ch*) which can grow chemolithoautotrophically on CO as the sole carbon and energy source[53,54] and express five Ni-CODHs. Using conventional kinetic assays, turnover frequencies as high as 30,000 s^{-1} at pH 8, 70 ℃ have been reported[5] for CO oxidation by two of these enzymes, CODH I_{Ch} and CODH II_{Ch}, both of which are monofunctional (i.e. they catalyze only the CO/CO_2 interconversion) and have similar spectroscopic properties.[5]

In Chapter 3, it was clearly shown CODH I_{Ch} performs reversible and rapid electrocatalysis on a PGE electrode with a low overpotential. The potential of zero-current under 50% CO and 50% CO_2 is close to thermodynamic value, ~ –520 mV at pH=7.0. Cyanide (which is isoelectronic with CO) mainly targets the C_{red1} state, while cyanate (which is isoelectronic with CO_2) mainly inhibits the C_{red2} state, which correlates with the similarity of electronic structure between inhibitors and substrates. In addition, sulfide reacts with CODH in the equivalent state of the C_{ox} state. The results of sulfide inhibition by PFE explain the discrepancy of the role of the sulfur atom in the active site observed from different crystal structures and spectroscopic evidence.[6,17,56,57]

Therefore, further investigations of CODH I_{Ch} and comparison between the properties of CODH I_{Ch} and CODH II_{Ch} may shed light on the catalytic mechanism of CODH and the possible biological role of CODH II_{Ch} .

4.3 Material and methods

Isolation and purification of CODH I_{Ch} and CODH II_{Ch} from *Carboxydothermus hydrogenoformans* were carried out as previously described.[63] All chemicals were of analytical or equivalent grade. The gases, carbon monoxide, carbon dioxide and argon were purchased from BOC. Potassium cyanide and potassium thiocyanate were obtained from Fisher Chemical and Fluka respectively. Sodium sulfide and potassium cyanate were purchased from Sigma-Aldrich. All electrochemical experiments were undertaken in a glovebox (Vacuum Atmospheres, O_2 < 5ppm). The electrochemical experiments and procedures are the same as described in Chapter 3.

The Eyring plot in Figure 4.2 was obtained by plotting the natural logarithms of {current value/ absolute temperature} against reciprocal absolute temperature according to equation 4.1, in which the reaction rate constant (k) is replaced by the electrocatalytic current since k is proportional to *i* (eq 2.1). The activation enthalpy can be obtained from the slope.

$$\ln\frac{k}{T} = \frac{-\Delta H^*}{R} \times \frac{1}{T} + \ln\frac{k_b}{h} + \frac{\Delta S^*}{R} \qquad equation\ 4.1$$

where k is the reaction rate constant; T is the absolute temperature; R is the ideal gas constant ΔH^* is the activation enthalpy; k_b is the Boltzmann constant; h is the Planck constant; ΔS^* is the activation entropy.

4.4 Results

4.4.1 The voltammogram of CODH I_{Ch} and CODH II_{Ch}

Voltammograms in Figure 4.1 reveal the electrocatalysis by CODH I_{Ch} and CODH II_{Ch} in which the scan was conducted from –0.76 V to 0.14 V under 50% CO and 50% CO_2. The positive electrocatalytic current indicates CO oxidation and the negative electrocatalytic current represents CO_2 reduction. CODH I_{Ch} and CODH II_{Ch} cut across the same potential of zero current at ~ –0.52 V (pH=7), which is close to the thermodynamic value.

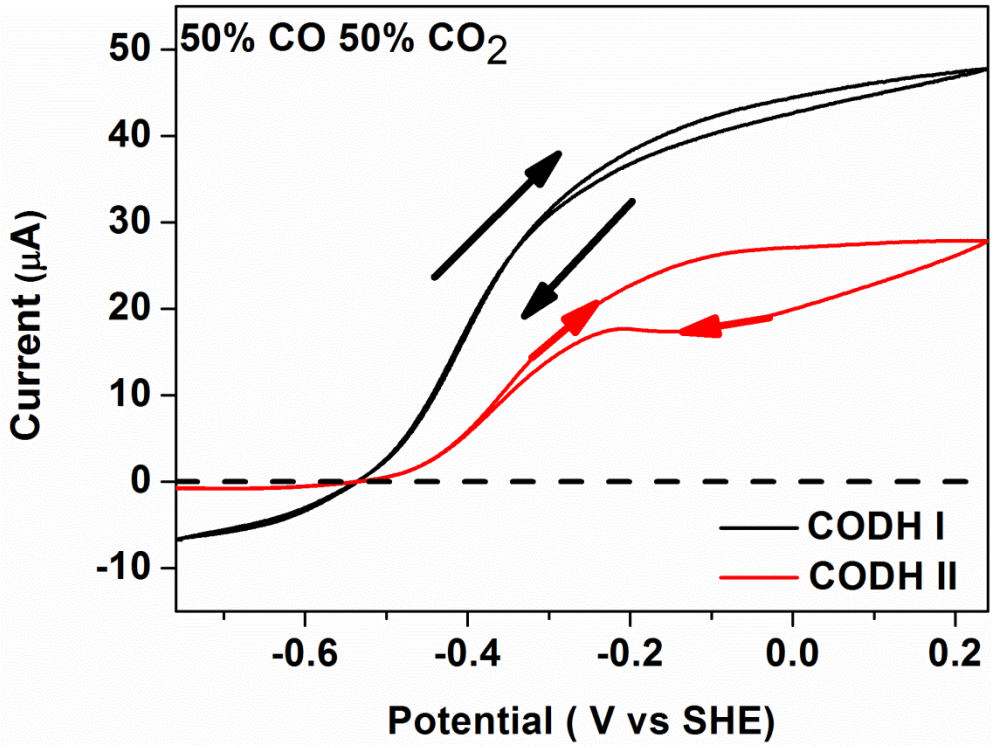

Figure 4.1 The voltammograms of CODH I_{Ch} and CODH II_{Ch} under 50% CO and 50% CO_2. Experimental conditions: 25℃, 0.2 M MES buffer (pH=7.0), rotation rate, 3500 rpm and scan rate, 2 $mVsec^{-1}$.

The voltammograms show there is a minimal overpotential requirement for the conversion between CO and CO_2 catalyzed by these two isoenzymes. However, the electrocatalytic current for CO_2 reduction by CODH II_{Ch} was barely observed in the voltammogram and it suggests much stronger CO product inhibition occurs in CODH II_{Ch}. The electrocatalytic current for CO_2 reduction and CO oxidation by CODH I_{Ch} is generally larger than CODH II_{Ch} over several experiments although it is difficult to estimate the concentration of enzyme on the electrode surface. The solution activity assay *via* methyl viologen has also shown that the activity of CODH I_{Ch} is slightly higher than CODH II_{Ch}.[5]

The K_m value for CO_2 reduction and the K_I value for CO product inhibition in CODH I_{Ch} by chronoamperometry have been shown in Chapter 3. A result for the CO product inhibition of CODH II_{Ch} analyzed by Lineweaver-Burk is shown in Figure 4.2 and all K_m and K_I values are summarized in Table 4.1. There are no great differences in the K_m value for CO_2 reduction between CODH I_{Ch} and CODH II_{Ch}. The higher K_m values for CO_2 reduction, in comparison with the K_m values for CO oxidation in the enzymes,[8] indicate the weak binding between CO_2 and the active site. Noticeably, the K_I value for CO product inhibition is larger for CODH I_{Ch} than CODH II_{Ch} as shown in Table 4.1 and the strongest product inhibition by CO occurs in CODH II_{Ch} at −560mV where the K_I value of CODH II_{Ch} is about one order of magnitude smaller than CODH I_{Ch}. This explains why a small electrocatalytic current for CO_2 reduction by CODH II_{Ch} was observed in Figure 4.1 under 50% CO and 50% CO_2. When more negative potentials in the region of CO_2 reduction are applied, the K_I values become bigger and the weak product inhibition occurs.

In previous studies, it has been shown that the apparent activation enthalpy from CODH I_{Ch} is 30 ± 3 kJ mole^{-1} for CO oxidation and 48 ± 9 kJ mole^{-1} for CO_2 reduction.[8] Under the same experimental conditions, the apparent activation enthalpy from CODH II_{Ch} is 27±4 kJ mole^{-1} for CO oxidation and 38±3 kJ mole^{-1} for CO_2 reduction (Figure 4.3). There are no great differences in the activation energy of CO oxidation but a smaller activation enthalpy of CO_2 reduction for CODH II_{Ch} is observed.

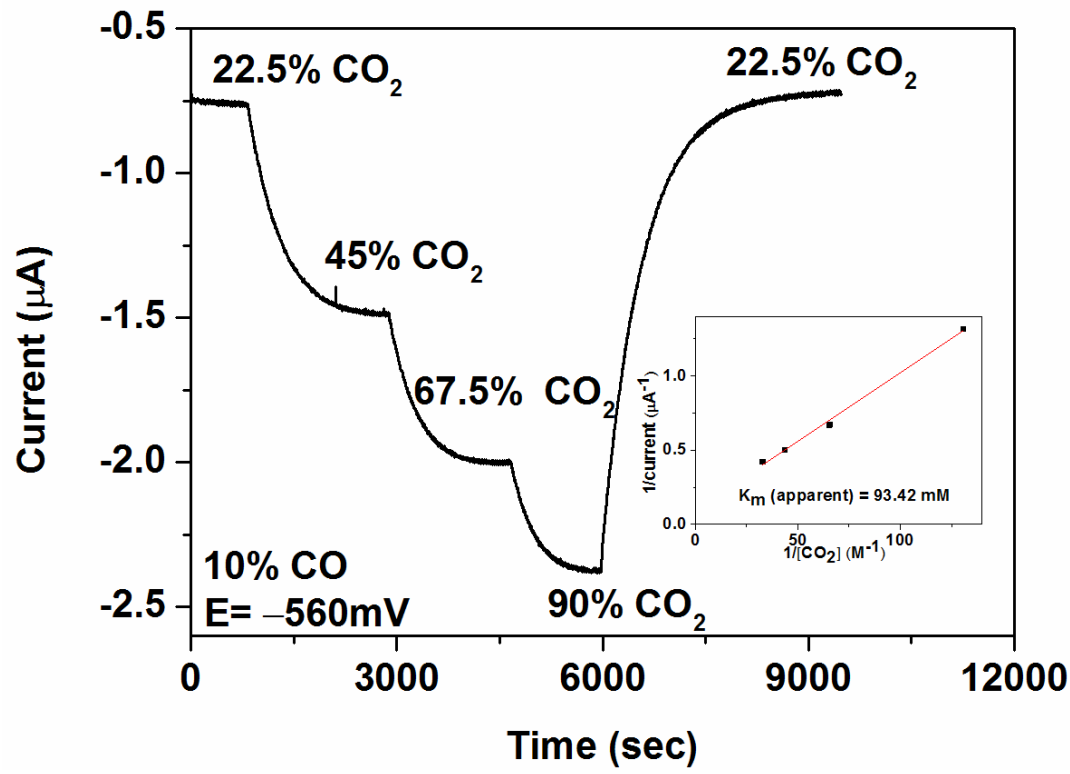

Figure 4.2 Inhibition of CODH II_{Ch} by CO product was recorded at –560 mV. The proportion of CO concentration was constant 10% over the experiment. The percentage number in the figure indicates the percentage of CO_2 was used in the total gas atmosphere. Argon was used to control the total gas balance. The inset figure shows the result of the Lineweaver-burk plot.

Table 4.1 Summary of K_m and K_I (CO product inhibition) values at two different potentials of CO_2 reduction between CODH I_{Ch} and CODH II_{Ch}

Potential	-560mV		-760mV	
	K_m (CO_2) (mM)	K_I (CO) (μM)	K_m (CO_2) (mM)	K_I (CO) (μM)
CODH I	8.06±2.07	45.2	7.08±0.70	337.0
CODH II	8.00±1.62	5.4	5.99±0.99	84.5

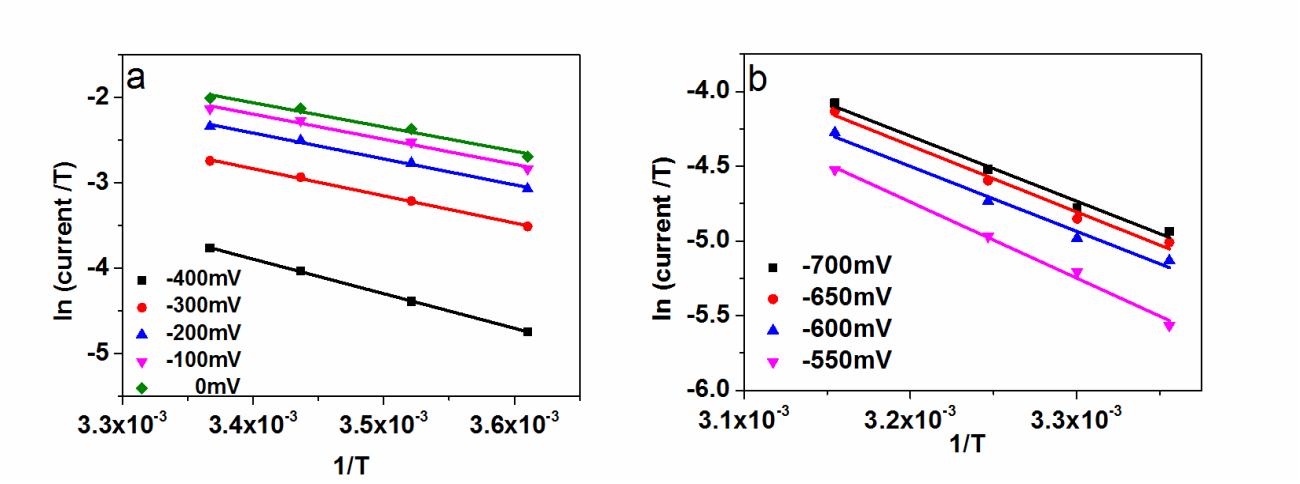

Figure 4.3 The activation enthalpy of CODH II_{Ch} by a Eyring plot. These plots yield (a) $\Delta H^{\ddagger}$= 27±4 kJ $mole^{-1}$ for CO oxidation at pH 7 under 100 % CO and (b) $\Delta H^{\ddagger}$=38±3 kJ $mole^{-1}$ for CO_2 reduction at pH 6 under 100 % CO_2.

4.4.2 Inhibition by cyanide

CODH inhibition by cyanide has been widely studied by different biophysical methods[16,56,63] since its electronic structure resembles CO. Conventional solution activity assay and spectroscopic evidence[56,59] indicate that cyanide only inhibits CO oxidation. However, CODH I_{Ch} inhibition by cyanide is also observed in the high potential window of CO_2 reduction on the electrode (Chapter 3). Therefore, it is useful to use cyanide as a probe to investigate differences between CODH I_{Ch} and CODH II_{Ch}.

Voltammograms showing CODH I_{Ch} and CODH II_{Ch} inhibition by cyanide under 100% CO are presented in Figure 4.4. 1 mM cyanide (final concentration in the solution) was injected at two different potentials in which the injection at the low potential is in the potential window of the C_{red1} state and the injection at the high potential is in the potential window of the C_{ox} state which is formed very slowly. Cyanide fully inhibits CO oxidation without any potential-dependence. The inhibition rate of CODH II_{Ch} by cyanide is slower than CODH I_{Ch} though both are inhibited by cyanide almost completely.

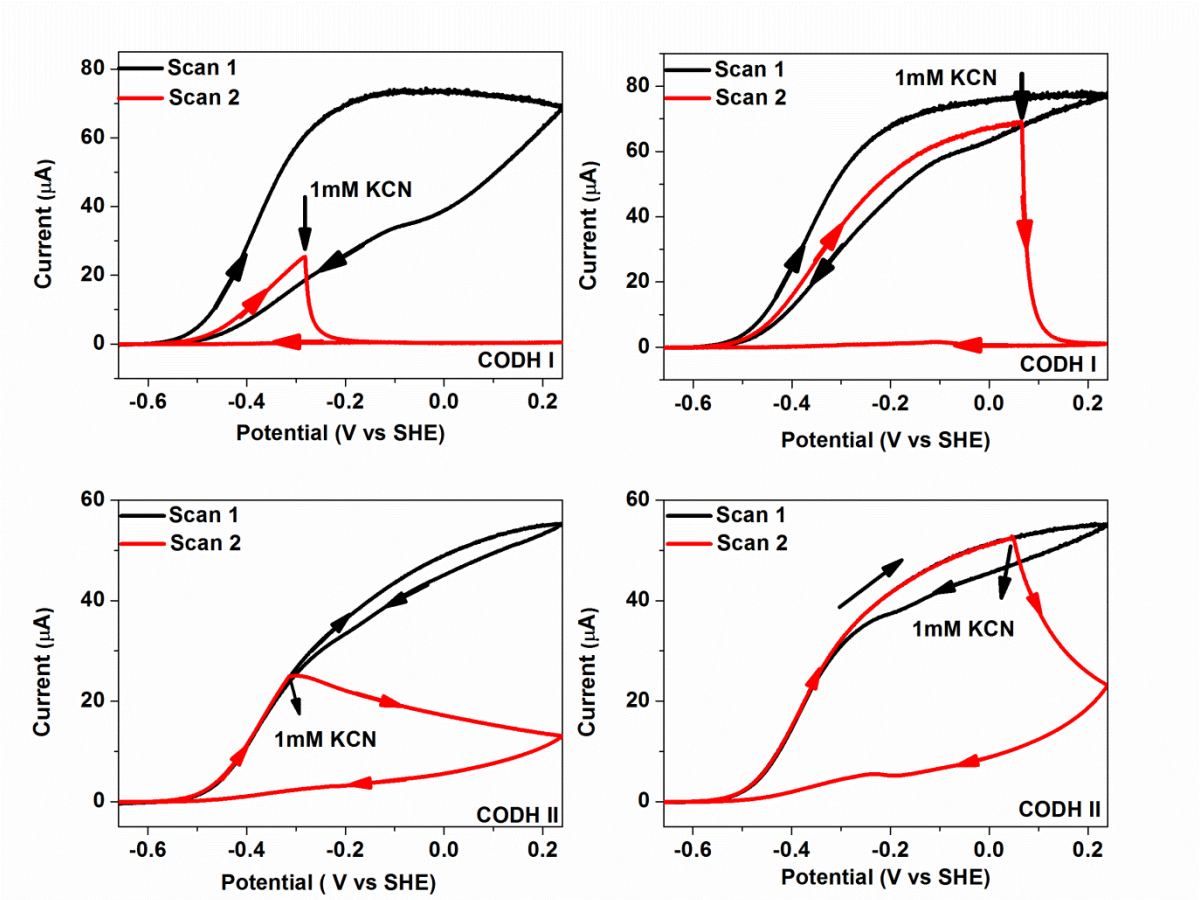

Figure 4.4 Inhibition of CODH I_{Ch} (upper figures) and CODH II_{Ch} (lower figures) by cyanide under 100 % CO. A final concentration of 1mM KCN was injected in Scan 2. The inhibition of CO oxidation by cyanide in CODH I_{Ch} is faster than CODH II_{Ch} (the lower figures). Experimental conditions: 25 ℃, 0.2 M MES buffer (pH=7.0), rotation rate, 3500 rpm and scan rate, 1 mV sec^{-1}.

Figure 4.5 reveals the result of cyanide injection under 100% CO_2. Like CODH I_{Ch}, CODH II_{Ch} is also inhibited by cyanide in the potential region where the C_{red1} state dominates. However, a more negative potential (by approximately 70 mV) is required to reductively

reactivate CODH II_{Ch} (CN^- is released by C_{red2}), implying that the C_{red1}/C_{red2} binding differential is about an order of magnitude higher (tighter binding) for CODH II_{Ch}. This phenomenon correlates with the stronger CO product inhibition displayed by CODH II_{Ch}.

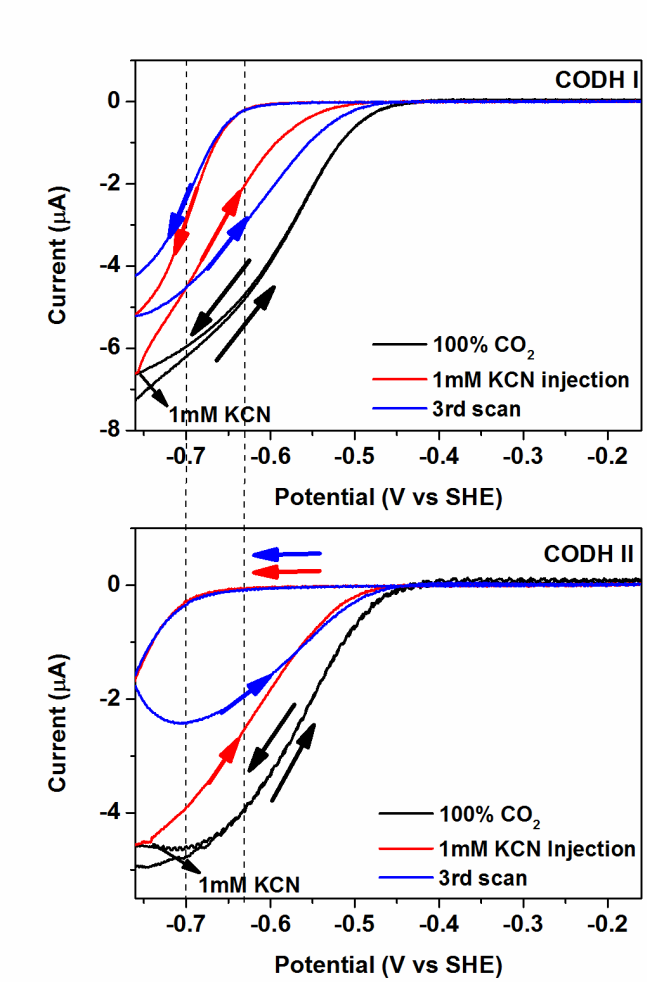

Figure 4.5 Inhibition of CODH I_{Ch} and CODH II_{Ch} by cyanide under 100% CO_2. The upper figure shows CODH I_{Ch} is inhibited by cyanide and CODH II_{Ch} inhibited by cyanide is shown in the lower figure. The more negative (approximate by ~70 mV) is required to reactivate CODH II_{Ch}. Experimental conditions: 25℃, 0.2 M MES buffer (pH=7.0), rotation rate, 3500 rpm and scan rate, 1 mV sec^{-1}.

In order to elucidate the mechanism of cyanide inhibition in the high-potential region of CO_2 reduction in cyclic voltammetry, chronoamperometry was used to measure the half-life time for inactivation (association)($t_{inact1/2}$) and the half-life time for reactivation (dissociation) ($t_{re\text{-}act1/2}$)*. A pseudo first order reaction in the inhibition process is assumed since the injection of cyanide concentration (final concentration, 0.5 mM in the electrochemical cell) is much higher than enzymes on the electrode surface and some results are shown in Figure 4.6. All half-life times which were measured from CODH I_{Ch} and CODH II_{Ch} at different potentials are summarized in Table 4.2. In CODH I_{Ch}, there are no great differences in the half-life time for inactivation by cyanide among different potentials measured; they are all approximately ~ 90 seconds though a slightly shorter half-life time is observed (~ 64 seconds) at −760mV.

* Here, the half-life time ($t_{1/2}$) is represented instead of the reaction rate constant (k) because the differences in terms of reaction rate constants (reciprocal of the life time) are not obvious.

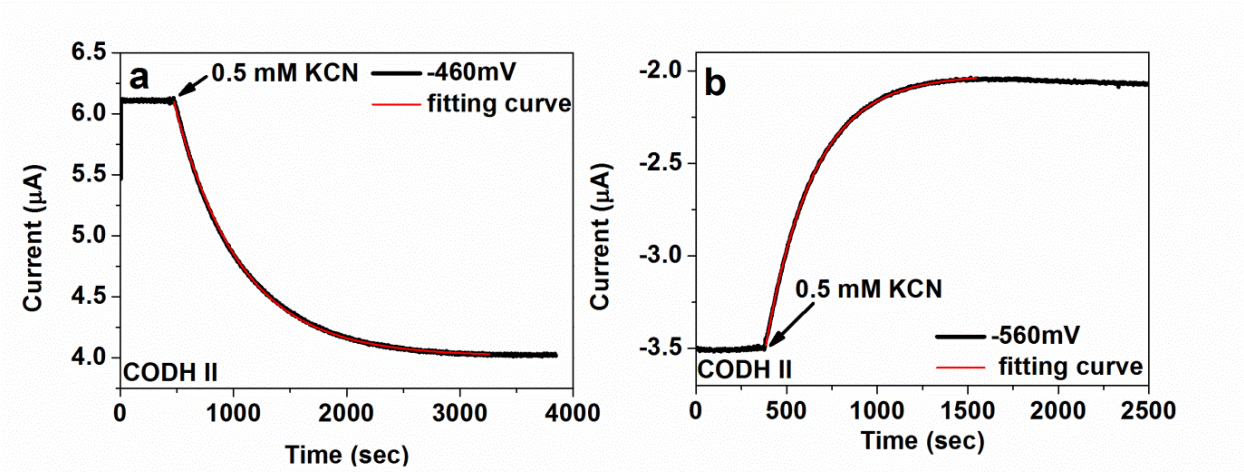

Figure 4.6 The measurement of the inactivation rate by cyanide in CODH II_{Ch} at −460 mV (CO oxidation) and −560 mV (CO_2 reduction). An aliquot of cyanide (giving 0.5 mM final concentration in the solution) was injected into the electrochemical cell to measure the half-life time. Experimental conditions: 25 ℃, 0.2 M MES buffer (pH=7.0) and rotation rate, 3500 rpm.

Table 4.2

The half-life for inactivation and reactivation of CODH I_{Ch} by KCN

Potential	$t_{inact1/2}$ (seconds)	$t_{re\text{-}act\ 1/2}$ (seconds)
+140mV	83.18±15	
-460mV	94.67±14.68	
-560mV	94.96±15.46	Still inhibited
-660mV	73.06±15.04	142.79±1.37
-760mV	64.12±10.54	19.41±6.93

The half-life for inactivation and reactivation of CODH II_{Ch} by KCN

Potential	$t_{inact1/2}$ (seconds)	$t_{re\text{-}act\ 1/2}$ (seconds)
+140mV	129.99	
-460mV	306.97±75.60	
-560mV	161.21±16.10	still inhibited
-760mV	54.48±3.26	<< *limit of detection*

However, greater differences in the half-life times for reactivation in CODH I_{Ch} at different potentials for CO_2 reduction were observed. The potential was first poised at –260mV (in the potential region of CO oxidation) in the presence of 0.5 mM KCN for 10 minutes in order to fully inactivate CODH and then the potential was switched to three different potentials, which are in the potential region of CO_2 reduction. It is difficult to observe any reactivation current upon switching to –560mV (Figure 4.7a), but the reactivation current is observed at –760mV with a half-life time of about 19 seconds in CODH I_{Ch} (Figure 4.8a), being shorter than the half-life time for inactivation at the same potential. These differences between $t_{inact1/2}$ and $t_{re\text{-}act1/2}$ explain why the hysteretic profile was observed in cyclic voltammetry because the rate for inactivation is much larger than the rate for reactivation in the high potential regions of CO_2 reduction (–560 mV), whereas the rate for reactivation is slightly faster than the rate for inactivation in the low potential regions of CO_2 reduction (–760 mV).

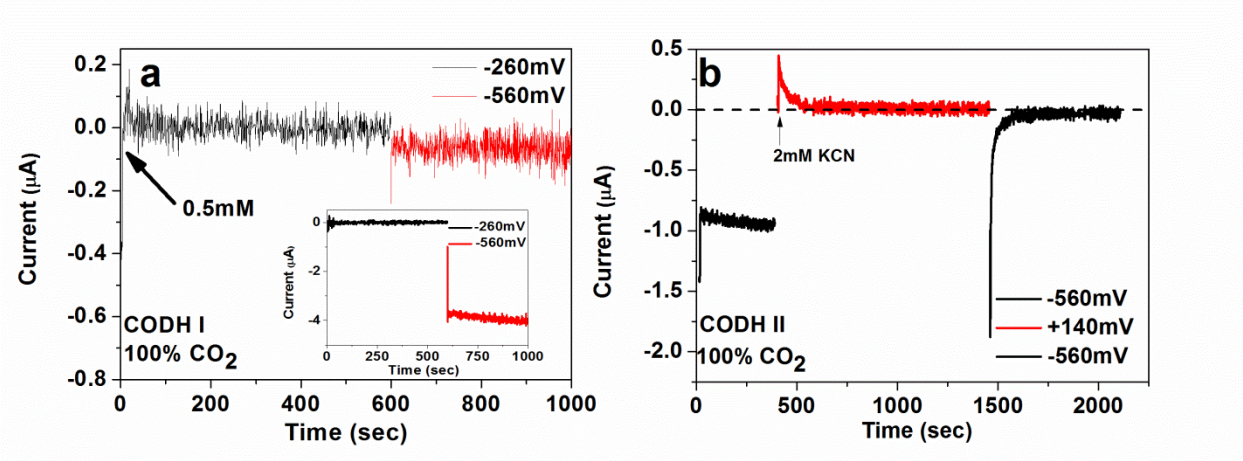

Figure 4.7 The measurement of the reactivation rate of cyanide-inhibited CODH I_{Ch} and CODH II_{Ch} at −560 mV by chronoamperometry. Once the potential is switched into −560 mV from (a) −260 mV (CODH I_{Ch}) and (b) +140 mV (CODH II_{Ch}), no electrocatalytic current was observed in the presence of KCN at −560 mV. The inset of Figure 4.7a exhibits the electrocatalytic current in the absence of KCN. Experimental conditions: 25℃, 0.2 M MES buffer (pH=7.0), and rotation rate 3500 rpm.

As opposed to CODH I_{Ch}, greater differences between half-life times for inactivation in CODH II_{Ch} were observed and longer half-life times were obtained. As the potential is in the potential window of the C_{ox} state (+140mV), the half-life time for inactivation is shorter. The half-life time for inactivation at −460 mV is about 2.4 times longer than at +140 mV. The longer half-life times for inactivation obtained by chronoamperometry in CODH II_{Ch} are consistent with the slower CO oxidation inhibition by cyanide observed in the voltammograms (Figure 4.4). Another main difference is that the half-life time for reactivation is much faster at −760 mV. Once the potential was switched to −760 mV after

the presence of cyanide for 10 minutes at –260 mV, the electrocatalytic current appeared immediately (Figure 4.8b) without any exponential increase as observed in CODH I_{Ch} (Figure 4.8a). This explains why the upward concave curve (the blue line in Figure 4.5) in the low potential region of CO_2 reduction (from –760mV to –660mV) was observed in the voltammogram of CODH II_{Ch} due to $k_{re\text{-}act} >> k_{inact}$ ($t_{re\text{-}act1/2} << t_{inact1/2}$). The faster reactivation of the cyanide-bound CODH II_{Ch} occurs in the low potential region of CO_2 reduction and then starts to bind faster again as soon as the potential is more positive than –0.6 V. In comparison, $k_{re\text{-}act}$ in CODH I_{Ch} is only one order of magnitude larger than k_{inact} in the low potential of CO_2 reduction. (–760mV)

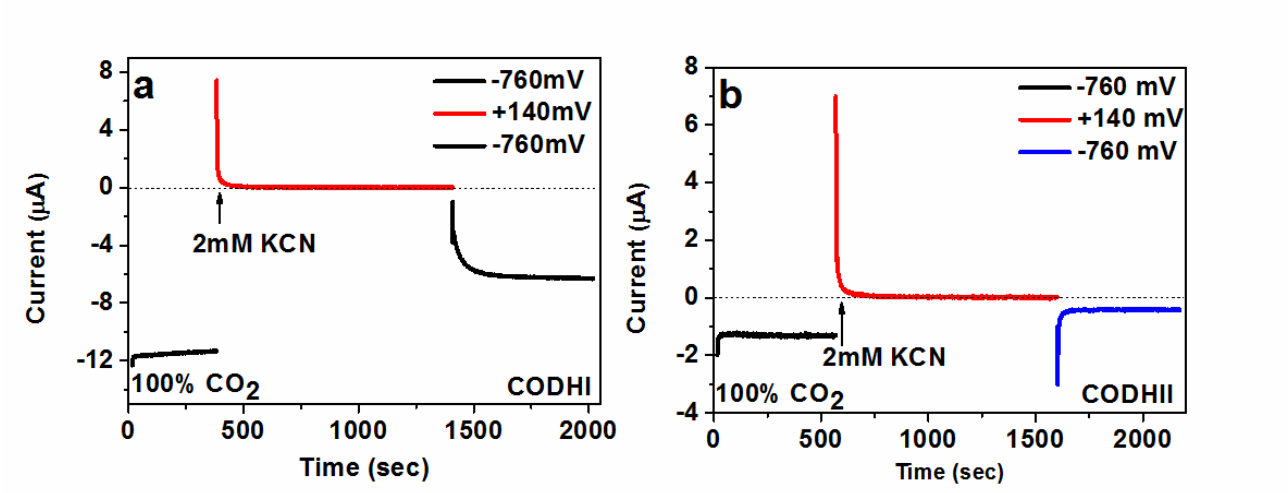

Figure 4.8 The measurement of the reactivation rate for cyanide-bound CODH I_{Ch} and CODH II_{Ch} at –760mV by chronoamperometry. The reactivation rate of cyanide from CODH II_{Ch} at –760mV is faster than the instrumental response. Experimental conditions: 25℃, 0.2 M MES buffer (pH=7.0) and rotation rate 3500 rpm.

4.4.3 Inhibition by cyanate

Cyanate is isoelectronic with CO_2 and it has been shown that CO oxidation catalyzed by CODH/ACS_{Mt} from *Moorella thermoacetica* is inhibited by cyanate and a new EPR signal was observed upon adding cyanate into the C_{red1} state.[55] Full inhibition of CO_2 reduction by cyanate in CODH I_{Ch} was observed in electrochemical experiments (described in Chapter 3). Therefore, cyanate is another way to probe the catalytic state in CODH and to investigate differences between CODH I_{Ch} and CODH II_{Ch}. When final concentration of 8 mM cyanate was injected into the electrochemical cell at −760mV under the atmosphere of 20% CO and 80% CO_2[*], a greater inhibition in the region of CO_2 reduction and weak inhibition under the low driving force window of CO oxidation (between – 0.6 V and −0.5 V) was observed as shown in Figure 4.9. As for CODH I_{Ch}, cyanate mainly inhibits CO_2 reduction by CODH II_{Ch}. There is no difference between CODH I_{Ch} and CODH II_{Ch} in terms of potential-dependence. However, the dissociation constant of cyanate in CODH II_{Ch} (3.3 mM) is slightly larger than CODH I_{Ch} (1.9 mM) at −760mV(Chapter 3).

[*] Instead of 50% CO and 50% CO_2, a gas mixture of 20% CO and 80% CO_2 was used in CODH II_{Ch} because it has strong CO product inhibition.

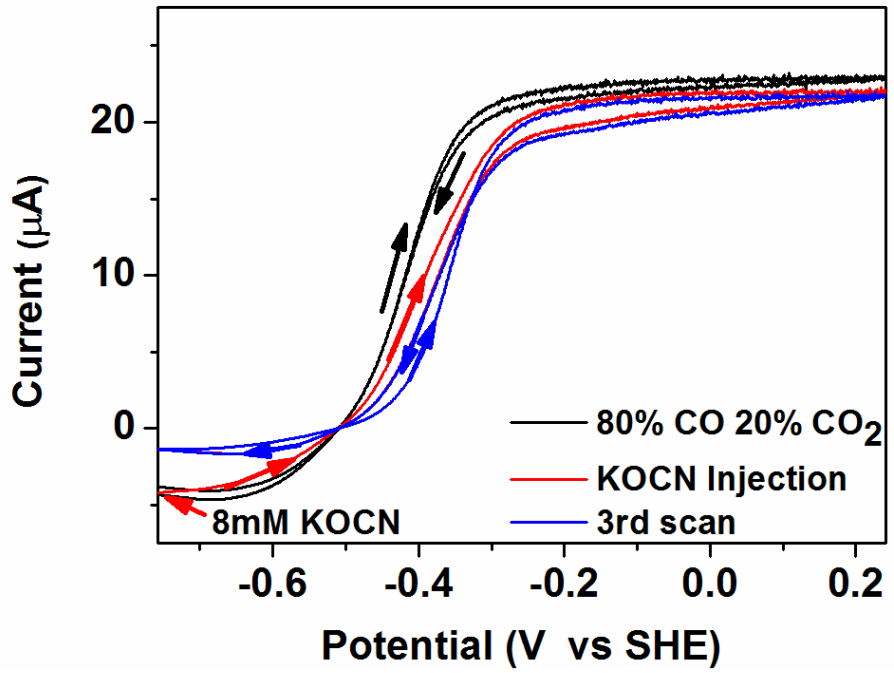

Figure 4.9 CODH II_{Ch} inhibition by cynante. An aliquot of cyanate solution (giving the final concentration 8 mM in the solution) was injected into the electrochemical cell at –760 mV under 20% CO and 80% CO_2. Experimental conditions: 25℃, 0.2 M MES buffer (pH=7.0), rotation rate, 3500 rpm and scan rate, $2mVsec^{-1}$.

In order to elucidate how cyanate reacts with CODH I_{Ch} and CODH II_{Ch}, chronoamperometry was undertaken to measure the half-life times for inactivation and reactivation in CODH I_{Ch} and CODH II_{Ch} respectively. Two methods were used for measuring the inactivation: first, the potential was poised at –160mV in the presence of 6.7 mM cyanate for 10 minutes. (No inhibition is observed at this potential) before stepping the potential to two different values, –560mV or –760mV respectively, where inhibition occurs. The second method was to inject cyanate directly at these potentials and measure the half-time of the subsequent reaction. (Figure 4.10) The half-life time for inactivation is about 90

seconds in CODH I_{Ch} at both potentials (Table 4.3) and a similar pattern occurs in CODH II_{Ch} except there are longer half-life times for inactivation (about 270 seconds). Unlike cyanide, no apparent potential dependence of the half-life time for cyanate inactivation is observed.

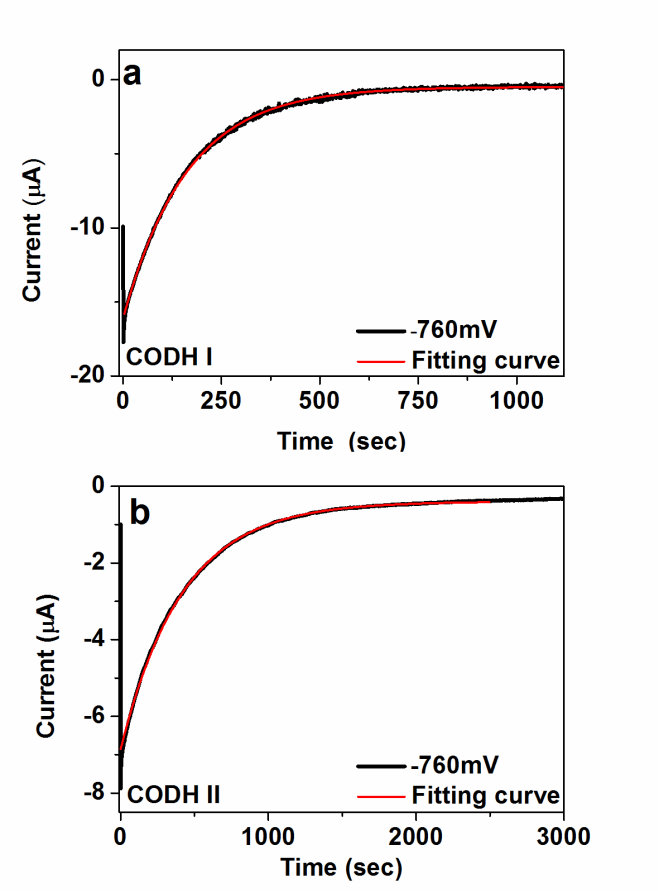

Figure 4.10 The measurement of the inactivation rate of CODH I_{Ch} (a) and CODH II_{Ch} (b) by cyanate at −760mV. First, 6.6 mM KOCN (final concentration) was added to the electrochemical cell and poised at −160mV for 10 minutes before switching into −760mV to measure the half-life time for inactivation. The same experiments were also conducted at −560mV. Experimental conditions: 25℃, 0.2 M MES buffer (pH=7.0), and rotation rate 3500 rpm.

Table 4.3

The half-life time for inactivation of CODH I_{Ch} and CODH II_{Ch} by KOCN

Potential	CODH I_{Ch} (seconds)	CODH II_{Ch} (seconds)
-560mV	84±6	288±29
-760mV	100±11	262±1

In contrast, it is unable to obtain the half-life time for reactivation in our electrochemical instrument. Once the potential was switched to –160 mV from –760 mV which is held for 10 minutes in the presence of 6.67mM cyanate in order to form cyanate-bound CODH, it was observed that the electrocatalytic current immediately jumped to the highest positive current and then started to decay slowly due to the film loss (Figure 4.11). This suggests that the reactivation rate is faster than two seconds since the dead-time for switching between two potentials (i.e. a realistic dead-time for the experiment, which produces a current spike due to charging) is about two seconds in the electrochemical instrument.

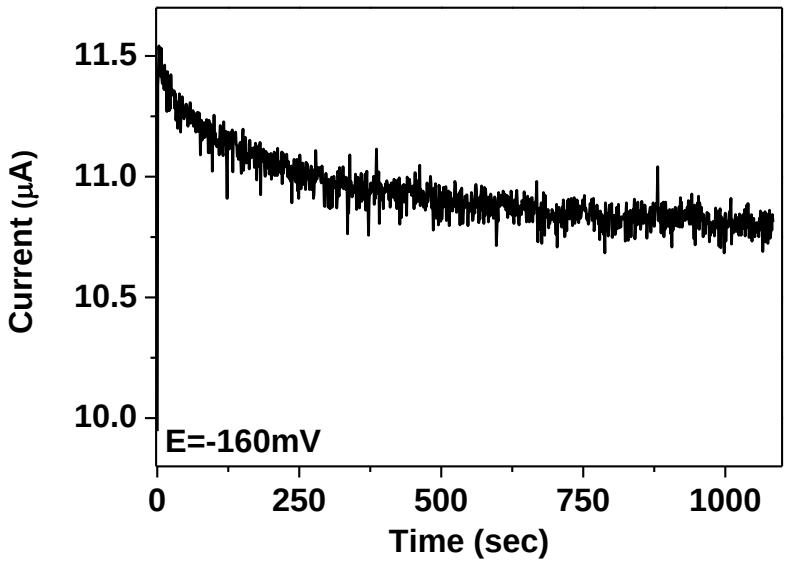

Figure 4.11 The measurement of the reactivation rate from cyanate-bound CODH I_{Ch} at −160 mV. The potential was poised at −760 mV for 10 mins in the presence of 6.66 mM KOCN before changing the potential to −160 mV. Experimental conditions: 25℃, 0.2 M MES buffer (pH=7.0), and rotation rate 3500 rpm.

In brief, the inactivation rate is quite slow but the reactivation rate is much faster. Potential is a crucial factor in controlling the inhibition and reactivation processes between cyanate and CODH.

In addition, different ratios of CO_2 and Ar in the headspace (100% CO_2 and 10% CO_2/90% Ar) were used in order to investigate whether cyanate is a competitive inhibitor with CO_2. A longer half-life time for inactivation was observed in both CODH I_{Ch} and CODH II_{Ch} when a higher concentration of CO_2 was used. This implies that cyanate should bind to C_{red2} and is a competitive inhibitor. (Figure 4.12)

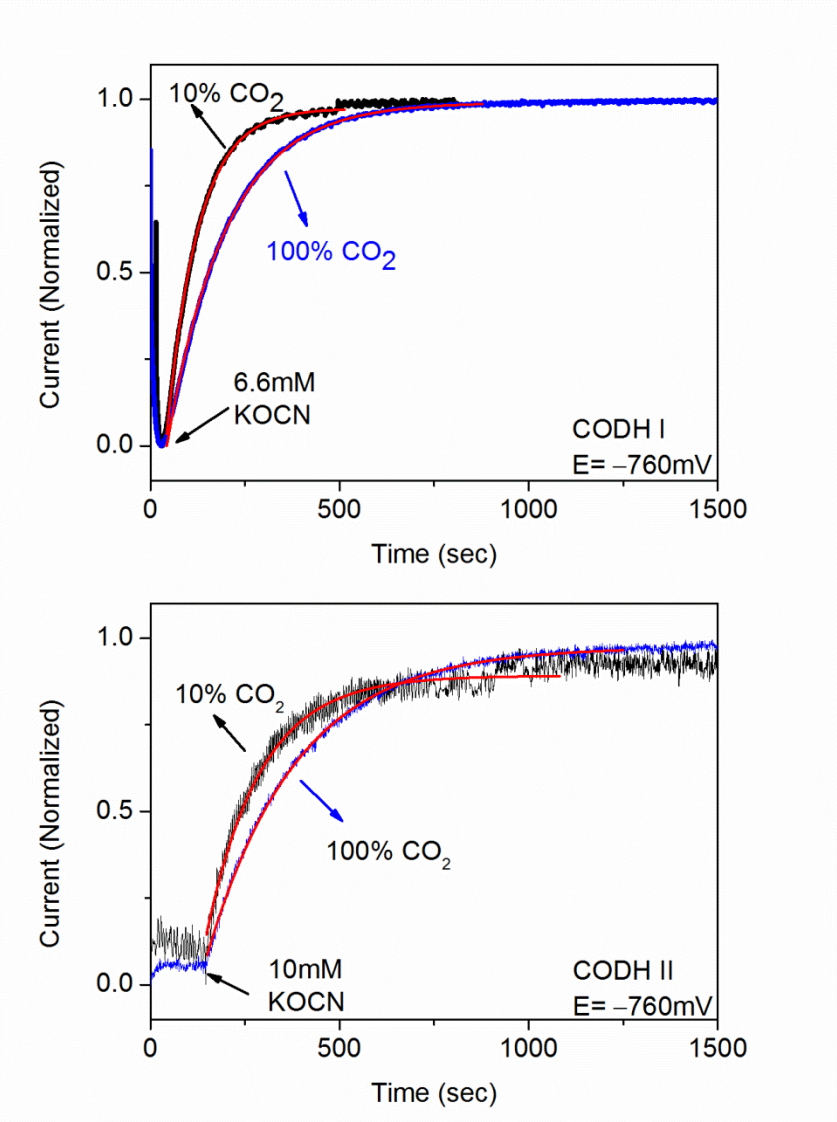

Figure 4.12 Investigations of the rate of inactivation of CODH I_{Ch} and CODH II_{Ch} by cyanate at –760 mV under different CO_2 concentrations (10% CO_2 or 100% CO_2). The normalized current is shown in figures and the fit to a single exponential decay curve is represented in the red line. Injections of KOCN were made into the electrochemical cell to give final concentrations of 6.6 mM for CODH I_{Ch} (upper figure) and 10 mM for CODH II_{Ch} (lower figure). Experimental conditions: 25℃, 0.2 M MES buffer (pH=7.0) and rotation rate 3500 rpm .

4.4.4 Inhibition by thiocyanate

Thiocyanate, like cyanate, is a linear molecule but an oxygen atom in cyanate is replaced by a sulfur atom in thiocyanate. Thus, it is useful to compare the inhibition mechanisms between cyanate and thiocyanate. As in the previous study, the change of EPR signal from CODH/ACS$_{Mt}$ was only observed in the C_{red1} state in the presence of thiocyanate and thiocyanate partially inhibits CODH/ACS$_{Mt}$ activity in the solution activity assay.[55] The voltammograms of CODH I$_{Ch}$ and CODH II$_{Ch}$ in the presence of thiocyanate under 100% CO are shown in Figure 4.13.

A partial drop in the electrocatalytic current was only observed when the potential was above –0.4V in the presence of 6.6 mM thiocyanate for CODH I$_{Ch}$ and 10 mM thiocyanate for CODH II$_{Ch}$ under 100% CO, which correlates with the partial inhibition of CODH/ACS$_{Mt}$ by thiocyanate reported before. Unlike cyanate, no inhibition in the potential region of CO_2 reduction was observed. A reversible inhibition/reactivation mechanism occurs and the switch-potential is –180 mV for CODH I$_{Ch}$ and – 90 mV for CODH II$_{Ch.}$ In brief, the results from the electrochemical experiment are consistent with previous studies from CODH/ACS$_{Mt}$.

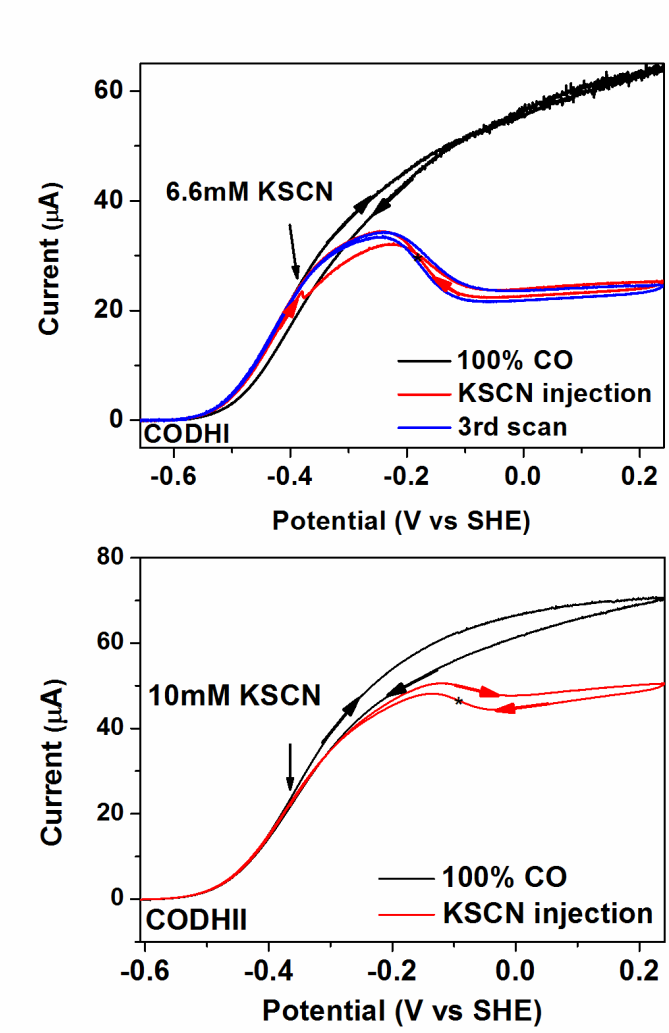

Figure 4.13 CODH I_{Ch} and CODH II_{Ch} inhibition by thiocyanate. A final concentration of 6.6 mM (CODH I_{Ch}) and 10 mM (CODH II_{Ch} was injected to the electrochemical cell respectively and the reversible inactivation/reactivation process occurs at −180 mV (CODH I_{Ch}) and –90 mV (CODH II_{Ch}) as marked by the asterisk. Experimental conditions: 25℃, 0.2 M MES buffer (pH=7.0), rotation rate, 3500 rpm and scan rate, 1 mV sec^{-1} (for CODH I_{Ch}) and 2 mV sec^{-1} (for CODH II_{Ch}).

4.4.5 Inhibition by sulfide

The potential dependence of CODH I_{Ch} inhibition by sulfide has been described in Chapter 3. The target state of sulfide inhibition is believed to be "the equivalent state of the C_{ox} or the highly oxidized state" (Chapter 3). The same results are also observed in CODH II_{Ch} (Figure 4.14). The inactivation of CODH II_{Ch} by sulfide starts at about 0 V. The reactivation potential of CODH II_{Ch}, −260 mV, is similar to the value obtained by CODH I_{Ch}. These potential-dependant inhibitions by sulfide on CODH II_{Ch} consolidate the evidence from CODH I_{Ch} and clarify the previous conflicting evidence about the role of sulfide in CODH.[17,56,57]

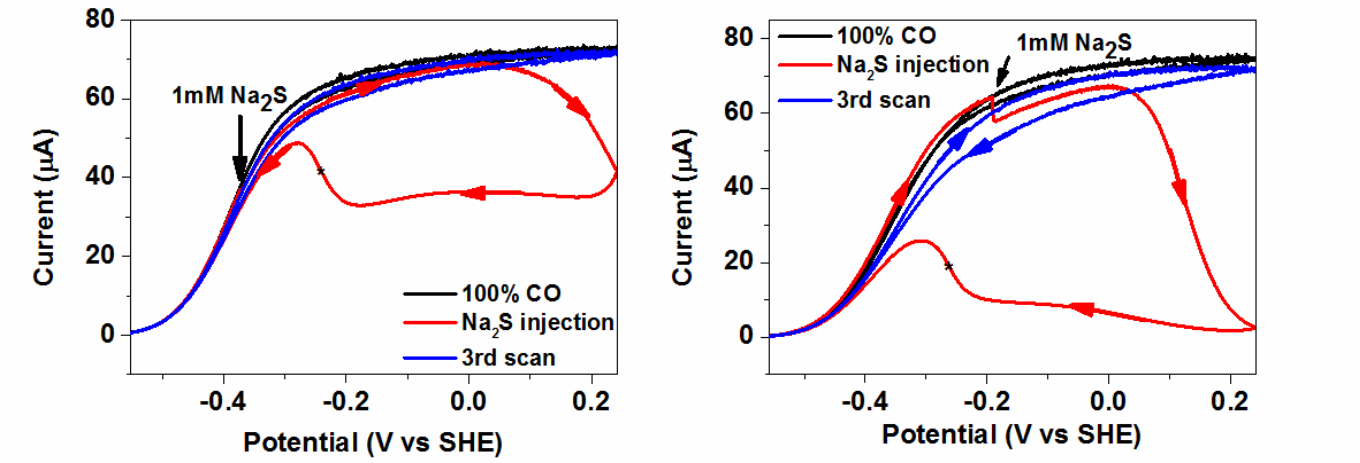

Figure 4.14 The inhibition of CODH II_{Ch} by sulfide. 1 mM Na_2S (final concentration) was injected to the electrochemical cell. The asterisk indicates the reactivation potential occurs at −260mV. Experimental conditions: 25℃, 0.2 M MES buffer (pH=7.0), rotation rate, 3500 rpm and scan rate, 1 mV sec^{-1}.

4.5 Discussion

The features of CODH II_{Ch} inhibition by these small inhibitors, CO product, CN^- NCO^-, SCN^- and HS^- (S^{2-}) are similar to CODH I_{Ch}. The inhibition by these molecules are highly potential-dependent. Cyanide inhibition occurs throughout the potential region of CO oxidation and the high potential region of CO_2 reduction; cyanate inhibition occurs weakly in the low potential region of CO oxidation and in the fully potential region of CO_2 reduction. The inhibition pattern implies that these two molecules are isoelectronic with CO and CO_2 respectively. In brief, in terms of inhibition of CO_2 reduction (C_{red2}) by these molecules, the inhibition strength is NCO^- > CN^- > CO >> HS^- (S^{2-}) and SCN^-. In terms of inhibition of CO oxidation in the low potential region (C_{red1}), the inhibition strength is CN^- > NCO^- > HS^- (S^{2-}) ~ SCN^-. In terms of the high potential region of CO oxidation (the potential window of C_{ox}), the inhibition strength is HS^- (S^{2-}) > CN^- > SCN^- > >NCO^-.

The main differences between CODH I_{Ch} and CODH II_{Ch} are CO product inhibition and cyanide inhibition. The stronger inhibition by cyanide and CO occurs in CODH II_{Ch}. Recently, several CODH crystal structures from different species with cyanide or CO bound to the Ni atom in the C-cluster have been published. CN–ACS/$CODH_{Mt}$[28] and CO(formyl)–ACDS/$CODH_{Mb}$[68] present the *bent* N–C–Ni structure with the bond angle ~114° and the *bent* O–C–Ni structure with the bond angle ~107°. In addition, the hydroxide ion (water) still binds to the dangling Fe atom in these two structures. After superimposing with CO_2–CODH II_{Ch},[6] the nitrogen atom from CN–ACS/$CODH_{Mt}$ and the oxygen atom from CO–ACDS/$CODH_{Mb}$ almost overlap with the oxygen atom from CO_2 in CO_2–CODH II_{Ch}. However, the carbon atom from CN–ACS/$CODH_{Mt}$ and CO–ACDS/$CODH_{Mb}$ is displaced

from the carbon atom from CO_2–CODH II_{Ch}. Therefore, the Drennan group[28] and Chan group[68] suggest carbon shift takes place in the catalytic mechanism of CO oxidation: Firstly, CO binds to the nickel atom and forms the unstable bent-binding structure to lower the energy barrier for reaction. Sequentially, carbon shift occurs to facilitate the nucleophilic attack by the hydroxide ligand on the dangling Fe atom.

According to suggestions by the Drennan group, the isoleucine residue plays an important role in the bent binding structure between CO/CN^- and the Ni atom due to the steric effect.[19] However, sequence alignments among several CODHs; including CODH I_{Ch} and CODH II_{Ch}, all show that this isoleucine residue is conserved. The crystal structure of CN–CODH II_{Ch} shows cyanide coordinates onto the Ni atom in the *straight* N-C-Ni binding manner with square plane geometry, in which the isoleucine is distant from CN^- although hydroxide bound to the dangling Fe in CN–CODH II_{Ch} is not observed (Figure 1.3c). The evidence indicates that the conserved residue isoleucine should not cause different rates and binding affinities of inactivation/reactivation by CN^- or CO between CODH I_{Ch} and CODH $II_{Ch.}$

Furthermore, several obligate residues coordinating to the C-cluster and important residues involving the proton channel and catalytic reaction as suggested by mutagenesis studies[73]are all *conserved* between CODH I_{Ch} and CODH II_{Ch}. Therefore, it is difficult to give definitive suggestions about which residues play a role in controlling the different affinity for CN^- binding and CO product inhibition between CODH I_{Ch} and CODH II_{Ch}.

Comparing multiple sequence alignments between CODH I_{Ch}, CODH II_{Ch} and ACS/$CODH_{Mt}$, only three residues are found to be near the active site in ~10 Å and are the

same in CODH II_{Ch} and ACS/$CODH_{Mt}$ but different in CODH I_{Ch} as shown in Figure 4.15. The residues Ala566 and Trp570 from CODH II_{Ch} or Ala589 and Trp593 from ACS/$CODH_{Mt}$ are replaced by the residues Ser566 and Tyr570 in CODH I_{Ch}.

```
CODH I Ch    PPVLHVGSCVDNSRAVALAVAVADRLGVDTDQLPVVASAAEAVAEKAVSIGTYAVALGLP 577
CODH II Ch   PPVLHMGSCVDNSRAVALVAALANRLGVDLDRLPVVASAAEAMHEKAVAIGTWAVTIGLP 577
CODHMt       PPVFHMGSCVDNSRAVDLLMAMANDLGVDTPKVPFVASAPEAMSGKAAAIGTWWVSLGVP 600
             ***:*:********** *  *:*: ****  ::*.****.**:  **.:***: *:*:*
```

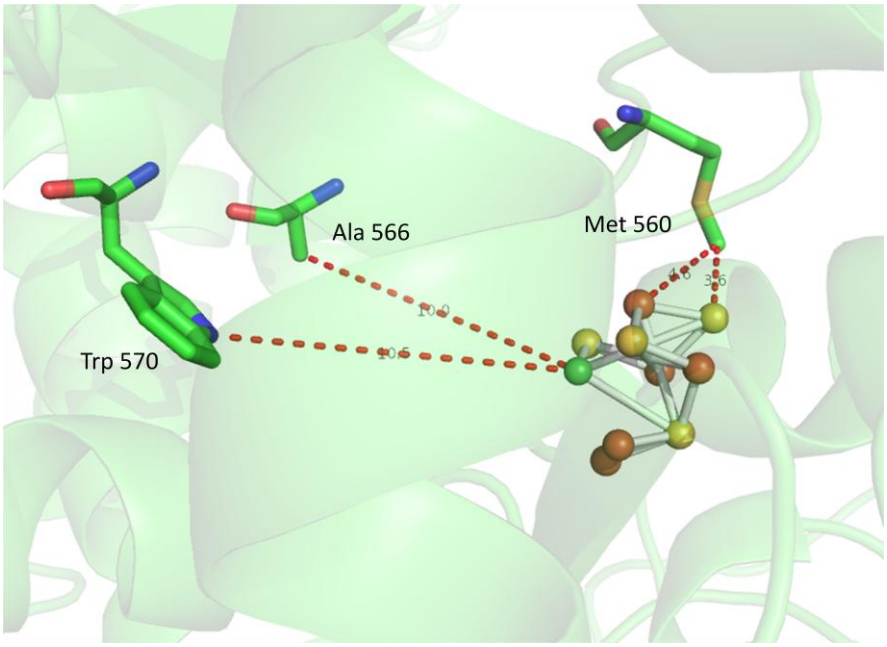

Figure 4.15 Multiple sequence alignments between CODH I_{Ch}, CODH II_{Ch} and ACS/$CODH_{Mt}$. The asterisk indicates amino acids are fully conserved. The colon indicates the conservation of amino acids between groups have strongly similar properties. The period indicates the conservation of amino acids between groups have weakly similar properties. Three residues labelled by red (as shown in the below figure based on the CODH II_{Ch} structure) which are 10 Å distant from the active site are found to be the same in CODH II_{Ch} and ACS/$CODH_{Mt}$ but are different in CODH I_{Ch} based on sequence alignments.

Ala566 and Tyr570 are found in the putative gas channel suggested by the crystal structure of CODH II_{Ch} with n-butyl-isocyanide,[74] which might imply they play a role as the regulatory gate in regulating substrate entry in enzyme. This replacement to Ser566 and Tyr570 might cause the steric effect for CO or cyanide entry to the C-cluster. It is also found that the inhibition rate of cyanide on ACS/$CODH_{Mt}$ (Chapter 5) is slower than CODH I_{Ch} in our electrochemical experiment. Further mutagenesis experiments are needed to examine this hypothesis.

The feature of CODH II_{Ch} inhibition by cyanate, thiocyanate and sulfide are similar to CODH I_{Ch} (Chapter 3) except the slightly higher K_d value for CODH II_{Ch} and the more positive switch potential was observed for reversible SCN^- inhibition/reactivation in CODH II_{Ch}. The strong and rapid inhibition by sulfide occurs when the potential is positive than 0 V. No inhibition of CO_2 reduction by sulfide in CODH II_{Ch} is observed. These results consolidate the proposed inhibition mechanism of CODH I_{Ch} by these molecules in Chapter 3.

The half-life time for inactivation and reactivation by cyanide and cyanate from chronoamperometry is on the magnitude of tens of seconds. The turnover rate for CODH *via* the conventional solution activity assay is approximately 5900 s^{-1} at 50 ^oC.[5] Therefore, the conversion time between C_{red1} and C_{red2} in the CO/CO_2 redox couple should be approximately10^{-3}-10^{-4} sec. The inhibition (association) rates of cyanide or cyanate observed here are much slower than the turnover rate. This implies that at least there is a fast reversible reaction between these two inhibitors and the C-cluster before the slow reaction rate is observed by electrochemical experiments. The fast reaction (k_{on} and k_{off}) possibly relates to

the initial weak interaction between cyanide/cyanate and the C-cluster when inhibitors go through the CODH substrate channel. The slow reaction ($k_{iso\text{-}on}$ and $k_{iso\text{-}off}$) should be associated with isomerisation or other rearrangement in CODH after binding between CODH and inhibitors. This fast-slow reaction mechanism for cyanide inhibition was previously proposed by the Ragsdale group.[63] The discovery of at least two-step reaction mechanisms for cyanide and cyanate inhibition reactions might correlate with the idea of carbon shift, which involves different structural conformations to facilitate the reaction in the C-cluster.

An obvious issue concerns the acid-base properties of the inhibitors and the likely requirements for proton transfer steps during transport in and out of the enzyme (the natural substrates are neutral molecules) and to allow tight binding to occur. Under our experimental conditions, NCO^- (p*K* 3.7) is present entirely as the conjugate anion and might require to be protonated to reach the active site, whereas CN^- (p*K* 9.2) is present entirely as neutral HCN and would certainly require deprotonation in order to become a viable ligand for binding to a metal. The differences may also reflect polarity (CN^- has a higher dipole moment than CO; NCO^- is dipolar but CO_2 is quadrupolar).

Unlike CODH I_{Ch} which is known to involve energy generation in microorganisms, the biological role of CODH II_{Ch} is less understood. The observation of stronger CO product inhibition from CODH II_{Ch} suggests CODH II_{Ch} has possible different roles in biological system.

This chapter has clearly shown that precise potential control is required to understand the reaction mechanism between CODH and a specific inhibitor. Although sequences

between CODH I_{Ch} and CODH II_{Ch} are highly similar, some electrochemical properties are different. This implies that CODH II_{Ch} has a different role in the cell.

Chapter 5 *Unidirectional electrochemical catalysis by acetyl-CoA synthase /carbon monoxide dehydrogenase from Moorella thermoacetica on pyrolytic graphite edge electrode*

5.1 Abstract

Acetyl-CoA synthase/carbon monoxide dehydrogenase (ACS/CODH) from *Moorella thermoacetica* was investigated by protein film electrochemistry. In comparison with bidirectional (reversible) eletrocatalysis of CO oxidation and CO_2 reduction by carbon monoxide dehydrogenase (CODH) from *Carboxydothermus hydrogenoformans* on the pyrolytic graphite edge (PGE) electrode, the unidirectional electrocatalysis for CO oxidation by ACS/CODH is observed with an overpotential of 0.1 V. In order to identify whether ACS influences the performance of CODH, several chemical reagents, such as sodium dodecyl sulfate (which separates CODH and ACS partially), 1, 10-phenanthroline, (which removes the requisite Ni atom in the active site of ACS) and acetyl-CoA (the product of the reaction carried out by ACS/CODH) are added. However, it is still unable to observe any electrocatalytic current from CO_2 reduction or lower overpotential for CO oxidation by ACS/CODH.

Several small inhibitors, cyanide, cyanate and azide, were added to ACS/CODH, which shows that cyanide fully inhibits CO oxidation and cyanate and azide partially inhibits CO oxidation. The inhibition of ACS/CODH by these anionic inhibitors from electrochemical results is consistent with previous studies from electron paramagnetic resonance and solution activity assay. In comparison, no inhibition of CO oxidation by azide and only weak inhibition by cyanate between −0.55 V and −0.5 V are observed in monofunctional CODH from *Carboxydothermus hydrogenoformans*. These findings indicate that ACS plays an important role in controlling CODH activity in ACS/CODH.

5.2 Introduction

Acetyl-CoA synthase/carbon monoxide dehydrogenase (ACS/CODH) plays an important role in some anaerobic archaea and bacteria in which it is involved in the final step for synthesizing acetyl-CoA in the Wood–Ljungdahl pathway as shown in eq 5.1.[9] This reaction carried out by ACS requires CO from CO_2 reduction by CODH as shown in eq 5.2, a methyl group from corrinoid iron-sulfur protein (CoFeSP) and CoA.

$$CO + [CH_3\text{-}Co(III)FeSP]^{2+} + CoASH \rightleftharpoons CH_3COSCoA + [Co(I)FeSP]^{+} + H^{+} \quad (5.1)$$

$$CO_2 + 2H^{+} + 2e^{-} \rightleftharpoons CO + H_2O \quad (5.2)$$

Several X-ray crystal structures, including ACS/CODH [28] from *Moorella thermoacetica*, CODH[6] and ACS[10] respectively from *Carboxydothermus hydrogenoformans* have been solved. These structures clearly show several $[Fe_4S_4]$ clusters involving electron transfer (called the B-cluster and D-cluster respectively) and two unique metal clusters in which the C-cluster in CODH reduces CO_2 to the intermediate CO product and the A-cluster in ACS condenses CO, CoA and a methyl group into acetyl-CoA. The C-cluster consists of a distorted $[NiFe_3S_4]$ cubane-like cluster and a dangling Fe atom which links to the cluster as shown in Figure 5.1a. The A-cluster consists of two Ni atoms which are bridged by two thiolates and a $[Fe_4S_4]$ cluster bridging with the proximal Ni ion by a cysteine thiolate as shown in Figure 5.1b. It has been shown that only the distal Ni atom is redox-inactive Ni (II) ion in the catalytic cycle.

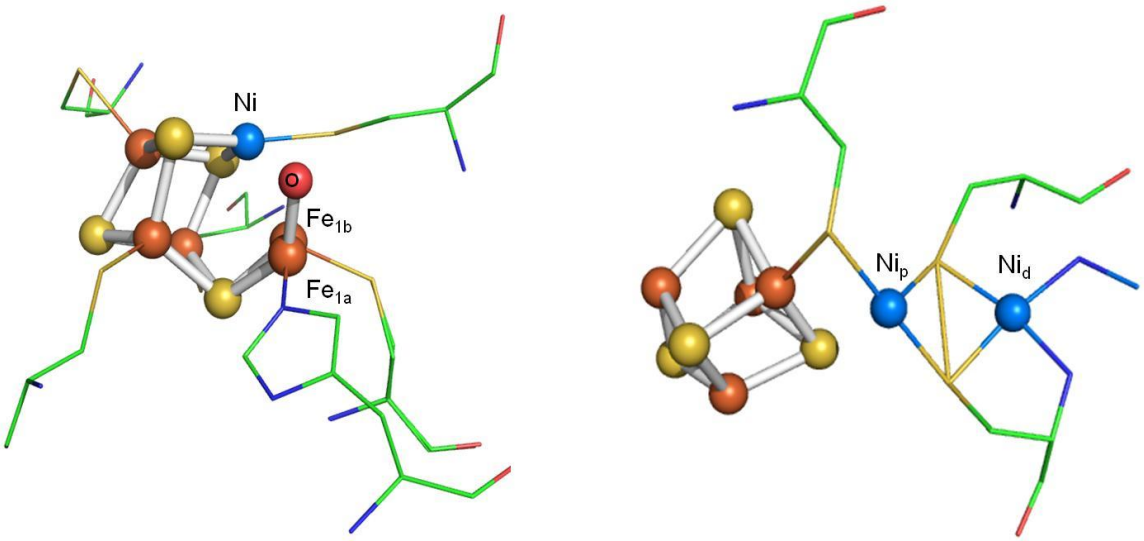

Figure 5.1 The active site of the C-cluster in CODH[6] (left figure) and the A-cluster in ACS[10] from *Carboxydothermus hydrogenoformans*. In the C-cluster, the dangling Fe atom (Fe_{1a} and Fe_{1b}) is found in two different positions in the CODH crystal structure. In the A-cluster, the proximal Ni (Ni_p) ion which links to the [Fe_4S_4] cluster is believed to be the redox-active site.

In contrast with the well-established mechanism of CO/CO_2 interconversion catalyzed by the C-cluster in CODH, the mechanism of acetyl-CoA synthesis in the A-cluster is still the subject of debate. Two possible mechanisms are proposed, the paramagnetic and diamagnetic mechanism depending on different ways to evaluate the oxidation state of the proximal Ni atom.[9] Essentially, CO deriving from CO_2 reduction by CODH migrates and bonds to the proximal Ni atom on the A-cluster and then a methyl group from the methyl carrier protein, CoFeSP binds to the A-cluster. The recent evidence from isotope trap experiments suggests that CO and a methyl group randomly bind to the active site without sequential order.[63] Following the formation of carbon-carbon bond between the carbonyl and methyl group, the

acetyl group forms. Finally, an intermediate complex (the acetyl group) reacts with CoA to form an acetyl-CoA. The observation of the exchange reaction between isotope acetyl ($CH_3{}^{14}CO$)-CoA and ^{12}CO occurs in ACS/CODH , which indicates this reaction is reversible and the carbonyl group is exchangeable.[75]

The catalytic cycle in the C-cluster in CODH has been discussed in Chapter 1 and Chapter 3, mainly based on the study of ACS/CODH from *Moorella thermoacetica*.[20] In addition, several small anionic molecules, cyanide (CN^-), cyanate (NCO^-) and azide (N_3^-) were added to the C_{red1} and C_{red2} state in ACS/CODH from *Moorella thermoacetica* and studied by EPR.[55,76] In brief, the new EPR signal was only observed in the C_{red1} state in the presence of these inhibitors, rather than the C_{red2} state.

In previous studies, most studies focus on the single role of ACS or CODH itself in ACS/CODH and less study address how ACS influences CODH activity. For example, the turnover number for CO_2 reduction by ACS/CODH is determined indirectly by measuring the amount of CO-product binding to hemoglobin.[77,78] However, several studies have shown CO from CO_2 reduction is an intermediate product and directly diffuses into the A-cluster without escaping from ACS/CODH during the synthesis of acetyl-CoA.[30,79] Therefore, it is difficult to understand CO_2 reduction by ACS/CODH unambiguously. In PFE, the electrocatalytic current directly reflects enzyme activity because the electrocatalytic current is correlated to the electron transfers which are used for enzymatic catalysis. In addition, as previous two chapters have shown, the inhibition of monofunctional CODH by different inhibitors is highly potential-dependent on the PGE electrode. The lack of precise potential-control could lead to different results, especially for CO_2 reduction which requires potentials

more negative than –0.5 V. Therefore, protein film electrochemistry is a useful tool to reinvestigate CODH performance in the complex enzyme ACS/CODH.

5.3 Material and methods

The preparation of ACS/CODH from *Moorella thermoacetica* follows methods described in previous publications.[61,80] All chemicals used are analytic grade or the best quality. Sodium dodecyl sulphate (SDS) was purchased from Acros. 1, 10-phenanthroline, acetyl-Coenzyme A (>93%), sodium aizde and potassium cyanate were purchased from Sigma-Aldrich. Potassium cyanide was obtained from Fisher chemical. CO and CO_2 cylinder were purchased from BOC.

Approximately 2μL of enzyme solution (~ 20 mg/mL) was discharged from a pipette onto the PGE surface. Sodium dodecyl sulphate and 1, 10-phenanthroline respectively was added to the coating solution at different ratios described in each figure legend. For experiments of the addition of acetyl-Coenzyme A or substrate-mimic inhibitors, polymyxin (Sigma-Aldrich) was added to the coating solution in a 3:1 ratio over enzyme as described in Chapter 3 to improve the stability of the enzyme film on the electrode.

The electrochemical experiments, instrumental setup and data analysis were the same as described in Chapter 3 and chapter 4.

5.4 Results

5.4.1 Unidirectional electrocatalysis for CO oxidation by ACS/CODH

The cyclic voltammograms in Figure 5.2 reveal the activity of ACS/CODH on the PGE electrode under 100% CO, 100% CO_2 and 50% CO/50% CO_2 respectively. In comparison with monofunctional CODH from *C. hydrogenoformans* in PFE (Chapter 4), two significantly different features are recognized. First, the electrocatalytic current for CO oxidation by ACS/CODH (~10^{-7} A) is about 100 times smaller than CODH I_{Ch} and CODH II_{Ch} (~10^{-5} A).

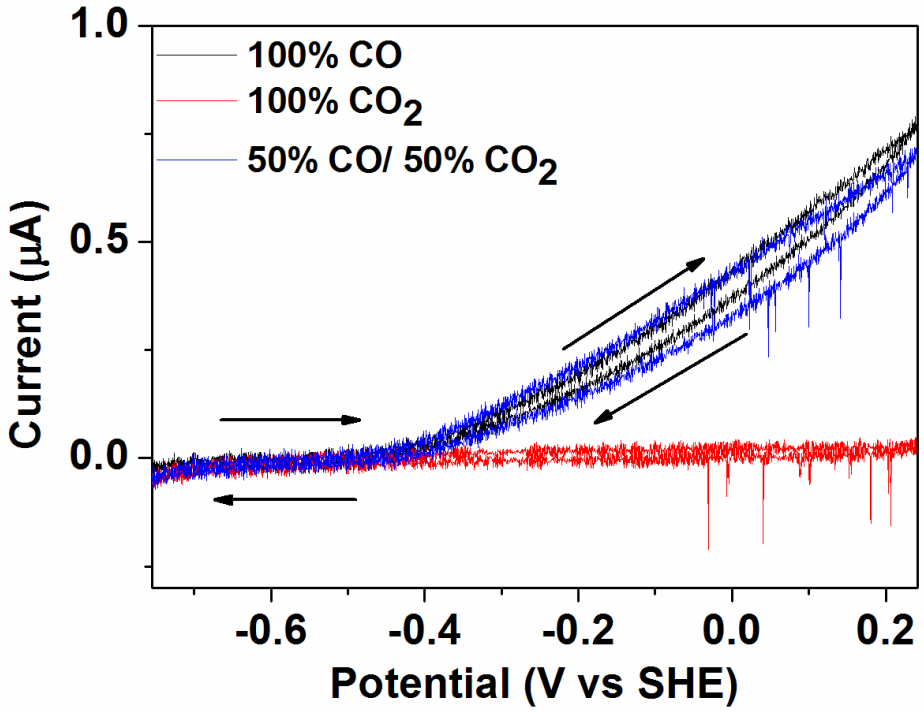

Figure 5.2 The voltammograms of ACS/CODH on the PGE electrode were recorded at different gas ratios. Only the electrocatalytic current for CO oxidation is observed. Experimental conditions: 25℃, 0.2 M MES buffer (pH=7.0), rotation rate 3500 rpm and scan rate 1 mV s^{-1}.

The smaller electrocatalytic current correlates with the observation that the specific activity of CO oxidation by ACS/CODH (~400 µmol min^{-1} mg^{-1}) from *Moorella thermoacetica*[5] is much lower than CODHs (~15000 µmol min^{-1} mg^{-1}) from *Carboxydothermus hydrogenoformans* by conventional solution activity assay with methyl viologen as a redox indicator dye.[69] The larger size of ACS/CODH would cause fewer enzymes on the electrode surface, which also leads to the smaller electrocatalytic current. Secondly, unlike monofunctional CODH which conducts bidirectional (reversible) electrocatalysis on the electrode (CO oxidation and CO_2 reduction), only the electrocatalytic current for CO oxidation was observed from ACS/CODH. In addition, a higher overpotential is observed for CO oxidation, which starts above ~ –0.4 V (at pH=7.0) as opposed to the monofunctional CODH with the minimal overpotential. (Chapter 3 and Chapter 4) The activation enthalpy ($\Delta H^{\ddagger}$) for CO oxidation is about 32.3 ±1 kJ /mole (Figure 5.3), which is similar to the value obtained from CODH I_{Ch} and CODH $II_{Ch.}$ (Chapter 4)

No electrocatalytic current for CO_2 reduction was observed at the even lower scan potential, −1 V. It is difficult to analyze results below −1V since proton reduction starts to occur on the PGE electrode at ~ –1V.

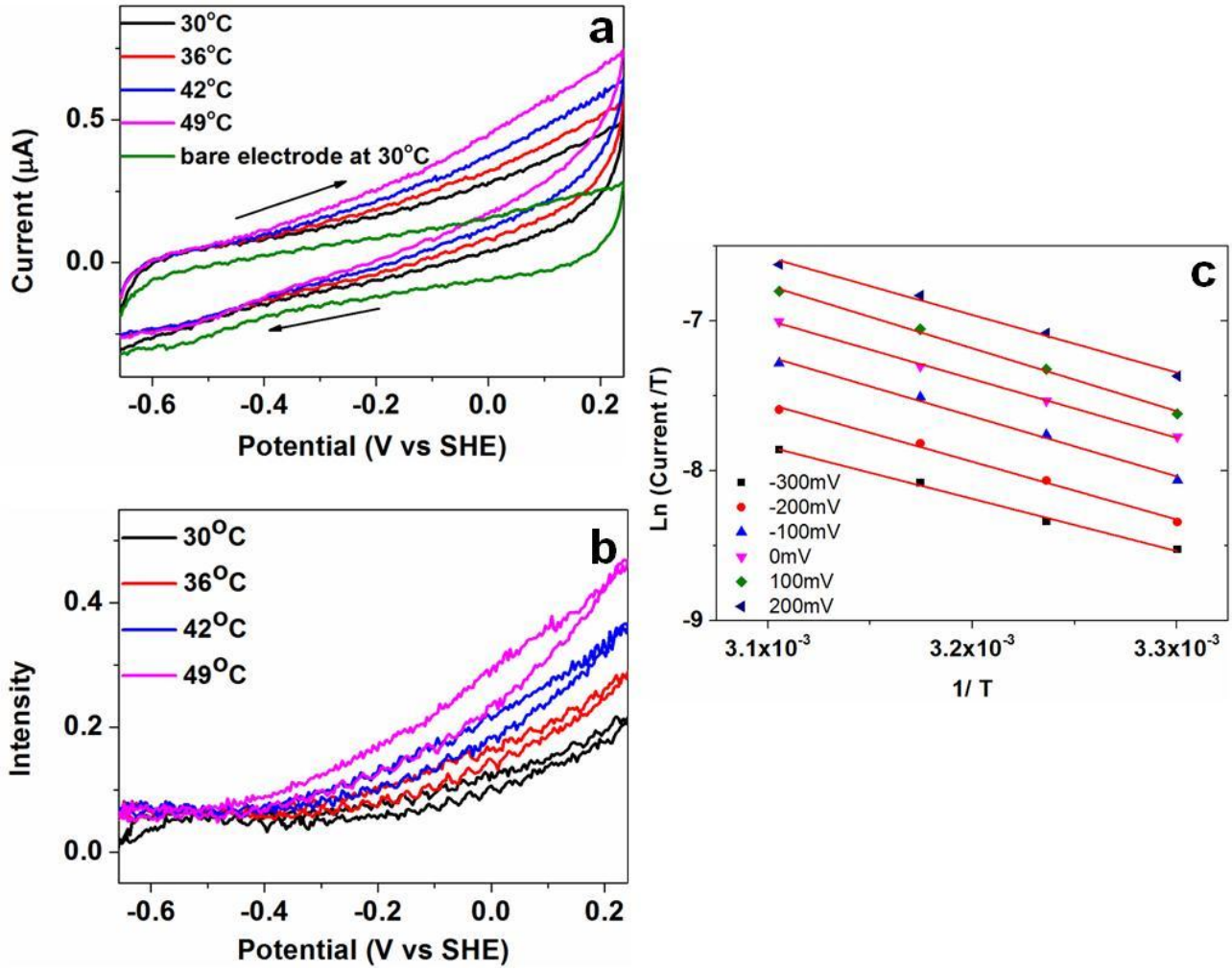

Figure 5.3 The voltammograms of ACS/CODH at different temperatures under 100% CO. (a) Raw data under 100% CO; (b) voltammograms are obtained by subtracting the background current and (c) the Eyring plot for CO oxidation from the date of Figure 5.3b. Experimental conditions: 0.2 M MES buffer (pH=7.0), rotation rate 4000 rpm and scan rate 30 mV s^{-1}.

5.4.2 In the presence of sodium dodecyl sulfate

It has been shown that the incubation of an intact $\alpha_2\beta_2$ ACS/CODH structure with SDS (sodium dodecyl sulfate) can yield a stable $\alpha\beta_2$ structure and a α subunit(ACS) in which the stable $\alpha\beta_2$ structure of CODH (β_2 subunit) still remains the activity of CO oxidation.[81] Therefore, SDS was added to investigate whether CO_2 reduction occurs when ACS (α-subunit) dissociates from ACS/CODH. Different ratios of the coating solution of SDS and enzymes were prepared and incubated for an hour before employing electrochemical experiments. In the presence of SDS, the electrocatalytic current for CO oxidation was observed. Although the very small plausible electrocatalytic current for CO_2 reduction was observed as shown in Figure 5.4, the lack of reproducibility of experiments, very small current and no direct evidence, such as detection by gas chromatography, hesitate us to suggest the electrocatalytic current for CO_2 reduction occurs. The electrocatalytic current is smaller when the concentration of SDS is 10 times more than enzymes concentration (Figure 5.5). This indicates that the high concentration of SDS might cause more unstable ACS/CODH structures or the less stable film of ACS/CODH on the PGE electrode.

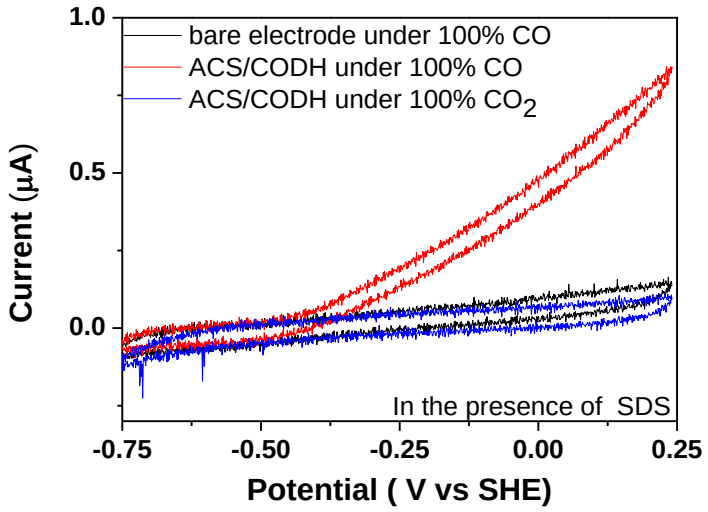

Figure 5.4 Voltammograms of the mixture of ACS/CODH and SDS (0.1 times concentration of ACS/CODH) on the PGE electrode were recorded. Only the electrocatalytic current for CO oxidation is observed. Experimental conditions: 37^{o}C, 0.2 M MES (pH=7.0), rotation rate: 1000 rpm and scan rate 1 mV sec^{-1}.

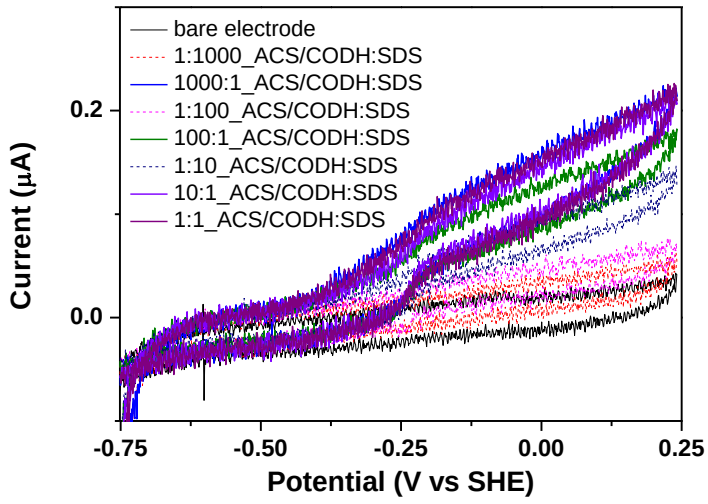

Figure 5.5 Different ratios of ACS/CODH and SDS under 100% CO. Experimental conditions: 37 ^{o}C, 0.2 M MES (pH=7.0), rotation rate 1000 rpm and scan rate 4 mVsec^{-1}.

5.4.3 In the presence of 1, 10-phenanthroline

The Lindahl group has shown that 1, 10-phenanthroline selectively removes the requisite Ni atom from the A-cluster in ACS/COSH, which causes the exclusive loss of ACS activity but still remains CODH activity for CO oxidation.[82] The electrocatalytic current for CO oxidation was still observed after incubating 1, 10-phenanthroline with ACS/CODH in a 4:1 ratio for 24 hours but the electrocatalytic current became smaller. (Figure 5.6) However, still no electrocatalytic current for CO_2 reduction was observed.

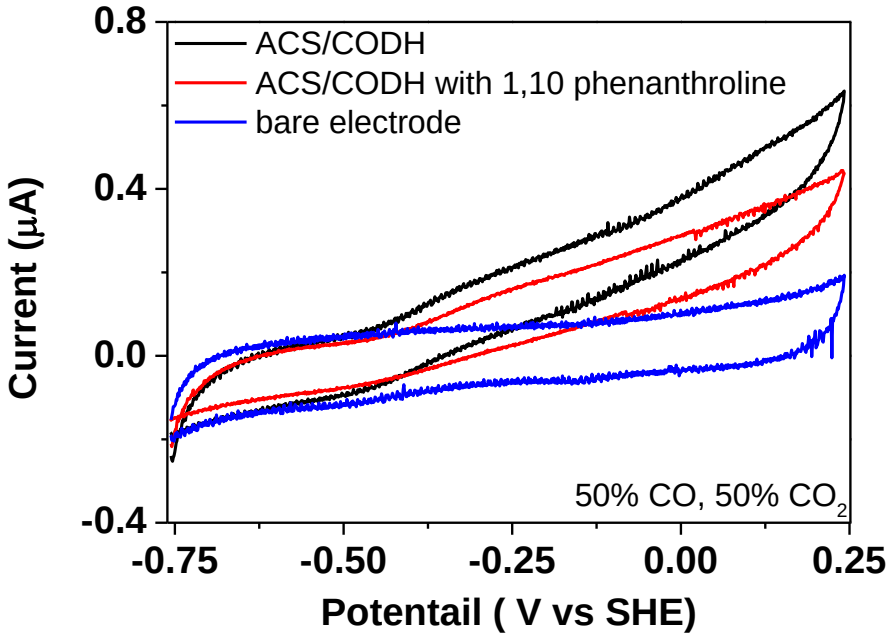

Figure 5.6 The mixtures of ACS/CODH and 1, 10 phenanthroline (four times concentration of ACS/CODH) on the PGE electrode were recorded. Only the electrocatalytic current for CO oxidation is observed. Experimental conditions: 37^{o}C, 0.2 M MES (pH=7.0), rotation rate 1000 rpm and scan rate 1 mVsec^{-1}.

5.4.4 In the presence of acetyl-CoA

It has been reported that the exchange reaction between the carbonyl group of acetyl-CoA and CO occurs in ACS/CODH and suggested that the A-cluster can cleave acetyl-CoA to form CO in the reverse direction.[75] Therefore, the addition of acetyl-CoA is to examine whether CO_2 reduction occurs in the presence of product. The electrocatalytic current for CO oxidation in the presence of ~1.5 mM acetyl-CoA in the electrochemical cell solution under 50% CO and 50% CO_2 is shown in Figure 5.7. In comparison with the result in the absence of acetyl-CoA, the electrocatalytic current in the presence of acetyl-CoA (blue line) was smaller. Although the very small plausible electrocatalytic current for CO_2 reduction was observed as shown in Figure 5.7, the lack of direct evidence, such as detection by gas chromatography, and very small current values hesitate us to suggest the electrocatalytic current for CO_2 reduction occurs. The electrocatalytic current was restored (pink line) after the cell buffer solution containing acetyl-CoA was replaced by fresh buffer. The smaller current in the presence of acetyl-CoA might relate to the fact that the slow exchange occurs between CO and the carbonyl group of acetyl-CoA, which causes some ACS/CODH to only engage in the exchange reaction in ACS rather than CO oxidation to CO_2 in ACS/CODH. The small electrocatalytic current for CO oxidation with the high overpotential still exists in three different methods and it suggests that the activity of CODH is affected by associated ACS structure.

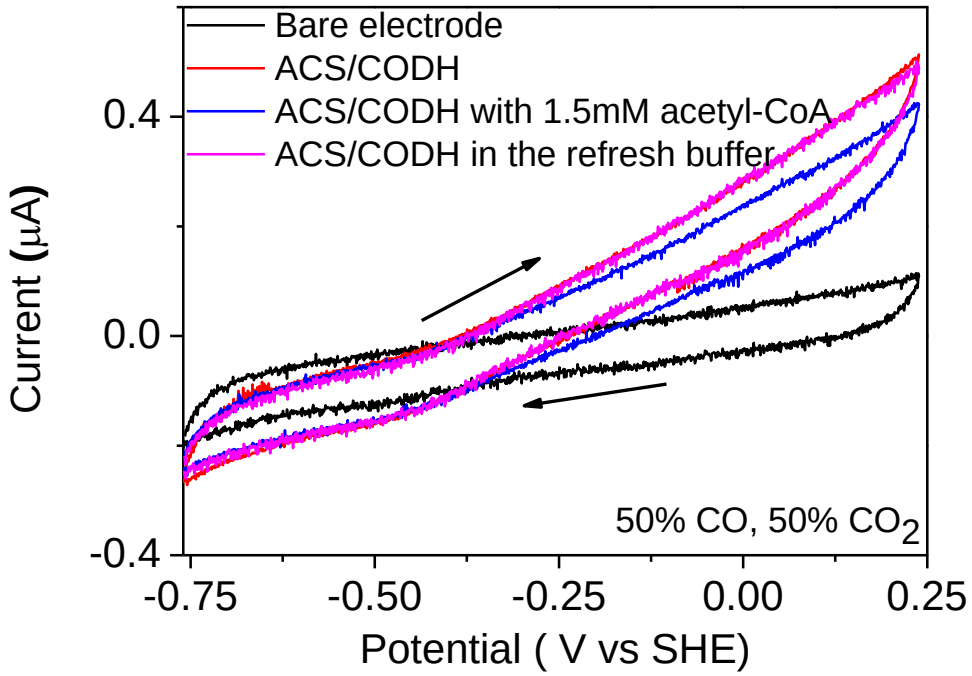

Figure 5.7 The voltammograms of ACS/CODH on the PGE electrode in the presence of acetyl-CoA (1.5 mM) under 50% CO and 50% CO_2. The electrocatalytic current for CO oxidation is smaller in the presence of acetyl-CoA. Experimental conditions: 37^{o}C, 0.2 M MES (pH=7.0), rotation rate 1000 rpm and scan rate 1 mV sec^{-1}.

5.4.5 Inhibition by cyanide, cyanate and azide

Several small molecules, CN^-, NCO^- and N_3^- were added to CODH/ACS from *M. thermoacetica* respectively under 100% CO as shown in Figure 5.8. The full inhibition of CO oxidation by CN^- in ACS/CODH is similar to results from monofunctional CODH I_{Ch} and CODH II_{Ch} (Figure 5.8a) The inhibition rate is slower than CODH I_{Ch} in the same experimental condition (in comparison with Figure 4.4). The partial inhibition of CO oxidation by NCO^- in ACS/CODH was observed in all ranges of potential scans under 100% CO oxidation in comparison with the shorter potential range of inhibition (between –0.5 V and –0.6 V) in CODH I_{Ch} and CODH II_{Ch}. The results are consistent with previous EPR studies and solution activity assay in which partial CO inhibition by NCO^- was observed in ACS/CODH.[55]

No inhibition of CODH I_{Ch} and CODH II_{Ch} by N_3^- is observed. In contrast, the current drop was observed from ACS/CODH samples as shown in Figure 5.8c when 10 mM NaN_3 (giving final concentration in solution) was injected. The same amount of buffer solution in the absence of sodium azide was injected in the 4th scan and it reveals almost the same current value as the 3rd scan in the presence of sodium azide. (The slightly smaller current in the 4th scan should be attributed to the film loss). It indicates that the current drop in the 3rd scan should be due to azide inhibition, not dilution effect from injecting solution. This result correlates with the EPR study in which a new EPR signal is formed upon adding N_3^- into the C_{red1} state and the partial inhibition of ACS/CODH by azide was also observed in the solution activity assay.[55,76] However, no change of the EPR signal of the C_{red1} state from CODH I_{Ch} was observed in the presence of NaN_3. (results from collaborators) The consistent results

between electrochemistry and EPR spectroscopy indicate that ACS influences CODH activity.

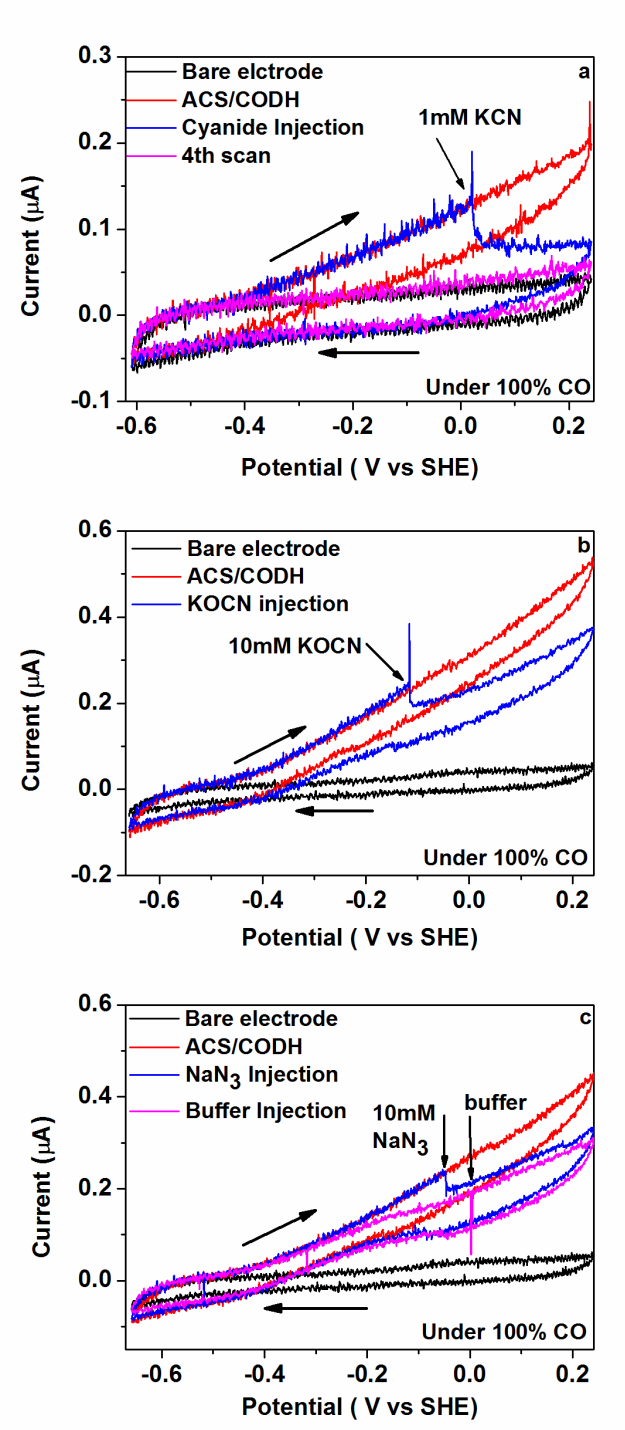

Figure 5.8 The voltammograms of ACS/CODH in the presence of (a) 1mM KCN (b) 10 mM KOCN and (c) 10 mM NaN_3 under 100% CO. Experimental conditions: 25^{o}C, 0.2 M MES (pH=7.0), rotation rate 3500 rpm and scan rate 1 mV sec^{-1}.

5.5 Discussion

The sequence alignments between the CODH subunit from ACS/CODH from *M. thermoacetica* and monofunctional CODH I_{Ch} and CODH II_{Ch} from *C. hydrogenoformans* are similar.[12] Therefore, it is reasonable to expect that the activity and function of CODH should be quite similar. For example, the similar features of cyclic voltammograms and intensity of the electrocatalytic current between CODH I_{Ch} and CODH II_{Ch} are observed. The selective inhibition of different catalytic states by small inhibitors is the same although there are slight differences in inhibition constants and potentials in which inhibition occurs (Chapter 4). However, the activity of CO oxidation from ACS/CODH in our electrochemical study and the conventional solution enzyme activity assay[69 83] both show much smaller activity than monofunctional CODH I_{Ch} and CODH II_{Ch}.[5] The high overpotential for CO oxidation by ACS/CODH is observed in our electrochemical results. Compared to monofunctional CODH, the lower activity of CO oxidation from ACS/CODH might relate to the fact that the function of ACS/CODH is to synthesize acetyl-CoA. Acetyl-CoA synthase might need to regulate CODH activity to obtain the maximum efficiency for acetyl-CoA synthesis in ACS/CODH.

Interestingly, only electrocatalytic CO oxidation is observed with ACS/CODH adsorbed on the PGE electrode in comparison with the reversible electrocatalysis for CO oxidation and CO_2 reduction by monofunctional CODH. Several possible aspects can be discussed. In terms of the interaction between ACS/CODH and PGE surface, the scan potential is proportional to the electrocatalytic current for CO oxidation. This indicates that the C-cluster buried inside the bigger ACS/CODH enzyme complex can convey electrons toward the PGE electrode

through iron-sulfur clusters, such as the B-cluster and D-cluster. In addition, the current is still observed after several scans, which suggests enzyme films is stable on the electrode surface for certain periods and the wide range of potential scans do not damage enzyme. These results show ACS/CODH is able to conduct electrocatalysis on the PGE electrode.

The association of the gas channel between ACS and COSH might involve this phenomenon of the unidirectional electrocatalysis reaction on the electrode. It is well-known that there is a 70Å gas channel between ACS and CODH. It has been suggested that when CO from CO_2 reduction catalyzed by the C-cluster is formed, it drifts into the A-cluster without escaping from the interior enzyme in which the gas channel between the C-cluster and A-cluster is open and then the CO-bound A-cluster reacts with a methyl group and CoA to form acetyl-CoA. No electrocatalytic current for CO_2 reduction was observed maybe due to the fact that the lack of a methyl group and CoA is unable to connect the gas channel between the C-cluster and A-cluster for completing a turnover for acetyl-CoA synthesis in ACS/CODH. However, the CO product from CO_2 reduction by ACS/CODH is observed by the CO product binding to hemoglobin in the absence of co-substrates (a methyl group and CoA).[77,78] Moreover, it is still impractical to observe any electrocatalytic current from CO_2 reduction on the PGE electrode in presence of acetyl-CoA. These findings indicate that co-substrates are not required for CO_2 reduction by ACS/CODH. In the solution activity assay, we notice that CO_2 reduction by CODH[77,78] and the acetyl-CoA synthesis by ACS[84] are both required to be in the reducing condition (by a strong reducing agent, such as sodium dithionite) and this suggests the reduced state of the A-cluster in ACS/CODH might be required for CO_2 reduction. The ACS/CODH crystal structure from *M. thermoacetica* reveals the D-cluster is exposed to the protein surface and the A-cluster is far from any electron-relay

iron-sulfur clusters (> 50Å). Since the reversible CO/CO_2 conversion by CODH I_{Ch} and CODH II_{Ch} on the PGE electrode with the high electrocatalytic current is observed, it is reasonable to expect that the enzyme surface of CODH near the D-cluster should contact the graphite surface, which facilitates electron transfer between the C-cluster and electrode. Under the same orientation of ACS/CODH on the PGE surface, the A-cluster in ACS/CODH is ~ 20 Å away from the electrode surface. Therefore, it is difficult to conduct electron transfer between the A-cluster and the electrode surface or electron relay centers in enzymes in comparison with the solution assay which contains free-diffusion mediators or reductants. The higher overpotential for CO oxidation from ACS/CODH on the PGE electrode also suggests a higher energy barrier for electron transfer between the PGE electrode and ACS/CODH since EPR-titration show two-electron interconversion between C_{red1} and C_{red2} in ACS/CODH is approximately –520 mV.[7]

Another reason for no observation of electrocatalytic currents from CO_2 reduction in PFE is the inherent low turnover rate of CO_2 reduction by ACS/CODH (1.3 s^{-1}).[52] In our electrochemical results of CODH from *C. hydrogenoformans*, the electrocatalytic current for CO_2 reduction is usually more than 10 times smaller than CO oxidation. If monofunctional CODH represents an innate property of this enzyme, it is reasonable to expect that the electrocatalytic current for CO_2 reduction from ACS/CODH should be around 10^{-8} Amps since the observed electrocatalytic current for CO oxidation from ACS/CODH is in the range of 10^{-7} Amps. The measurement of CO oxidation by solution activity assay shows the rate of monofunctional CODH from *C. hydrogenoformans* is about 30 times faster than ACS/CODH from *M. thermoacetica*.[5,69] In addition, it is reported that the rate of CO oxidation from

ACS/CODH is at least 100 times faster than CO_2 reduction by ACS/CODH.[55,77] Therefore, it is reasonable to expect the range of electrocatalytic current for CO_2 reduction by ACS/CODH should be about 10^{-8} Amps, which is equal to or smaller than the background current (capacitance current). This small current is difficult to be observed in our electrochemical system. The slow turnover rate (electrocatalytic current) also implies that ACS plays a role in modulating CODH activity.

Several inhibitors, such as cyanate, cyanide and azide were added to investigate the catalytic states in CODH. The inhibition of CODH by these inhibitors in ACS/CODH has been studied thoroughly. A new EPR signal is formed g_{av}~1.72 (g= 1.87, 1.78, and 1.55) in the presence of cyanide from the signal of the C_{red1} state, g_{av} ~1.82 (g = 2.01, 1.81 and 1.65).[60] A new EPR signal is also formed when anionic inhibitors, cyanate, azide and thiocyanate are injected into the C_{red1} state rather than C_{red2} in ACS/CODH.[55] The EPR spectrum of the C_{red1} state from the C-cluster in the presence of theses anionic inhibitors are converted to a two-component spectrum with g_{av} = 2.15 (g = 2.34, 2.067, 2.03) and g_{av} = 2.17 (g = 2.34, 2.115, 2.047).[55]

In the electrochemical experiments for monofunctional CODH inhibition by these inhibitors (Chapter 4), cyanide, thiocyanate and cyanate inhibit CODH but azide inhibition is not observed in CODH. In addition, no EPR signal change is observed in CODH I_{Ch} in the presence of 20 mM NaN_3 (results from collaborators).

Here, the same electrochemical condition was also used in ACS/CODH. As with previous EPR studies and solution activity assay, all these anions, including azide, inhibit CO oxidation by ACS/CODH. No changes in the electrochemical signals and EPR signals of CODH I_{Ch} and CODH II_{Ch} in the presence of azide indicate azide does not react with

monofunctional CODH. The different inhibition by azide between ACS/CODH and CODH suggests ACS plays an important role in modulating CODH performance.

Lindahl and his co-worker have shown the activity of ACS synthase in ACS/CODH decreases when CO concentration is over 100 μM and CO becomes an inhibitor in the high concentration of CO. They suggest the channel crowding of the high concentration of CO in ACS/CODH leads to have a slow residual activity.[85,86] CO as a product inhibitor in CODH in the low driving force of CO_2 reduction has been described in Chapter 3 and 4. The low activity of ACS in the presence of high concentration of CO might also relate to the observation of CO product inhibition of CODH since the K_I value (inhibition of ACS activity by CO) for ACS/CODH is the same scale range we obtained for CO product inhibition of CODH ($K_I \sim$ μM). It seems likely that CO product inhibition of CODH is also a part of the inhibition process of acetyl-CoA synthesis in ACS/CODH.

Here, some different features of electrocatalysis and inhibition in ACS/CODH, in comparison with CODH I_{Ch} and CODH II_{Ch}, suggest that ACS has a unique role in controlling CODH activity.

Chapter 6 *Investigating the reaction of oxygen and nitrous oxide with carbon monoxide dehydrogenase from Carboxydothermus hydrogenoformans by protein film electrochemistry*

6.1 Abstract

Anaerobic Ni-Fe containing carbon monoxide dehydrogenase (CODH) catalyzes the reversible conversion between carbon monoxide (CO) and carbon dioxide (CO_2). Dioxygen (O_2) is known to damage the enzyme irreversibly but the mechanism is still unclear. Here, evidence from protein film electrochemistry clearly shows O_2 attacks the active site, possibly at the Ni atom. Further experiments show O_2 damages enzymes irreversibly when oxygen is added in the potential region of the C_{red1} state (for CO oxidation). In contrast, the inactive state, C_{ox} in CODH prevents oxygen attack and is reactivated by low-potential reduction.

Nitrous oxide (N_2O), isoelectronic with CO_2, is a sluggish gas due to its poor properties of σ-donor and π-acceptor as CO_2. Here, it is shown that N_2O is reduced by CODH and acts as the suicide substrate toward CODH by protein film electrochemistry. The electrocatalytic current for N_2O reduction is observed below –0.55 V but the catalysis of N_2O reduction also damages on CODH irreversibly.

6.2 Introduction

Carbon monoxide dehydrogenase (CODH) is known to catalyze CO/CO_2 reaction reversibly as shown in eq 6.1 with the minimal overpotential (E = –520 mV at pH = 7.0).[9] The X-ray crystal structures of CODH II[6,17] from *Carboxydothermus hydrogenoformans* reveal a unique metal cluster [$NiFe_4S_4$], also known as the C-cluster, involving the catalytic reaction, and two extra [Fe_4S_4] clusters (the B-cluster and D-cluster) conducting electron transfers between the C-cluster and the external redox partner in the dimer structure as shown in Figure 6.1. Chapter 3 and Chapter 4 have shown the electrocatalytic oxidation of CO and reduction of CO_2 by CODH I and CODH II from *Carboxydothermus hydrogenoformans,* adsorbed on the pyrolytic graphite edge (PGE) electrode.

$$CO_2 + 2H^+ + 2e^- \leftrightarrow CO + H_2O \qquad E = -0.52\ V \qquad (6.1)$$

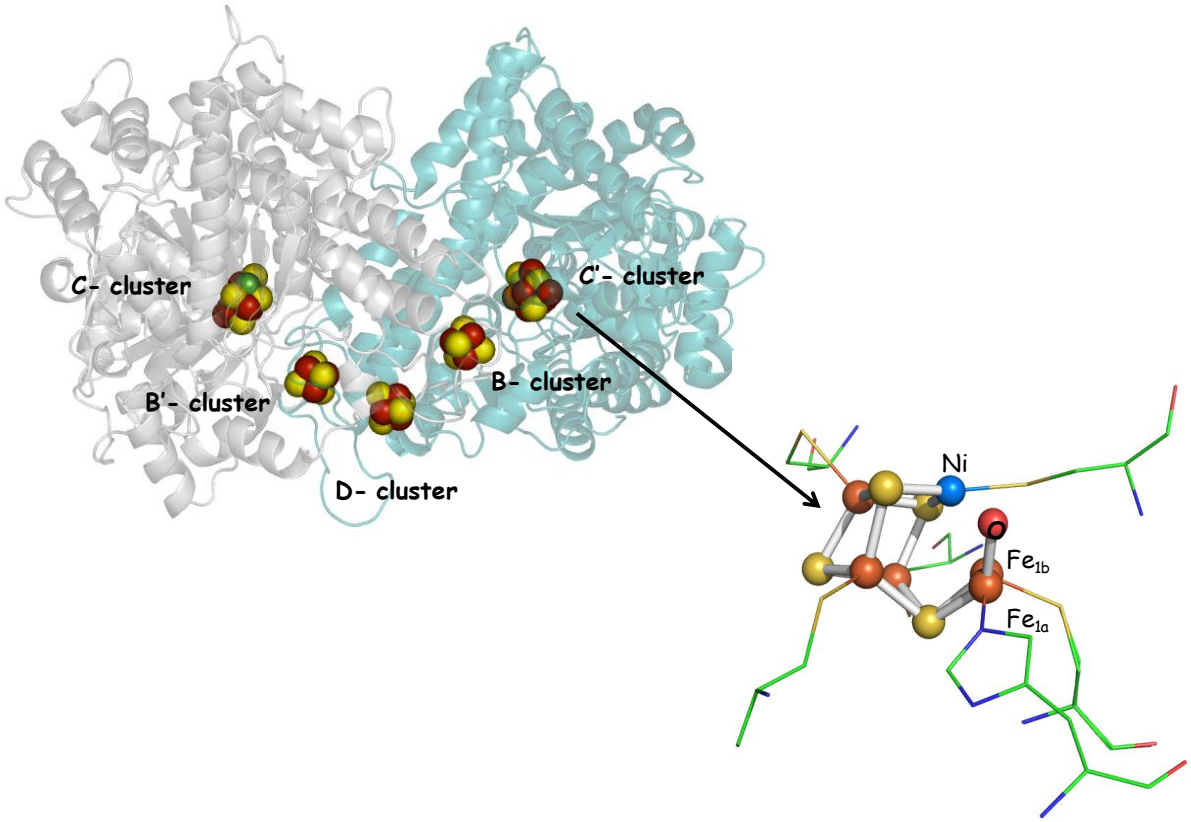

Figure 6.1 The structure of CODH II_{Ch} (PDB: 3B53) from *Carboxydothermus hydrogenoformans*. Two positions are found for the dangling Fe-atom in the crystal structure, labelled Fe_{1a} and Fe_{1b}, respectively.

The electrocatalytic reduction of CO_2 by anaerobic Ni-Fe containing CODH with minimal overpotential, the highest turnover rate and the tiny side-reaction product in aqueous solution (Chapter 7) has so far been the best catalyst in comparison with artificial molecular catalysts.[34,87] The superior performances show the great potential for developing bio-mimic catalysts based on the structural environment near the active site in CODH. However, several studies have shown anaerobic CODH is inactivated in the presence of air and that oxygen

causes irreversible damages.[5,61,88-90] However, it is still unclear where and how oxygen damages CODH.

If oxygen, known as an oxidant, reacts with the active site in CODH, it could be expected that the inactive C_{ox} state forms. However, the inactive C_{ox} state is an EPR-silent state and the complicated metal cluster of the C-cluster is not easily analyzed by bioinorganic spectroscopy, such as X-ray absorption spectroscopy. Therefore, it is difficult to realize whether O_2 inactivates (or destroys) the active site or other iron-sulfur clusters in CODH. In Chapter 3 and 4, we have shown it is possible to control inhibitors s*electively* to target different active states by potential control. Cyanide, isoelectronic with CO, is known to inhibit CO oxidation by CODH. Several X-ray crystal structures and spectroscopic evidence clearly shows cyanide binds to the C-cluster.[16, 28] Protein film electrochemistry further indicates full inhibition by cyanide occurs above ~ – 0.65 V and CN-inhibited CODH is reactivated rapidly at low potentials (such as −760mV). Therefore, the cyanide-bound C-cluster might prevent oxygen attack if oxygen attacks the active site. Here, protection of CODH II_{Ch} by cyanide in the presence of oxygen is studied since the dissociation rate of cyanide from CODH II_{Ch} is much faster than CODH I_{Ch} at low potentials, such as −760mV. (Chapter 4)

Nitrous oxide (N_2O), also known as laughing gas, is widely used for anaesthesia in operation. The greenhouse effect by N_2O is 300 times stronger than CO_2.[91] In terms of electronic structure, N_2O is isoelectronic with CO_2. Nitrous oxide, like CO_2, is a poor ligand for transition metals due to the weak σ-donating and π-accepting property. Although thermodynamically nitrous oxide is favoured by splitting to N_2 and H_2O (eq 6.2), the high

kinetic energy barrier hinders the reduction reaction to N_2. In biological systems, nitrous oxide reductase reduces N_2O to N_2 and H_2O by the unusual active site of the μ-4-sulfide bridged four copper ions in the final step of the denitrification cycle.[92] Only a few examples of transition metal complexes have been shown to have activity toward N_2O, such as oxo transfer, insertion of the oxygen atom into alkyl-metal or metal-hydride, and N-N bond breaking.[91]

$$N_2O + 2H^+ + 2e^- \leftrightarrow N_2 + H_2O \qquad E = 1.77\ V \qquad (6.2)$$

It was reported that ACS/CODH (acetyl-CoA synthase/carbon monoxide dehydrogenase) from *Moorella thermoacetica* is capable of catalyzing N_2O to N_2.[93] However, no clear conclusion indicates the reaction occurs in the C-cluster or the A-cluster which involves the synthesis of acetyl-CoA in ACS/CODH and no clear mechanisms were described for how this reaction may happen. Here, we demonstrate CODH on PGE has the ability to react with N_2O under precise potential control. CODH I_{Ch} and CODH II_{Ch} show similar properties for N_2O reaction and CODH I_{Ch} is represented in this study since CODH I_{Ch} has the higher activity in our samples.

Protein film electrochemistry reveals CODH reacts with N_2O slowly and causes irreversible damage. This implies that the C-cluster in CODH is capable of catalyzing N_2O to N_2 but also forms unstable intermediates during the catalytic process of N_2O, which damage CODH.

6.3 Material and Methods

Cylinders of CO, CO_2 (CP grade), N_2O (99.99%) and O_2 (research grade) were all purchased from BOC. The oxygen-saturated buffer (1.3 mM) for oxygen injection experiment was prepared by bubbling O_2 through the well-sealed vial for 20 minutes.

The setup and procedures of electrochemical experiments are as described in Chapter 3.

6.4 Results

6.4.1 The effect of oxygen on CODH

Chronoamperometry was used to determine how oxygen attacks CODH II_{Ch} under 100% CO as shown in Figure 6.2. An aliquot of 0.5 mL oxygen-saturated buffer (1.3 mM) was injected into 3 mL solution at two different potentials. Injection at +140 mV corresponds to the potential region in which the C_{ox} state starts form slowly, whereas injection at −260 mV corresponds to the potential region where the C_{red1} state is dominate.

First, the oxygen-saturated buffer was injected at +140 mV as shown in Figure 6.2a. The electrocatalytic current for CO oxidation was observed at +140 mV under 100% CO and the electrocatalytic current declines with time mainly due to the formation of the inactive state, C_{ox}. The inactive state was reactivated by reductive reactivation after poising at −760 mV for 120 seconds. When 0.5 mL oxygen-saturated buffer (1.3 mM) was injected into 3 mL solution in the electrochemical cell at +140 mV, the electrocatalytic current dropped to zero rapidly. This result shows oxygen inactivates CODH II_{Ch}, which could form the inactive C_{ox} state or damaged CODH II_{Ch}. After injecting oxygen into solution, the potential was maintained at +140 mV for more than 1000 seconds in order to flush out all oxygen from the stock solution before switching to the low potential, −760 mV for reductive reactivation.

More than 50 % of the electrocatalytic current for CO oxidation was restored following the reactivation potential at −760 mV for 120 seconds. In contrast, less than 1% of electrocatalytic current was restored after performing a similar sequence step but O_2 was injected at −260 mV, the potential region of C_{red1}. (Figure 6.2b) This difference clearly

suggests oxygen damages CODH II_{Ch} in the C_{red1} state but does not damage CODH II_{Ch} in the C_{ox} state. These results suggest CODH II_{Ch} forms the inactive C_{ox} state after reacting oxygen at +140 mV and the inactive state is reactivated by reductive reactivation. When the oxygen-saturated solution was injected at –260 mV, the negative current was observed in Figure 6.2b due to oxygen reduction starting to occur below –0.05 V on the PGE electrode. It also suggests a lower concentration of O_2 reacts with CODH II_{Ch} at – 260 mV.

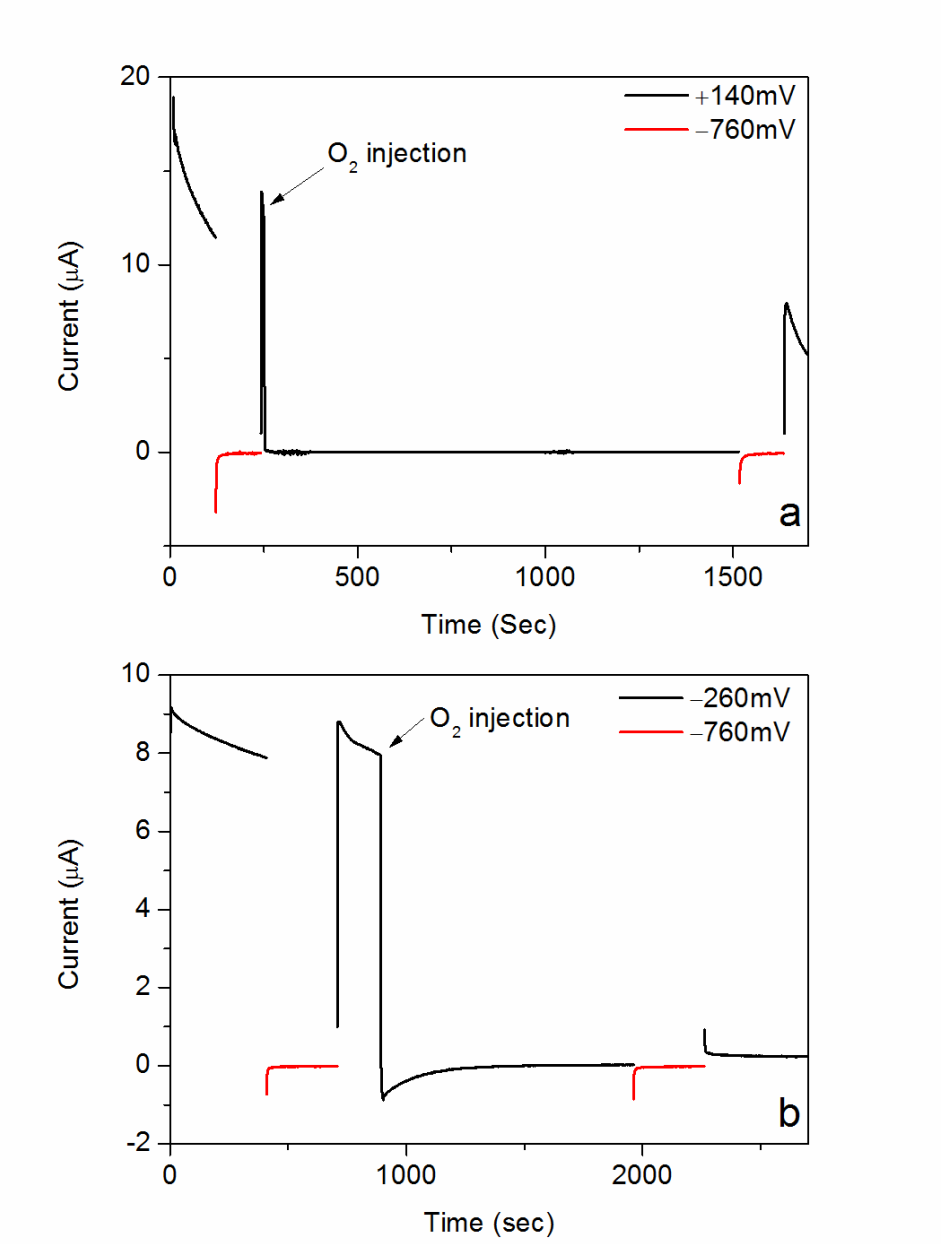

Figure 6.2 Injection of the oxygen-saturated buffer (0.5 mL) into the electrochemical cell (3.0 mL). The black line indicates the potential was poised at (a) +140mV or (b) –260 mV and the red line indicates the potential was poised at –760 mV. Experimental conditions: 25 ℃, 0.2 M MES buffer (pH = 7.0), rotation rate 2500 rpm and 100% CO.

These results clearly indicate that oxygen inactivates CODH II_{Ch} at any potential. Roughly 50% electrocatalytic current for CO_2 reduction still remained after oxygen-saturated buffer was injected at −760mV, the potential region of the C_{red2} state, in the same chronoamperometry experiment. However, oxygen reduction also occurs aggressively on the PGE electrode at such a low potential, making it difficult to analyze how much oxygen directly reacts with CODH II_{Ch}. However, the inactive state (C_{ox}) can protect oxygen attack, which has not been observed before. The partial damages of CODH II_{Ch} by oxygen observed at +140mV can be attributed to the reaction between the active C_{red1} state (indicated by the observable electrocatalytic current before injecting O_2-saturated buffer) and oxygen.

6.4.2 Cyanide protection

In Figure 6.3, the final concentration of 10mM potassium cyanide was injected to inhibit CODH II_{Ch} at −260 mV under 100% CO. When the electrocatalytic current reached ~ 0 μA by cyanide inhibition, 0.5 mL oxygen-saturated buffer was injected and the potential was maintained for more than 1000 seconds in order to flush out all oxygen from the solution. The high concentration of cyanide was removed by fresh buffer and then the potential was switched to −760 mV to remove cyanide from the active site. Replacement of buffer without a potential poise step at −760 mV is not capable of removing cyanide from CODH II_{Ch} rapidly (Figure 6.4). After poising at −760 mV for 60 seconds, replacement of the cell contents with fresh buffer was employed again to remove any cyanide released from the active site into the buffer solution. Finally, a potential poised at −260 mV in the fresh buffer shows approximately 50% activity of CODH II_{Ch} still remains. This is in comparison with

less than 1% activity remaining in the absence of cyanide protection in Figure 6.2b. These results suggest oxygen should attack the C-cluster in CODH.

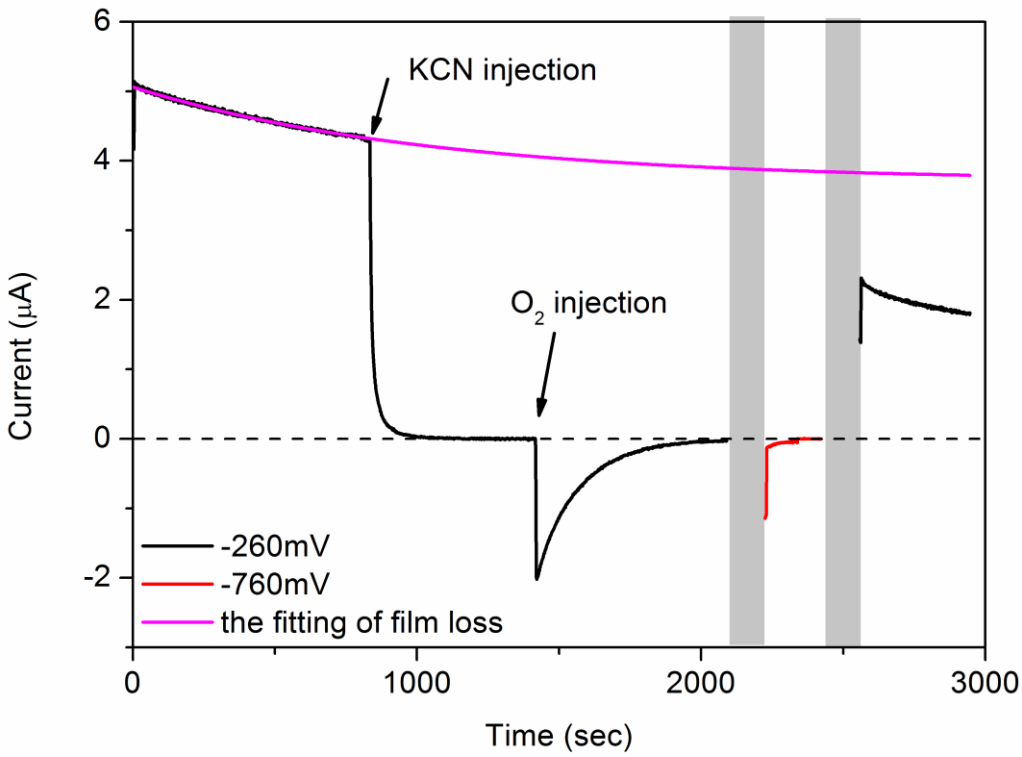

Figure 6.3 Inhibition of CODH II_{Ch} by cyanide protects from oxygen attack. The black line indicates the potential was poised at – 260mV and the red line was at – 760mV. The grey windows refer to the buffer exchange. The pink line is extrapolated for the film loss. Experimental conditions: 25℃, 0.2 M MES buffer (pH=7.0), rotation rate 2500 rpm and 100% CO.

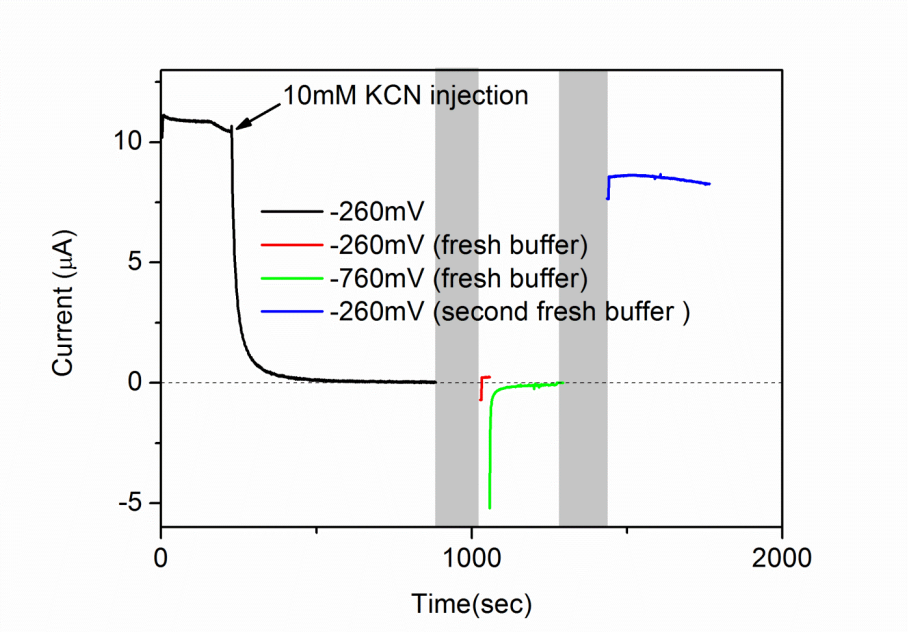

Figure 6.4 CODH inhibition by potassium cyanide is reactivated by the low potential and buffer exchange. 10 mM KCN (final concentration in the solution) was injected and the grey area indicates buffer exchange. The low potential with buffer exchange is required for restoring CODH activity from cyanide inhibition. Experimental conditions: 25℃, 0.2 M MES (pH=7.0), rotation rate 2500 rpm and 100% CO.

Only about 50% current is restored after O_2 injection into cyanide-protected samples over several experiments. There are several reasons for this. First, twice buffer exchange causes some film loss. Secondly, a small amount of cyanide still binds to (inhibits) CODH II_{Ch} even at the low potential −760mV. (Roughly 20% current loss after injecting cyanide into the solution, comparing before injection at −760 mV. For example, Figure 4.7 in Chapter 4) Finally, O_2 is likely to attack the surface-exposed D-cluster as well since only about 50% of the electrocatalytic current remains after O_2 injection into cyanide-protected samples in comparison with ~75% current restored in the absence of O_2 (Figure 6.3 vs. Figure 6.4) .

6.4.3 Prediction of gas channel by Hollow

In order to rule out the oxygen damage on the B-cluster [Fe_4S_4] in CODH, the gas channel between protein surface and metal clusters was simulated by the software, Hollow[94] based on the crystal structure of CN-CODH II_{Ch}.[16] The only channel is found between the C-cluster and protein surface as shown in Figure 6.5. No channel between the B-cluster and protein surface found by Hollow suggests it is highly unlikely that oxygen reacts with the B-cluster.

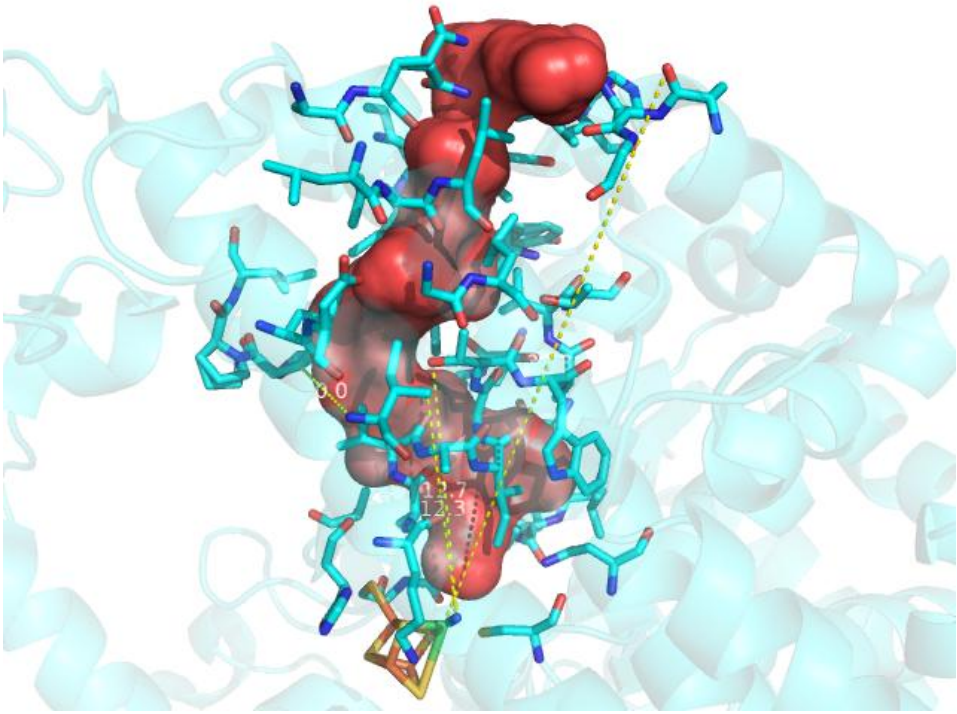

Figure 6.5 The gas channel toward the C-cluster is predicted by Hollow based on the crystal structure of cyanide-CODH II_{Ch} (PDB 3I39).

6.4.4 Suicide substrate, nitrous oxide

Cyclic voltammetry was sweeping the potential from –0.74 V to 0.24 V in the presence of 100% Ar, N_2O and CO_2 respectively in Figure 6.6a and revealed the negative electrocatalytic current for N_2O reduction started to occur when the potential was below –0.55 V. In order to eliminate the possibility of the small reduction current being due to the residual CO_2 in the solution, cyclic voltammetry was performed with a stationary electrode in Figure 6.6b for distinguishing whether the cathodic current comes from CO_2 or N_2O reduction. If the electrocatalytic current is due to CO_2 reduction, it should be possible to observe the positive (oxidation) current from CO-product oxidation near the stationary electrode when the scan potential is above –0.5 V as shown in the blue line of Figure 6.6b. However, only a negative current was observed in the presence of N_2O without any apparent oxidation current in the complete potential sweep. The evidence indicates that the observation of the electrocatalytic current in the presence of N_2O should be ascribed to N_2O reduction.

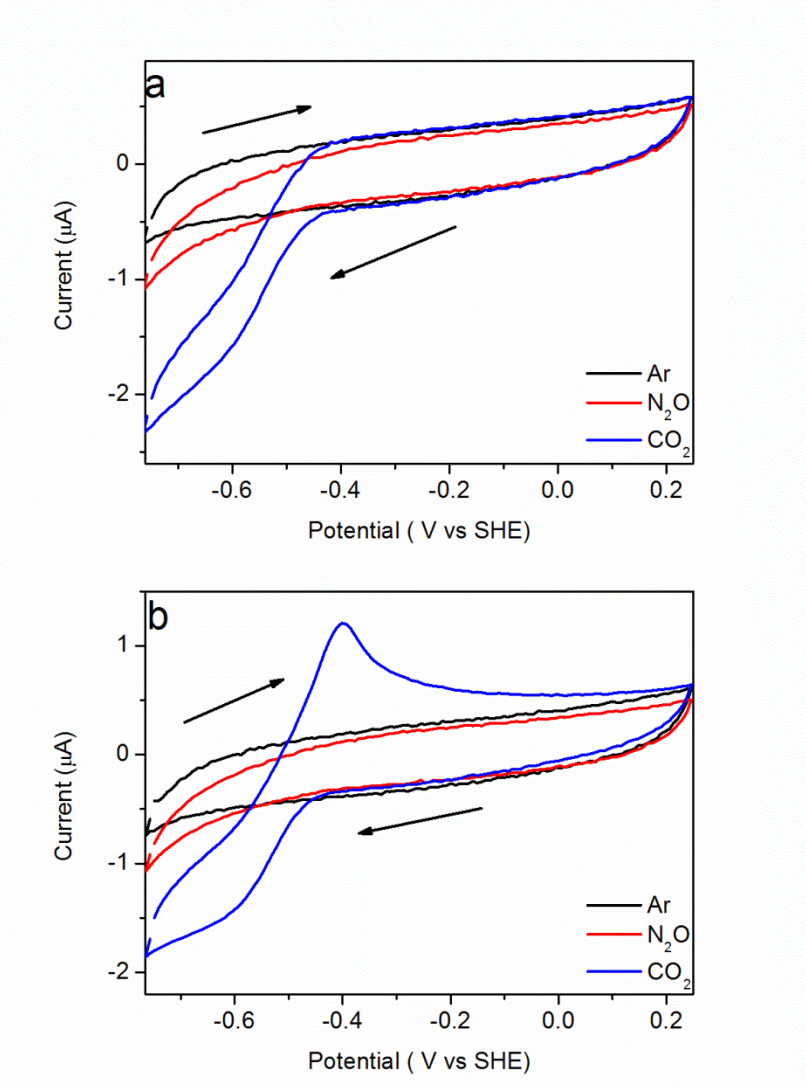

Figure 6.6 Voltammograms of CODH I_{Ch} in the presence of different gas. (a) The black line was performed under 100% Ar, the red line was under 100% N_2O and the blue line was under 100% CO_2. (b) Cyclic voltammetry was performed in the stationary electrode. Experimental conditions: 25 ℃, 0.2 M MES buffer (pH=7.0), Rotation rate 1000 rpm for the upper figure, and scan rate, 20 mVs^{-1}.

Chronoamperometry was employed to investigate the possible reaction between N_2O and CODH further. First, chronoamperometry from CODH I was poised at −209 mV (the potential for CO oxidation) as shown in Figure 6.7 to investigate whether CODH reacts with N_2O. Initially, 100% CO was used to flow through the headspace of the electrochemical cell and the electrocatalytic current, ~7.5 μA, was observed. The electrocatalytic current dropped to zero when CO was replaced by Ar. Following the replacement by 100% CO again, the current rose back to ~7 μA. The slight decrease in the current should be attributed to the protein film loss on the electrode. It shows no reaction occurs between Ar and CODH. When 100% N_2O was introduced into the headspace at 3010 seconds, no electrocatalytic current for N_2O reduction at −209 mV was observed. As the voltammograms shown in Figure 6.6, it is difficult to observe any electrocatalytic current in the high potential region. However, the electrocatalytic current for CO oxidation only reveals ~3.8 μA after flushing out N_2O with Ar and returning to 100% CO, after which shows only about 50% of CODH activity remains. This indicates N_2O could react with CODH slowly and cause damage onto CODH although no apparent reduction current was observed. It is difficult to ascribe the 50 % of current loss to film loss because the rate of film loss is much slower (The half-life time for film loss is about 5000 seconds in the absence of polymyxin. In the presence of polymyxin, the film becomes much more stable though slow film loss still occurs with time). No electrocatalytic current observed in the presence of N_2O could be due to the very slow turnover rate at −209 mV.

The current dropped to ~0 μA again as CO was flushed out by N_2O at 5900 seconds. The decrease in the electrocatalytic current by ~ 40% (relative to the current at 5850 seconds) was

observed after CO was introduced again at 6212 seconds. It was found that N_2O causes more irreversible damages on CODH with the small amount of CO over several experiments.

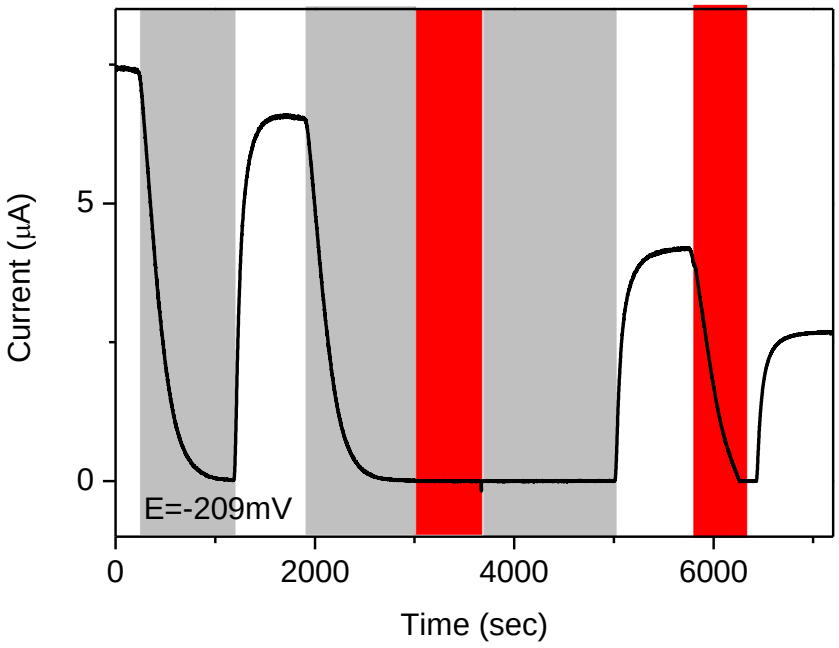

Figure 6.7 Chronoamperometry of CODH I_{Ch} at −209 mV. The white region indicates the presence of 100% CO; the red and grey region indicates 100% N_2O and 100% Ar respectively; Experimental conditions: 25℃, 0.2 M MES buffer (pH=7.0), and rotation rate 1500 rpm.

The same experiment was performed at a lower potential, −439 mV (the potential for CO oxidation) in Figure 6.8. The negative current was observed when N_2O was introduced into the headspace at 3200 seconds. The small negative current clearly indicates that N_2O is reduced by CODH at this lower potential compared to −209 mV (Figure 6.7). After flushing

out N_2O by Ar, CO was reintroduced for measuring the remains of CODH activity. The current loss is more than 50%, which is larger than at –209 mV (Figure 6.7).

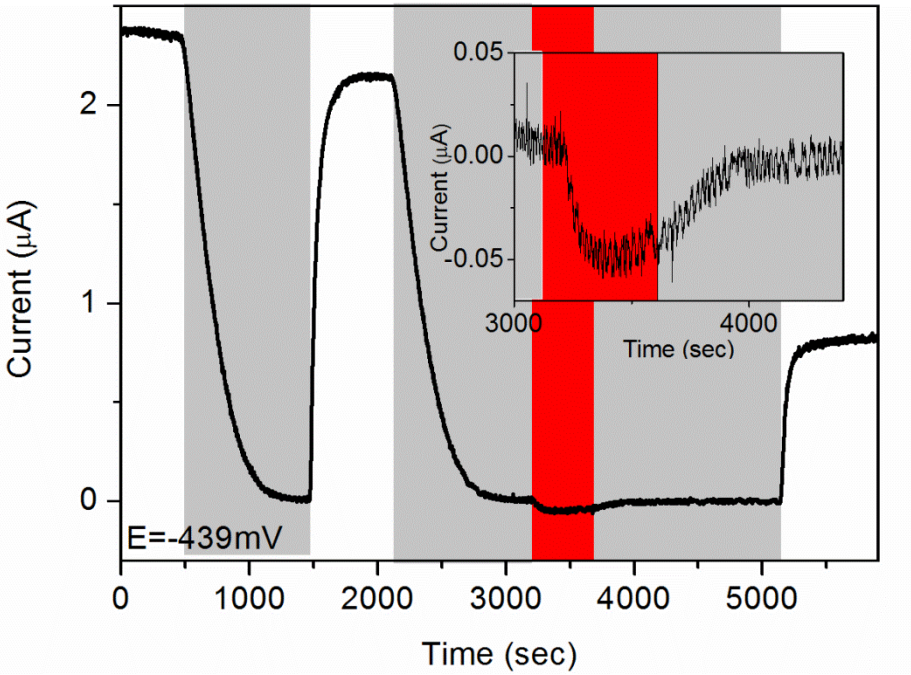

Figure 6.8 Chronoamperometry of CODH I_{Ch} at –439 mV. The white region indicates the presence of CO; the red and grey region indicates N_2O and Ar respectively. The inset figure enlarges the region of N_2O reduction. Experimental condition: 25℃, 0.2 M MES buffer (pH=7.0), and rotation rate 1500 rpm.

When the potential was poised at an even more negative potential, –760 mV (the potential for CO_2 reduction) in Figure 6.9, the even higher negative current for N_2O reduction was observed. When N_2O was introduced at 5720 seconds as shown in Figure 6.9, the electrocatalytic current for N_2O reduction sharply increased and then started to decay after about 400 seconds in the presence of N_2O. These results suggest CODH reduces N_2O more

efficiently in the low potential. The scale of N_2O turnover frequency by CODH should be about several hundred per second at −760 mV since the scale of the current for N_2O reduction (μA) is similar to the current for the obligate substrates, CO_2. N_2 was also introduced and no electrocatalytic current for N_2 was observed.

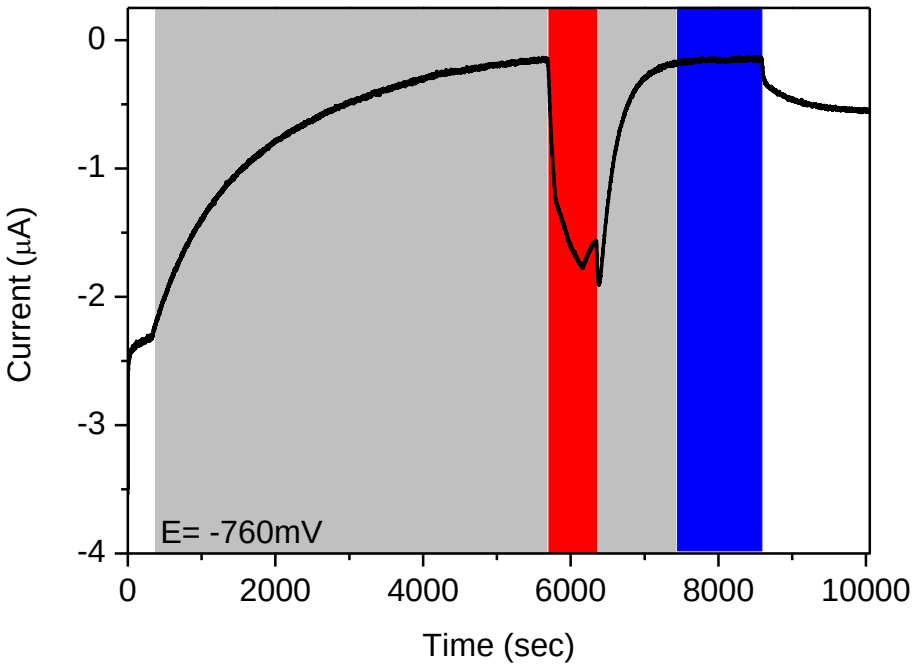

Figure 6.9 The chronoamperometry of CODH I_{Ch} at −760 mV. The white region indicates the presence of 100% CO_2; the blue and grey regions indicate the presence of 100% N_2 and 100% Ar respectively; the red region indicates the presence of 100% N_2O. Experimental conditions: 25 ℃, 0.2 M MES buffer (pH = 7.0) and rotation rate 1500 rpm.

6.5 Discussion

It has been shown CODH activity is inactivated (damaged) irreversibly after exposure to oxygen into CODH from different microorganisms.[5,61,88-90] The EPR signals from both CODH I_{Ch} and CODH II_{Ch} revealed the free iron signal (g~4.3) after 12 hr exposure to air.[5] All experiments in the literature are performed under the potential range of the C_{red1} state. Here, the electrochemical results are consistent with the previous observation. When oxygen is added at −260 mV (the potential in which the C_{red1} state is dominate) and at 140 mV (the potential in which the C_{ox} state is formed), the inactivation of CODH by oxygen rapidly occurs. The more interesting result is that the C_{ox} state is capable of preventing oxygen attack and then is reactivated by low-potential reduction. This indicates that the C-cluster in the C_{ox} state, which might form a peroxo or oxy bridge between the Ni atom and dangling Fe atom, hinders the reaction between the active site and oxygen. A similar mechanism is suggested in the [NiFe] hydrogenase.[95,96]

Another interesting comparison is the sulfide inhibition (as discussed in Chapter 3 and 4), which reveals that sulfide rapidly and fully inhibits CODH at potentials above 0 mV, the potential region of the C_{ox} state which starts to be formed. In contrast, the slow and weak inhibition occurs in the potential region of the C_{red1} state. Partial reactivation from full inhibition of CODH by sulfide occurs in the low potential (–250mV). The possible inactive structure could be a sulfide (or hydrosulfide) bridge between the Ni atom and the dangling Fe atom in the C-cluster since several crystal structures of sulfide bridged between the Ni atom and dangling Fe atom in CODH II_{Ch} have been shown.[17] It is proposed that sulfide inhibits the equivalent state of the C_{ox}. The inactivation mechanism by oxygen in the potential region

of C_{ox} might occur in the similar mechanism. The equivalent state of the C_{ox} state in the high potential is able to rapidly react with oxygen and oxidants probably accelerates the formation of the inactive C_{ox} state when the applied potential is in the potential region of C_{ox} as shown in scheme 6.1.

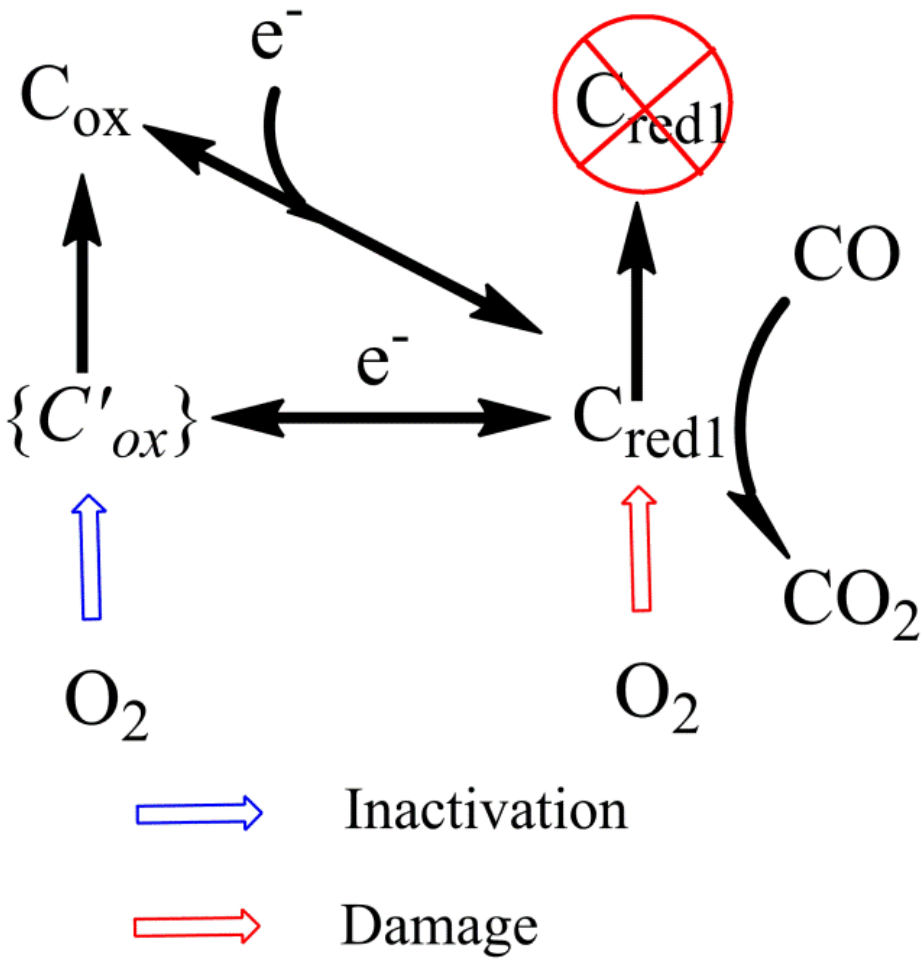

Scheme 6.1 Summary of the effect of oxygen on different catalytic states in CODH

However, CODH is damaged seriously when oxygen is injected at the potential of the C_{red1} state and the low reduction potential is unable to reactivate CODH. This implies that

oxygen might react with the C-cluster and form some reactive oxygen species (ROS) which destroy the C-cluster. A similar mechanism was reported in the [FeFe] hydrogenase in which the distal iron reacts with oxygen and forms ROS which destroy the proximal iron-sulfur cluster.[97]

Further experiments in which the protection of the C-cluster by cyanide-bound CODH were performed in the presence of oxygen suggest that oxygen should react with the Ni atom in the C-cluster because several CODH crystal structures from different species have shown that cyanide binds to the Ni atom.[16, 28] The simulation of gas channel by Hollow also indicates the gas channel toward the C-cluster, not the B-cluster. However, we cannot rule out the possible damage from the surface-exposed D-cluster since it is impractical to fully restore the activity of CODH.

The only *negative* current observed in the presence of N_2O in the low potential suggests CODH is capable of catalyzing N_2O to N_2. Since the monofunctional CODH was used in this study, the reaction center should occur in the unique C-cluster metal clusters. The irreversible decrease in the electrocatalytic current for CO oxidation or CO_2 reduction after N_2O reaction with CODH, suggests the unstable intermediates might form and break down the C-cluster during N_2O reduction. Since CODH in biological systems is involved in the interconversion between CO and CO_2, the structural design for the N_2O reaction in CODH is not elementary. N_2O acts as a suicide substrate, which opens a door to further investigate the reaction mechanism in the active site by spectroscopy such as ENDOR or ESSEM. It also suggests the unique active site, [$NiFe_4S_4$], is a possible model to design new catalysts for the difficult N_2O reduction reaction.

Here, we clearly show how and where O_2 reacts with the C-cluster and N_2O is catalyzed by the C-cluster and acts as a suicide substrate.

Chapter 7 *The evidence for the formation of a Ni-H intermediate state in the catalytic cycle of carbon monoxide dehydrogenase*

7.1 Abstract

Ni-containing carbon monoxide dehydrogenase (CODH) uses a unique cluster [$NiFe_4S_4$] to catalyze CO oxidation and CO_2 reduction rapidly and reversibly. The detection of hydrogen formation by CODH in the direction of CO oxidation in the presence of CO and formate formation by CODH in the direction of CO_2 reduction in the presence of CO_2 suggests that Ni-hydride is an intermediate state during the catalytic cycle. The small solvent kinetic isotope value from CO oxidation further suggests the hydride transfer between the Ni atom and the possible intermediate, a Ni-bound carboxylate occurs by the β-hydride elimination/migration process. This discovery may correlate with the rapid turnover rate of CODH in either direction with minimal overpotential requirement and aid in the design of better catalysts for CO_2 reduction.

7.2 Introduction

As described in the chapter 1, the key chemistry for CO_2 reduction lies in the multiple proton-coupled electron transfer. The important aspect of catalyst design for CO_2 reduction would be taken measures to orchestrate multiple proton-coupled electron transfer. Transition metals with the aid of the proton relay center in the second coordination sphere appear to be a rational design for the catalyst. It is expected that the electrophilic carbon in CO_2 binds to a transition metal, which leads to the geometrical change from a linear molecule to a bent molecule upon electron reduction. However, this process requires the huge amount of reorganization energy.[98] The proton transfer or hydrogen-bond from the second coordination sphere is expected to stabilize an electron-reduced CO_2 intermediate and lower an energy barrier. In biological systems, several enzymes reveal this important feature such as CO_2 reduction into CO by Ni-containing carbon monoxide dehydrogenase (CODH)[73] and formate by formate dehydrogenase (FDH)[99] with the low overpotential requirement and the rapid turnover rate in electrocatalysis. The Dubois group uses this concept to design a molecular catalyst, a Ni-atom catalyst with the pendant amine(s) as the proton relay, which has been shown to catalyze formate oxidation[100], hydrogen production/oxidation and oxygen reduction with the high turnover rate.[101]

Ni-containing CODH has been shown to catalyze reversible and rapid interconversion between CO and CO_2 on the PGE electrode in previous chapters. It has a unique metal [$NiFe_4S_4$] cluster (called the C-cluster) carrying out the reaction and two extra [Fe_4S_4] clusters as electron relay centers (called the B-cluster and D-cluster). EPR and Mössbauer spectroscopy have shown that several redox states of the C-cluster are involved in the

mechanism of CO/CO_2 interconversion by CODH, C_{ox}, C_{red1} and $C_{red2,}$ as shown in Figure 7.1.[20] The inactive state, C_{ox}, which is EPR-silent, is reduced by one electron to C_{red1}, which exhibits a characteristic EPR signal, g_{av}~1.82 (g=2.01, 1.81, 1.65). It is proposed that C_{red1} has the hydroxide bridged between the Ni atom and the dangling Fe atom. As CO enters and binds to the Ni atom in the C_{red1} state, the nucleophilic attack of hydroxide on CO occurs and it forms the Ni-bound carboxylate intermediate. Following deprotonation from the Ni-bound carboxylate, CO_2 is released and the C-cluster forms another state, C_{red2} with a new EPR signal, g_{av}~1.86 (g=1.97, 1.87, 1.75). The catalytic cycle is shown in Figure 7.1. The reduction potential for the two-electron interconversion between C_{red1} and C_{red2} is ~ –520mV according to EPR potentiometric titrations.[7]

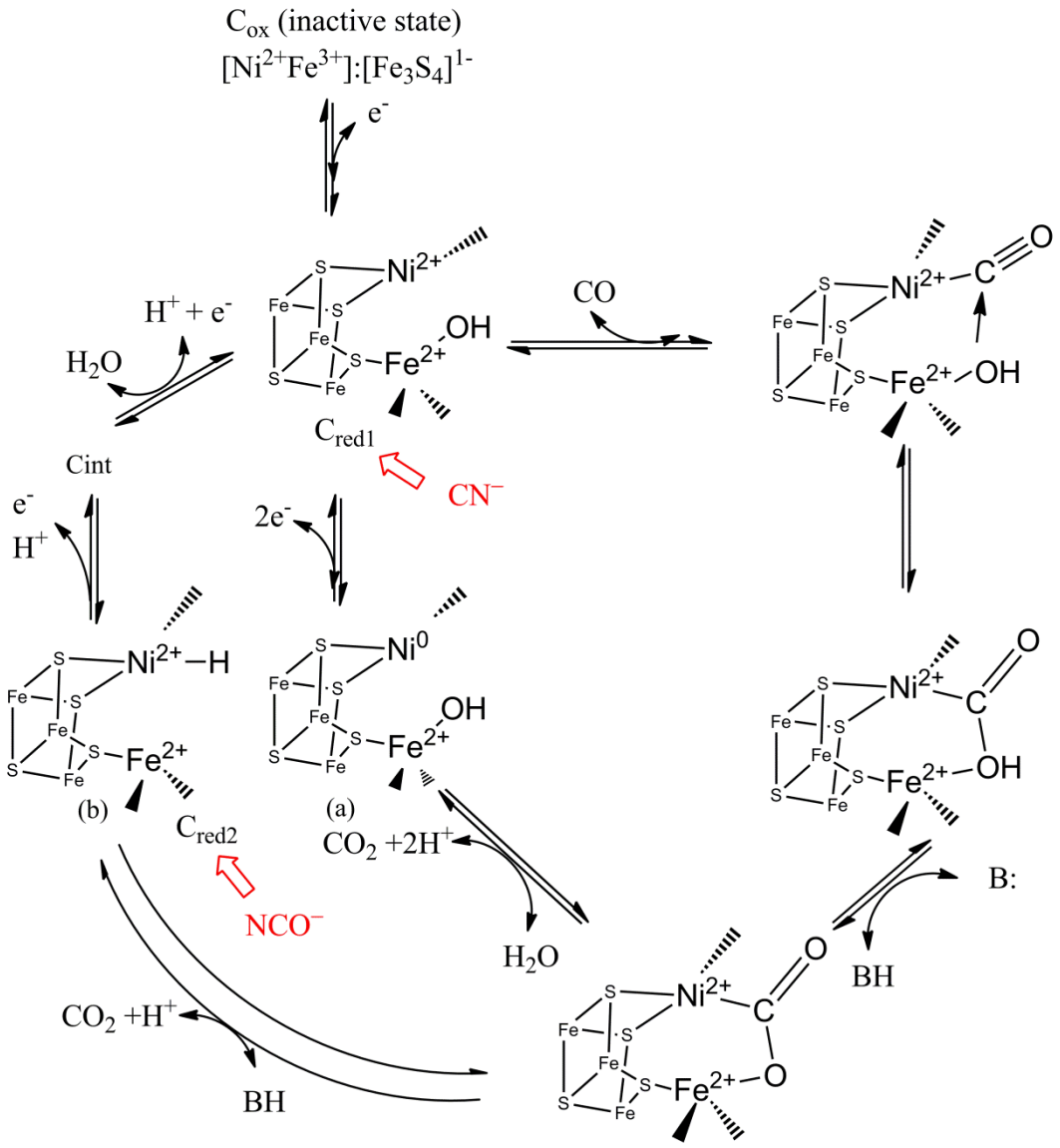

Figure 7.1 Two possible mechanisms of CODH proposed by (a) Dobbek[6] and Lindahl group[20], the Ni (0) state for the C_{red2} state or (b) Fontecilli-Camps group[21], the Ni(II)-H specie for the C_{red2} state. B refers to the amino acid which accepts proton, possibly His or Lys. The red colors represent substrate-mimic inhibitors in which cyanide (CN^-) inhibits the C_{red1} state and cyanate (NCO^-) inhibits the C_{red2} state.

The proposed mechanism of CO oxidation by CODH is quite similar to the well-studied water-gas shift (WGS) reaction. The key step in these two reactions involves nucleophilic attack on the carbon by a metal-bound hydroxide to generate a carboxylate-bound metal intermediate as shown in Figure 7.2.[102] The main difference is the final product in which the WGS reaction yields H_2 in comparison with two protons released from CODH. This difference leads us to ask a question: Why would CODH in the microorganism deliver these two electrons from CO oxidation to hydrogenase which catalyzes H_2 evolution[5] instead of direct H_2 evolution by CODH itself ? To the best of our knowledge, CODH from *Carboxydothemus hydrogenoformans* (*Ch*) has the highest turnover rate for CO oxidation and CO_2 reduction with minimal overpotential requirement in the aqueous solution. Does proton as the product/reactant in CO oxidation/CO_2 reduction catalyzed by CODH play a crucial role in rapid and reversible interconversion between CO and CO_2?

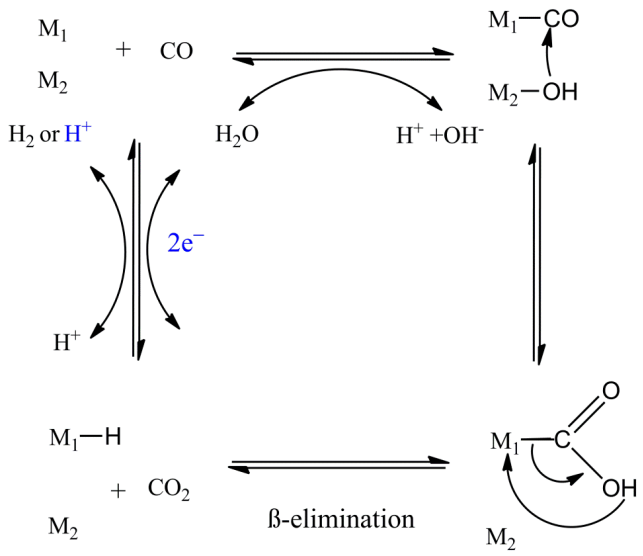

Figure 7.2 The general catalytic mechanism for the water gas shift reaction.[102] Blue colors represent reaction species are involved in CODH.

Recently, QM/MM calculation on several X-ray crystal structures of CODH II_{Ch}[6,16] by the Fontecilla-Camps group[21] suggests that the C_{red2} state has the hydride bound to the Ni(II) ion as shown in Figure 7.1(b) instead of the previous proposed state, Ni(0) coordinated by electron-rich sulfur atoms,[6] which seems to be less stable. The proposed intermediate, Ni hydride in the C_{red2} state is also similar to another key step in the WGS reaction in which metal-hydride is generated by β-elimination of the metal-bound carboxylate intermediate. In the final step of the WGS reaction, water reacts with metal-hydride to yield H_2 and return the initial state, a metal-bound hydroxide.

In this chapter, the kinetic isotope effect (KIE) value was measured by PFE and a small amount of hydrogen and formate were detected during the catalytic reaction by gas chromatography and NMR respectively. These results suggest a Ni-hydride intermediate is generated in the catalytic cycle.

7.3 Material and methods

All chemicals were analytical grade. Cylinders of CO and CO_2 (CP grade) were purchased from BOC. Chemicals for modification of the PGE electrode: Multi-walled carbon nanotubes (MWCT, carbon >90% (trace metal basis)), 1-pyrenebutyric acid (Py), 1-ethyl-3-(3-dimethylaminopropyl) carbodiimide (EDC), N-hydroxy sulfosuccinimide (NHSS) and dimethyl formamide (DMF) were all purchased from Sigma-Aldrich. Deionized (DI) water (18.2 MΩ· cm) made by Milli-Q water purification system (Millipore) and deuterium oxide (99.9%) purchased from Apollo Scientific were used in this study. 2-(*N*-morpholino) ethanesulfonic acid (MES) (Sigma-Aldrich) buffer was prepared in these two different isotope solvents and NaOH (Sigma-Aldrich) was used to adjust the pH or pD value. The

value of pD was measured by a pH electrode (Mettler Toledo) and then corrected by the relationship, pD= pH_{meter} +0.4.

7.3.1 The detection of H_2 produced by CODH

Attempts to measure H_2 evolution by CODH in the WGS reaction were conducted by solution assay, which is similar to the measurement of CO oxidation activity by CODH without redox mediators, methyl viologen.

The preparation of CODH samples from *Carboxydothermus hydrogenoformans* described in the previous publication was followed.[63] For measuring H_2 evolution by CODH I_{Ch} and CODH II_{Ch}, the following procedure was employed and all sample preparation was performed in the glove box (Vacuum atmospheres) with less than 5ppm O_2. The Pyrex pressure vessel was sealed tightly with a rubber septum and then purged with 96% CO/4% CH_4 for 20 mins. CODH I_{Ch} and CODH II_{Ch} in 0.2 M MES (pH=7.0) was injected into the vessel by syringe. The atmosphere in the headspace of the reaction vessel was withdrawn (20 μL) for detecting H_2 by GC (Agilent Technologies 7890A GC equipped with a Restek ShinCarbon ST micropacked column held isothermally at 34 ℃) using N_2 as a carrier gas and a thermal conductivity detector. For each measurement, the amount of H_2 formed by CODH was calculated against the internal standard CH_4.

7.3.2 The detection of formate produced by CODH

To detect the reduction of CO_2 to formate by CODH I_{Ch}, the electrocatalysis provide sufficient driving force to catalyze CO_2 reduction (which is more negative than –0.5 V at pH=7.0), which is otherwise difficult to achieve by chemical mediators or titrants. No

formate formation was observed by the mixture of polymyxin and CODH I_{Ch} on the PGE electrode in the three-day experiment. Therefore, PGE electrode surface was modified by MWCT to increase the amount of CODH I_{Ch} on the electrode surface for CO_2 reduction.

The method for PGE surface modification by MWCT is described[103] as follows: A suspension of MWCT in DMF (1 mg/mL) was dispersed by sonication for 1 h before placing 15 μL solution onto the PGE surface and drying overnight. The solution of MWCT in DMF (1mg/mL) was sonicated for 1 h before placing the 15 μL solution onto the PGE surface and drying overnight. The 20 uL of a solution of Py in DMF (10 mM) was added onto the MWCT-PGE electrode surface and placed for 1 hour to obtain π-π stacking interactions between MWCT and Py. The modified electrode was washed by DI water to remove free Py and brought into the glovebox for the further modification. The 5 μL of EDC (0.4 M) and NHSS (0.1 M) respectively was placed onto the modified PGE surface with Py and MWCT for 20 mins and then CODH I_{Ch} was added and left for 40 minutes with the eppendorf tube on the electrode top to keep the moisture environment for enzymes.

The detection of formate formed by CODH I_{Ch} is described below. CODH I_{Ch} was placed on MWCT-modified electrode and poised at −760 mV in 0.2 M MES (90% H_2O and 10% D_2O at pH=7) with continuous CO_2 flow (40 scc/m) in the headspace of the electrochemical cell. The rotation rate at 400 rpm was employed. The solution was collected and 500 MHz NMR (Bruker) was used to detect the proton signal from formate.

The electrochemical experiment and instrumental setup was the same as described in Chapter 3.

7.4 Results

7.4.1 Water–gas shift reaction carried out by CODH

H_2 evolution by CODH I_{Ch} and CODH II_{Ch} in the presence of 96% CO/ 4% CH_4 at 20°C in the time-course experiment is shown in Figure 7.3. The rate of H_2 evolution is 78.4 nmole/min · mg (0.16 s^{-1}) for CODH I_{Ch} and 7.5 nmole/min · mg (0.016 s^{-1}) for CODH II_{Ch}. The rate of H_2 evolution by these CODHs is much slower than CO oxidation rate (~1500 s^{-1} at 20°C).[63] In the presence of methyl viologen as an electron acceptor, the turnover number for H_2 evolution is smaller (~0.5 times slower). It was reported ACS/CODH from *Moorella thermoacetica(Mt)* is 590 nmole/min · mg (3 s^{-1}) at 25°C (pH=6.0) in the absence of any electron acceptor and the rate of H_2 evolution in the presence of electron acceptor is 1000-fold slower than CO oxidation.[104] In order to confirm hydrogen formation from CODH, not from the possible contamination of hydrogenase, cyanide, which inhibits CODH, is added. The hydrogenase is not inhibited by cyanide. The hydrogen evolution stops after adding cyanide into samples.

The small amount of H_2 observed by CODH from different species may imply that hydride plays an important role in catalyzing the reaction, which is similar to the mechanism of the WGS reaction. Since the turnover number of CO oxidation and CO_2 reduction by CODH I_{Ch} and CODH II_{Ch} is much faster than ACS/$CODH_{Mt}$, especially in CO_2 reduction (at least 1000 times faster), CODH from *Carboxydothermus hydrogenoformans* might have a different structural environment to protect hydride from proton or water attack for H_2 evolution during the catalytic process.

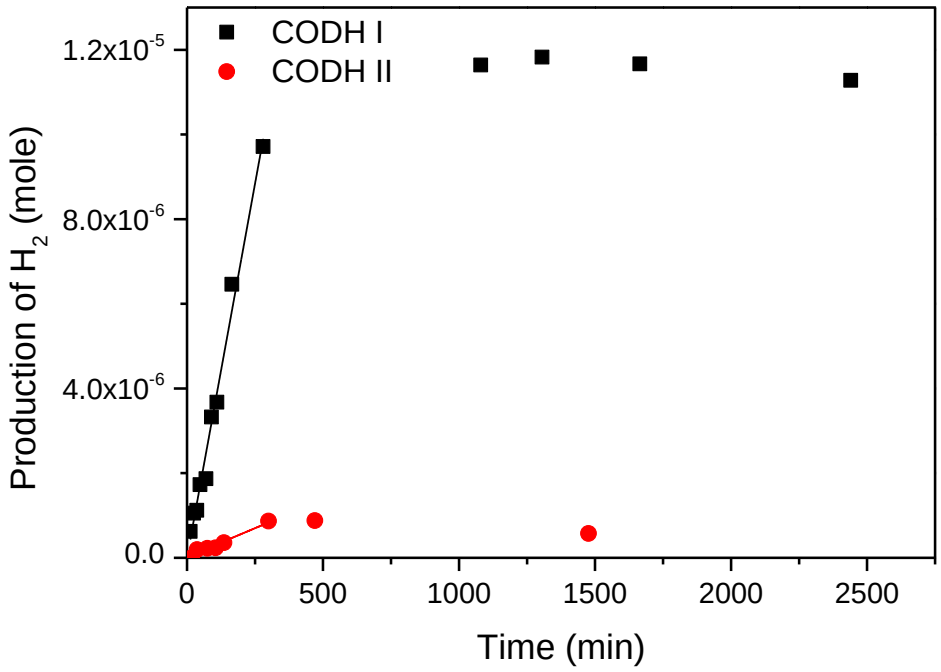

Figure 7.3 The rate of H_2 evolution by the WGS reaction in $CODH_{Ch}$ in the presence of 96% CO/ 4% CH_4. 30 μL CODH I_{Ch} (15 mg/ml) and 20 uL CODH II_{Ch} (18mg/mL) respectively were dissolved in 0.2 M MES buffer (pH=7.0). The final volume in the reaction vessel was 300 μL and the reaction occurred at 20 ^{o}C.

7.4.2 Kinetic isotope effect (H_2O/D_2O)

The electrocatalytic current in PFE directly correlates to the turnover number. It is easy to observe the solvent kinetic isotope effect (KIE) for CO oxidation and CO_2 reduction in PFE by changing solvent. However, the protein film is unstable in the D_2O solvent, especially in CODH II_{Ch}, which makes it quite difficult to obtain a precise KIE value. Since the turnover number of CODH I_{Ch} is faster in H_2 evolution and is more stable in D_2O solvent, the main research in our KIE study was concentrated on CODH I_{Ch}.

In order to obtain the KIE value as accurately as possible, a high rotation rate (1500 rpm) for increasing the rate of CO_2 dissolving into buffer and a fast scan rate (20mV/sec) was used. When observing the electrocatalytic current drop in successive scans, the scan was stopped and the buffer was changed. The biggest electrocatalytic current in voltammograms among successive scans in the same solvent was used for calculating KIE values.

Two different pH/pD values (7.0 and 5.2) were used to investigate KIE values for CO oxidation and CO_2 reduction respectively. Cyclic voltammograms was recorded at pH/pD=7.0 and pH/pD=5.2 in the presence of 100% CO and 100% CO_2 respectively as shown in Figure 7.4. The KIE value for CO oxidation is about 1.2-1.4 at pH/pD=7.0 and about 1.4-1.7 at pH/pD=5.2 (the KIE value is estimated by $I_{(\text{fresh H2O buffer})}/ I_{(\text{D2O buffer})}$). The KIE value is smaller in the high potential region of CO oxidation. However, the real KIE values should be bigger than the apparent values since the film loss on the D_2O buffer is unavoidable. Even in the presence of polymyxin in the D_2O buffer, it is still unable to decrease the rate of film loss. As shown in the equation 1.7a in Chapter 1, H_2O (solvent) is involved in CO oxidation; thus the small KIE value was expected and the small KIE values indicate H_2O or proton is involved in the rate-determining step in CO oxidation.

In contrast, the negligible KIE values for CO_2 reduction at these two pH/pD values were observed although the equation 1.7a in Chapter 1 clearly indicates protons are involved in CO_2 reduction. No apparent KIE values for CO_2 reduction suggest proton transfer is not the rate-determining step in CO_2 reduction. The KIE values from CODH II_{Ch} are similar by rough estimation although the greater film loss of CODH II_{Ch} in D_2O makes it difficult for us to obtain the value.

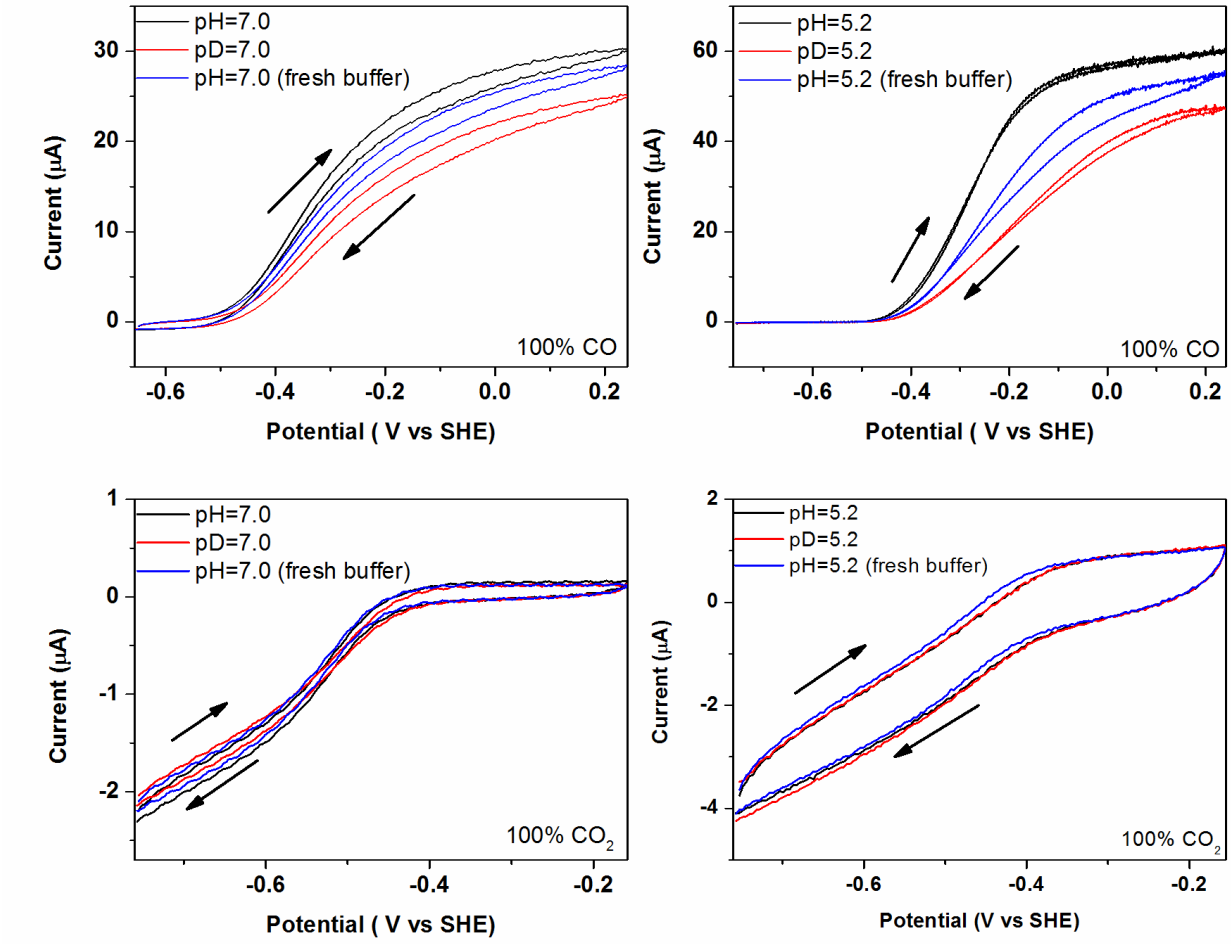

Figure 7.4 Cyclic voltammograms of CODH I_{Ch} were recorded in the proton/deuterium buffer respectively. Experimental conditions: 15 ^{o}C, 0.2 M MES (pH/pD=7.0 or pH/pD=5.2), rotation rate 1500 rpm and scan rate 20 mVs^{-1}.

The inactivation rate for CO_2 reduction by cyanate was studied (Chapter 4) and the measurement of the kinetic rate constant for cyanate inhibition is another probe for

investigating KIE between H_2O and D_2O solution. No kinetic isotope effect values between H_2O and D_2O buffer was observed, also suggested proton transfer (or proton-coupled electron transfer) is not involved in the crucial step for CO_2 reduction by CODH. However, the faster inhibition by cyanate occurs at the low pH value (pH=7.0 vs. pH=5.2). (Figure 7.5)

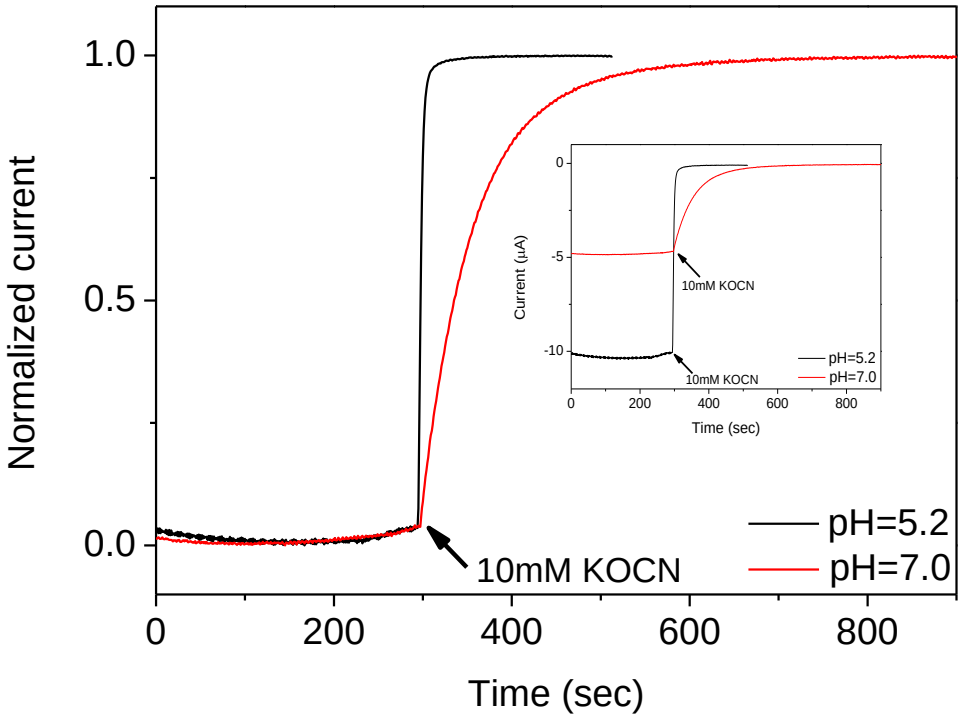

Figure 7.5 Inhibition rates of CODH I_{Ch} by cyanate at two different pH values. An aliquot of KOCN solution (giving final concentration of 10 mM in the cell) was injected at pH=5.2 and pH=7.0 respectively. The inset figure is the original data. Experimental conditions: 25 ^{o}C, 0.2 M MES (pH=7.0 or pH=5.2) and rotation rate 1000 rpm.

7.4.3 Formate formation by CODH I_{Ch}

CODH I_{Ch} on the MWCT-modified PGE electrode was poised at −760 mV with the continuous CO_2 flow in the headspace of the electrochemical cell for 3 days. The final solution was collected and examined by proton NMR for formate. The characteristic proton peak from formate was observed in NMR as shown in Figure 7.6.

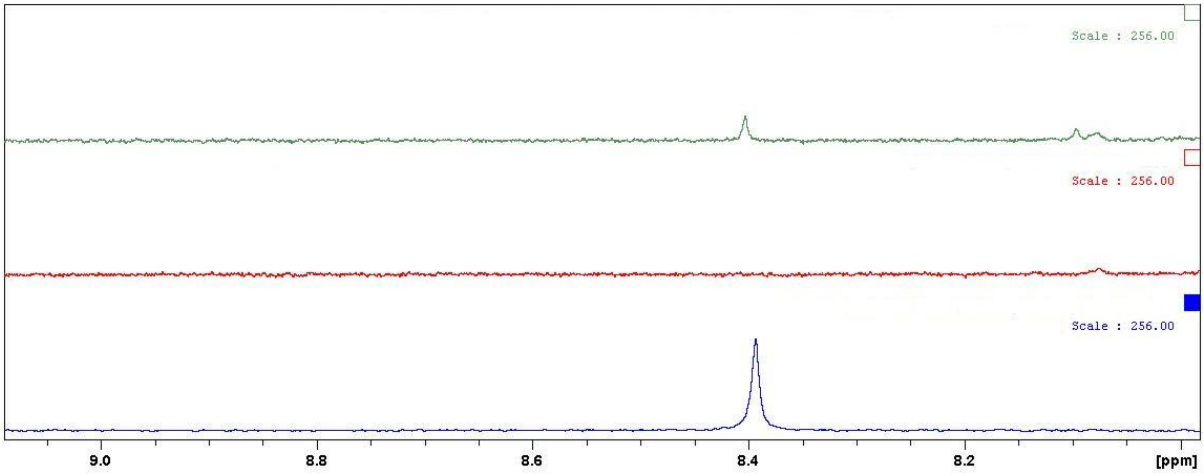

Figure 7.6 The formate production by CODH I_{Ch} during CO_2 reduction. The green line refers to the experimental sample in which CO_2 (40 scc/m) flows through the headspace for 3 days with CODH I_{Ch} on the modified PGE electrode at −760 mV. The red line indicates the control experiment in which N_2 was in the headspace without poising any potential on the modified PGE electrode with CODH I_{Ch} and the blue line indicates that 1 mM potassium formate in 100% D_2O. Experimental conditions: 25 ^oC, 0.2 M MES (pH=7.0 and 10% D_2O and 90% H_2O) and rotation rate 400 rpm.

The concentration of formate produced by CODH I_{Ch} is roughly 75 nmole in the 3 days in comparison with 9.36 mole CO based on the integral of the current with time in chronoamperometry as shown in Figure 7.7. The rate of formate formation is much slower than CO product. No formate signals were detected by NMR after placing CODH I_{Ch} on the MWCT-modified PGE electrode in the presence of CO flow for 4 days, which indicates that hydration of CO into formate by CODH is unlikely to have occurred.

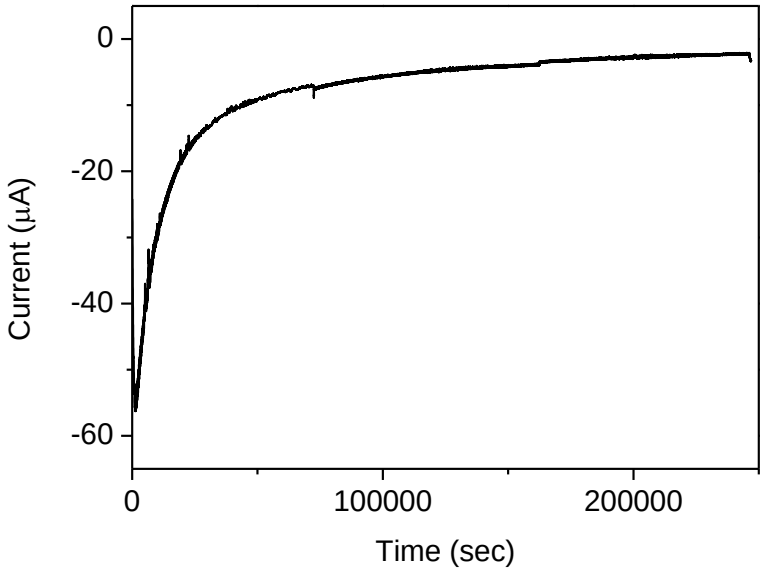

Figure 7.7 Chronoamperometry of CODH I_{Ch} on the MWCT-modified PGE electrode recorded at −760 mV under 100% CO_2 (40 scc/m). 1806599 coulombs is obtained by the integral of the current with time in chronoamperometry. Experimental conditions: 25 ^{o}C, 0.2 M MES (pH=7.0 and 10% D_2O and 90% H_2O) and rotation rate 400 rpm.

7.5 Discussion

Hydrogen formation by CODH I_{Ch} and CODH II_{Ch} in the presence of CO suggests CODH is likely to use the similar mechanism as the WGS reaction and the nickel hydride engages in the catalytic cycle. The hydrogen evolution is also observed in other CODH families. Aerobic CODH from *Oligotropha carboxydovorans* uses the Mo and Cu atom as an active site, which has been shown to generate H_2 with 7.5 nmole/min · mg (0.034 s^{-1}) in the presence of 100% CO.[105] In anaerobic bacterium, *Moorella thermoacetica*, $CODH_{Mt}$ coupled with acetyl-CoA synthase to form the bifunctional enzymes also reveals H_2 evolution with 590 nmole/min · mg (3 s^{-1}).[104] The evidence clearly indicates the mechanism of CO oxidation employed by CODH is similar to the WGS mechanism. The slow rate for H_2 formation in comparison with CO oxidation indicates that how the enzyme structure prevents a metal-hydride species from easily reacting with water or proton to yield H_2. This unusual property is likely to correlate to the high turnover number and reversibility of anaerobic [Ni-Fe] CODH.

Two possible mechanisms for hydride transfer inside the C-cluster could occur; the direct hydride transfer or β-hydride elimination from a metal-bound carboxylate intermediate. The small KIE value observed here suggests the direct hydride transfer is less likely because the direct hydride transfer involves a linear binding mode which has the higher frequency than a bent mode and therefore, the direct hydride transfer leads to a high KIE value. The studies in formate oxidation by several different molecular metal catalysts show KIE values for direct hydride transfer is larger than β-hydride elimination (the KIE value <2).[106-110] The mechanism of β-hydride elimination also supports the formation of the metal-carboxylate

intermediate species in CODH (Figure 7.2). The small solvent KIE values are also associated with results of internal proton transfer inside CODH suggested by NMR studies of CO/CO_2 exchange experiments.[63]

X-ray absorption spectroscopy (XAS) has revealed as-isolated CODH II_{Ch}, CO-treatment CODH II_{Ch} and dithionite-reduced CODH II_{Ch} all have the same oxidation state, Ni (II) and no great differences among three samples in the region of pre-edge XAS suggest the coordination environment of the Ni atom is similar.[56,111] In comparison with EPR signals between C_{red1} and C_{red2}, small differences are observed and both average *g* values are less than 2, which indicate the spin density mainly resides on the Fe-S clusters rather than the Ni atom. [61]Ni-ENDOR also indicates the very weak electron coupling with the Ni-atom.[67] These results imply that the oxidation state of Ni does not change in the catalytic cycle and the proposed state of hydride-Ni (II) seems to correlate with these spectroscopic results. In addition, quantum mechanics/molecular mechanics calculation by the Fontecilli-Camps group suggests a hydride-Ni(II) intermediate species in the C_{red2} state is the most possible state which corresponds to results from Mössabauer spectroscopy.[21]

Here, the suggestion of CO_2 reduction by metal-hydride in CODH is not a rare concept. CO_2 insertion into the metal-hydride bond for formate formation has been reported in molecular metal catalysts.[98] Formate dehydrogenase has been shown to catalyze the reversible reaction on the PGE electrode for formate oxidation and CO_2 reduction[99] and been suggested that Mo-hydride should be an intermediate in the catalytic cycle in Mo-containing formate dehydrogenase.[112,113] Interesting, a small amount of formate observed by CODH I_{Ch} on PGE electrode further consolidates the idea of a Ni-hydride species in the catalytic cycle of CODH. However, in comparison with the usual proposed mechanism for molecular metal

catalysts in which carbon dioxide is reduced to formate by migrating the hydride to carbon and forming the metal-bound formate, the intermediate specie of a Ni-bound carboxylate in CODH is formed by migrating the hydride from Ni-hydride into one of the oxygen atoms in CO_2.(Figure 7.8) The Fontecilli-Camp group terms this abnormal insertion.[21] Following this, hydroxide is abstracted by the dangling Fe. The dangling Fe should play an important role in stabilizing the bent CO_2 intermediate state for inserting hydride by interacting with the oxygen atom. For example, several molecular catalysts for CO_2 reduction operated in the aqueous solution, such as the electrocatalyst, Ni-(cyclam) complex[114] and the catalyst, Ir-pincer complex[115], have been shown that the *H-bond* from the second coordination sphere plays an important role in stabilizing the activated CO_2 and facilitating formate formation. The dangling Fe should have a similar role in the C-cluster.

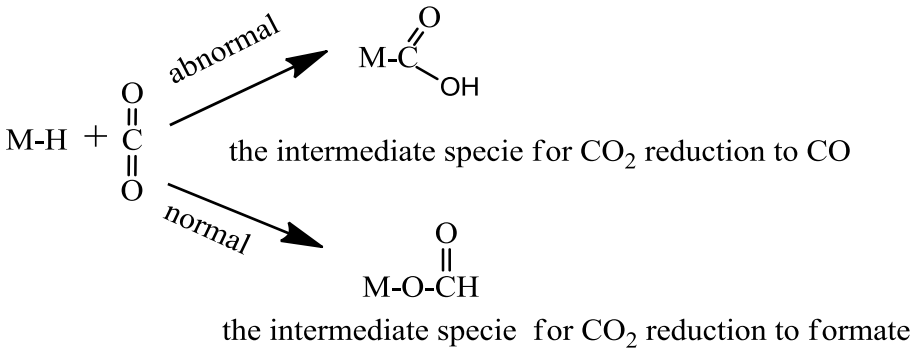

Figure 7.8 Illustration of possible mechanisms for hydride insertion to CO_2

Metal-hydride appears to be a better candidate to conduct the two-electron-and-proton transfer in the concerted mechanism for CO_2 reduction, which generally invokes a lower energy barrier than sequential proton and electron transfer. This might explain why CODH has a rapid turnover rate for CO_2 reduction with the low overpotential requirement. Chapter 3

and Chapter 4 have shown that cyanate mainly inhibits CO_2 reduction. More interestingly, the inactivation rate is much faster in the low pH buffer. It suggests HNCO ($pK_a = 3.7$) without charge has the stronger affinity toward the C_{red2}. This strong affinity between neutral HNCO and CODH supports a *neutral* Ni-bound carboxylate intermediate formed by abnormal hydride insert into CO_2.

Finally, the Lindahl group has conducted mutagenesis experiments in ACS/$CODH_{Mt}$ to identify the possible pathways for proton transfer.[73] In comparison with the electron transfer pathways *via* $[Fe_4S_4]$ clusters, the proton transfer pathways are quite discrete. It is interesting to further examine how these two discrete pathways play roles in the formation of Ni-H in CODH.

The development of efficient electrocatalysts for CO_2 reduction (or combined with photo-catalysts) plays the important role in converting CO_2 to carbon-based fuel in a clean and sustainable way. The evidence of the metal-hydride intermediate in CODH provides a new aspect in the design of catalysts. The similar mechanism between the WGS reaction and CODH also provide hints toward reinvestigating and redesigning WGS catalysts, which might be able to catalyze CO_2 reduction preferentially.

Chapter 8 ***Conclusion***

In this thesis, different CODH samples have been studies by protein film electrochemistry. The availability of a wide range of potentials in PFE reveals some important features of CODH, which are inaccessible to be performed by traditional solution titration, especially in the low potential region required for CO_2 reduction.

Several small substrate-mimic inhibitors, cyanide, cyanate, sulfide, thiocyanate and azide are added into CODH I_{Ch} and CODH II_{Ch} for investigating the catalytic mechanism. Inhibition of CO oxidation and the more positive potential region of CO_2 reduction by cyanide, (which is isoelectronic with CO) is found. Inhibition of CODH by cyanide is reactivated in the more negative potential region of CO_2 reduction. Inhibition of CODH II_{Ch} by cyanide is about one-order-of-magnitude stronger than CODH I_{Ch}, which correlates with the observation that CODH II_{Ch} has the stronger CO product inhibition. In comparison, cyanate, isoelectronic with CO_2, mainly inhibits CO_2 reduction.

Hydrogen sulfide (or sulfide) inhibits CO oxidation but not CO_2 reduction. The rapid inhibition occurs in the potential region of the same oxidation level as $C_{ox.}$ This result explains why previous studies reveal different conflicting roles of the sulfur atom in the active site, an activator or inhibitor. Partial and reversible inhibition by thiocyanate is only observed in CO oxidation rather than CO_2 reduction. Finally, no inhibition by azide in these two monofunctional CODHs is found. These results show the electrode potential *selectively* controls binding between CODH and substrate-mimic inhibitors.

In comparison with monofunctional CODH, a much smaller electrocatalytic current for CO oxidation with the higher overpotential and no electrocatalytic CO_2 reduction from ACS/$CODH_{Mt}$ are observed. In the presence of chemical reagents, sodium dodecyl sulfate (which separates CODH and ACS partially), 1, 10-phenanthroline (which removes the

requisite Ni atom in the active site of ACS), and acetyl-CoA (the product of the reaction carried out by ACS/CODH), it is still impractical to observe the electrocatalytic current for CO_2 reduction by ACS/CODH$_{Mt}$. Finally, inhibition of ACS/CODH$_{Mt}$ by azide is observed. These findings suggest that ACS plays an important role in modulating CODH performance.

The C-cluster is identified as a target of oxygen attack in CODH. Further studies revealed that oxygen damages CODH when it is the C_{red1} state. However, the inactive C_{ox} state can protect against oxygen attack and the inactive state is reactivated reductively by the low potential. The mechanism of the inactive process by oxygen in the high potential region might be similar to the sulfide inhibition in which the reactivation occurs in the low potential.

Nitrious oxide, isoelectronic with CO_2, is found to be catalyzed by CODH. This discovery opens a new direction to study the mechanism of CODH. In addition, the detection of hydrogen as the side product in the direction of CO oxidation and formate in the direction of CO_2 reduction as well as previous spectroscopic evidence and theoretical calculations strongly suggest the formation of a Ni-hydride intermediate during the catalytic cycle. The small solvent KIE values observed in CO oxidation suggest β− hydride elimination occurs in the catalytic cycle.

These discoveries lead us to understand how CODH catalyzes the interconversions between CO oxidation and CO_2 reduction *rapidly* and *reversibly* with a minimal overpotential. The inspiration from the enzymatic mechanism and structure, such as metal-hydride, can help design better catalysts for CO_2 reduction.

In future, mutagenesis study could further help understand how proton-coupled electron transfer occurs in CODH since CO_2 reduction is required for multiple proton and electron

transfers. From the application perspective, further understanding how O_2 destroys anaerobic [Ni-Fe] CODH in the C_{red1} state is an important question.

References

(1) James, O. O.; Mesubi, A. M.; Ako, T. C.; Maity, S. *Fuel Processing Technology* **2010**, *91*, 136.
(2) Meyer, O.; Schlegel, H. G. *Annual Review of Microbiology* **1983**, *37*, 277.
(3) Dobbek, H.; Gremer, L.; Kiefersauer, R.; Huber, R.; Meyer, O. *Proceedings of the National Academy of Sciences of the United States of America* **2002**, *99*, 15971.
(4) Daniel, S. L.; Hsu, T.; Dean, S. I.; Drake, H. L. *Journal of Bacteriology* **1990**, *172*, 4464.
(5) Svetlitchnyi, V.; Peschel, C.; Acker, G.; Meyer, O. *Journal of Bacteriology* **2001**, *183*, 5134.
(6) Jeoung, J. H.; Dobbek, H. *Science* **2007**, *318*, 1461.
(7) Lindahl, P. A.; Munck, E.; Ragsdale, S. W. *Journal of Biological Chemistry* **1990**, *265*, 3873.
(8) Parkin, A.; Seravalli, J.; Vincent, K. A.; Ragsdale, S. W.; Armstrong, F. A. *Journal of the American Chemical Society* **2007**, *129*, 10328.
(9) Bender, G.; Pierce, E.; Hill, J. A.; Darty, J. E.; Ragsdale, S. W. *Metallomics* **2011**, *3*, 797.
(10) Svetlitchnyi, V.; Dobbek, H.; Meyer-Klaucke, W.; Meins, T.; Thiele, B.; Romer, P.; Huber, R.; Meyer, O. *Proceedings of the National Academy of Sciences of the United States of America* **2004**, *101*, 446.
(11) Grahame, D. A. *Journal of Biological Chemistry* **1991**, *266*, 22227.
(12) Lindahl, P. A.; Chang, B. *Origins of Life and Evolution of the Biosphere* **2001**, *31*, 403.
(13) Wu, M.; Ren, Q. H.; Durkin, A. S.; Daugherty, S. C.; Brinkac, L. M.; Dodson, R. J.; Madupu, R.; Sullivan, S. A.; Kolonay, J. F.; Nelson, W. C.; Tallon, L. J.; Jones, K. M.; Ulrich, L. E.; Gonzalez, J. M.; Zhulin, I. B.; Robb, F. T.; Eisen, J. A. *Plos Genetics* **2005**, *1*, 563.
(14) Fox, J. D.; He, Y. P.; Shelver, D.; Roberts, G. P.; Ludden, P. W. *Journal of Bacteriology* **1996**, *178*, 6200.
(15) Soboh, B.; Linder, D.; Hedderich, R. *European Journal of Biochemistry* **2002**, *269*, 5712.
(16) Jeoung, J. H.; Dobbek, H. *Journal of the American Chemical Society* **2009**, *131*, 9922.
(17) Dobbek, H.; Svetlitchnyi, V.; Liss, J.; Meyer, O. *Journal of the American Chemical Society* **2004**, *126*, 5382.
(18) Drennan, C. L.; Heo, J. Y.; Sintchak, M. D.; Schreiter, E.; Ludden, P. W. *Proceedings of the National Academy of Sciences of the United States of America* **2001**, *98*, 11973.
(19) Kung, Y.; Drennan, C. L. *Current Opinion in Chemical Biology* **2011**, *15*, 276.
(20) Lindahl, P. A. *Angewandte Chemie-International Edition* **2008**, *47*, 4054.
(21) Amara, P.; Mouesca, J. M.; Volbeda, A.; Fontecilla-Camps, J. C. *Inorganic Chemistry* **2011**, *50*, 1868.
(22) Spangler, N. J.; Lindahl, P. A.; Bandarian, V.; Ludden, P. W. *Journal of Biological Chemistry* **1996**, *271*, 7973.
(23) Kumar, M.; Lu, W. P.; Liu, L. F.; Ragsdale, S. W. *Journal of the American Chemical Society* **1993**, *115*.
(24) Lu, W. P.; Jablonski, P. E.; Rasche, M.; Ferry, J. G.; Ragsdale, S. W. *Journal of Biological Chemistry* **1994**, *269*, 11646.
(25) Fraser, D. M.; Lindahl, P. A. *Biochemistry* **1999**, *38*, 15706.

(26) Lindahl, P. A.; Ragsdale, S. W.; Munck, E. *Journal of Biological Chemistry* **1990**, *265*, 3880.
(27) Darnault, C.; Volbeda, A.; Kim, E. J.; Legrand, P.; Vernede, X.; Lindahl, P. A.; Fontecilla-Camps, J. C. *Nature Structural Biology* **2003**, *10*, 271.
(28) Kung, Y.; Doukov, T. I.; Seravalli, J.; Ragsdale, S. W.; Drennan, C. L. *Biochemistry* **2009**, *48*, 7432.
(29) Doukov, T. I.; Blasiak, L. C.; Seravalli, J.; Ragsdale, S. W.; Drennan, C. L. *Biochemistry* **2008**, *47*, 3474.
(30) Seravalli, J.; Ragsdale, S. W. *Biochemistry* **2000**, *39*, 1274.
(31) Vincent, K. A.; Armstrong, F. A. *Inorganic Chemistry* **2005**, *44*, 798.
(32) Armstrong, F. A.; Hirst, J. *Proceedings of the National Academy of Sciences of the United States of America* **2011**, *108*, 14049.
(33) Woolerton, T. W.; Sheard, S.; Pierce, E.; Ragsdale, S. W.; Armstrong, F. A. *Energy Environ. Sci.* **2011**, *4*, 2393.
(34) Woolerton, T. W.; Sheard, S.; Chaudhary, Y. S.; Armstrong, F. A. *Energy Environ. Sci.* **2012**, *5*, 7470.
(35) Yeh, P.; Kuwana, T. *Chemistry Letters* **1977**, *10*, 1145.
(36) Eddowes, M. J.; Hill, H. A. O. *Journal of the Chemical Society-Chemical Communications* **1977**, *21*, 771.
(37) Armstrong, F. A.; Hill, H. A. O.; Walton, N. J. *Accounts of Chemical Research* **1988**, *21*, 407.
(38) Sucheta, A.; Ackrell, B. A. C.; Cochran, B.; Armstrong, F. A. *Nature* **1992**, *356*, 361.
(39) Armstrong, F. A.; Wilson, G. S. *Electrochimica Acta* **2000**, *45*, 2623.
(40) Blanford, C. F.; Armstrong, F. A. *Journal of Solid State Electrochemistry* **2006**, *10*, 826.
(41) Leger, C.; Bertrand, P. *Chemical Reviews* **2008**, *108*, 2379.
(42) Patel, A. N.; Collignon, M. G.; O'Connell, M. A.; Hung, W. O. Y.; McKelvey, K.; Macpherson, J. V.; Unwin, P. R. *Journal of the American Chemical Society* **2012**, *134*, 20117.
(43) Heering, H. A.; Hirst, J.; Armstrong, F. A. *Journal of Physical Chemistry B* **1998**, *102*, 6889.
(44) Leger, C.; Heffron, K.; Pershad, H. R.; Maklashina, E.; Luna-Chavez, C.; Cecchini, G.; Ackrell, B. A. C.; Armstrong, F. A. *Biochemistry* **2001**, *40*, 11234.
(45) Reda, T.; Hirst, J. *Journal of Physical Chemistry B* **2006**, *110*, 1394.
(46) Laviron, E. *Journal of Electroanalytical Chemistry* **1974**, *52*, 355.
(47) Bard, A. J.; Faulkner, L. R. *Electrochemical Methods:*; 2nd ed.; Wiley, New York, 2001.
(48) Hirst, J.; Armstrong, F. A. *Analytical Chemistry* **1998**, *70*, 5062.
(49) Pershad, H. R.; Duff, J. L. C.; Heering, H. A.; Duin, E. C.; Albracht, S. P. J.; Armstrong, F. A. *Biochemistry* **1999**, *38*, 8992.
(50) Moser, C. C.; Keske, J. M.; Warncke, K.; Farid, R. S.; Dutton, P. L. *Nature* **1992**, *355*, 796.
(51) Page, C. C.; Moser, C. C.; Chen, X. X.; Dutton, P. L. *Nature* **1999**, *402*, 47.
(52) Dobbek, H.; Svetlitchnyi, V.; Gremer, L.; Huber, R.; Meyer, O. *Science* **2001**, *293*, 1281.
(53) Ragsdale, S. W. *Critical Reviews in Biochemistry and Molecular Biology* **2004**, *39*, 165.

(54) Svetlichny, V. A.; Sokolova, T. G.; Gerhardt, M.; Ringpfeil, M.; Kostrikina, N. A.; Zavarzin, G. A. *Systematic and Applied Microbiology* **1991**, *14*, 254.
(55) Seravalli, J.; Kumar, M.; Lu, W. P.; Ragsdale, S. W. *Biochemistry* **1995**, *34*, 7879.
(56) Ha, S. W.; Korbas, M.; Klepsch, M.; Meyer-Klaucke, W.; Meyer, O.; Svetlitchnyi, V. *Journal of Biological Chemistry* **2007**, *282*, 10639.
(57) Feng, J.; Lindahl, P. A. *Journal of the American Chemical Society* **2004**, *126*, 9094.
(58) Ensign, S. A.; Hyman, M. R.; Ludden, P. W. *Biochemistry* **1989**, *28*, 4973.
(59) Anderson, M. E.; Lindahl, P. A. *Biochemistry* **1994**, *33*, 8702.
(60) Anderson, M. E.; Derose, V. J.; Hoffman, B. M.; Lindahl, P. A. *Journal of the American Chemical Society* **1993**, *115*, 12204.
(61) Ragsdale, S. W.; Clark, J. E.; Ljungdahl, L. G.; Lundie, L. L.; Drake, H. L. *Journal of Biological Chemistry* **1983**, *258*, 2364.
(62) Wang, V. C. C.; Can, M.; Pierce, E.; Ragsdae, S. W.; Armstrong, F. A. *Journal of the American Chemical Society* **2013**, *135*, 2198.
(63) Seravalli, J.; Ragsdale, S. W. *Biochemistry* **2008**, *47*, 6770.
(64) Diekert, G. B.; Thauer, R. K. *Journal of Bacteriology* **1978**, *136*, 597.
(65) Drake, H. L.; Hu, S. I.; Wood, H. G. *Journal of Biological Chemistry* **1980**, *255*, 7174.
(66) Doukov, T. I.; Iverson, T. M.; Seravalli, J.; Ragsdale, S. W.; Drennan, C. L. *Science* **2002**, *298*, 567.
(67) DeRose, V. J.; Telser, J.; Anderson, M. E.; Lindahl, P. A.; Hoffman, B. M. *Journal of the American Chemical Society* **1998**, *120*, 8767.
(68) Gong, W.; Hao, B.; Wei, Z.; Ferguson, D. J.; Tallant, T.; Krzycki, J. A.; Chan, M. K. *Proceedings of the National Academy of Sciences of the United States of America* **2008**, *105*, 9558.
(69) Chen, J. Y.; Huang, S.; Seravalli, J.; Gutzman, H.; Swartz, D. J.; Ragsdale, S. W.; Bagley, K. A. *Biochemistry* **2003**, *42*, 14822.
(70) Grahame, D. A.; Stadtman, T. C. *Journal of Biological Chemistry* **1987**, *262*, 3706.
(71) Ensign, S. A.; Bonam, D.; Ludden, P. W. *Biochemistry* **1989**, *28*, 4968.
(72) Hu, Z. G.; Spangler, N. J.; Anderson, M. E.; Xia, J. Q.; Ludden, P. W.; Lindahl, P. A.; Munch, E. *Journal of the American Chemical Society* **1996**, *118*, 830.
(73) Kim, E. J.; Feng, J.; Bramlett, M. R.; Lindahl, P. A. *Biochemistry* **2004**, *43*, 5728.
(74) Jeoung, J.-H.; Dobbek, H. *Journal of Biological Inorganic Chemistry* **2012**, *17*, 167.
(75) Ragsdale, S. W.; Wood, H. G. *Journal of Biological Chemistry* **1985**, *260*, 3970.
(76) Kumar, M.; Lu, W. P.; Smith, A.; Ragsdale, S. W.; McCracken, J. *Journal of the American Chemical Society* **1995**, *117*, 2963.
(77) Kumar, M.; Lu, W. P.; Ragsdale, S. W. *Biochemistry* **1994**, *33*, 9769.
(78) Menon, S.; Ragsdale, S. W. *Biochemistry* **1996**, *35*, 12119.
(79) Maynard, E. L.; Lindahl, P. A. *Journal of the American Chemical Society* **1999**, *121*, 9221.
(80) Andreese.Jr; Schaupp, A.; Neuraute.C; Brown, A.; Ljungdah.Lg *Journal of Bacteriology* **1973**, *114*, 743.
(81) Xia, J. Q.; Sinclair, J. F.; Baldwin, T. O.; Lindahl, P. A. *Biochemistry* **1996**, *35*, 1965.
(82) Shin, W.; Lindahl, P. A. *Journal of the American Chemical Society* **1992**, *114*, 9718.
(83) Heo, J. Y.; Staples, C. R.; Halbleib, C. M.; Ludden, P. W. *Biochemistry* **2000**, *39*, 7956.

(84) Barondeau, D. P.; Lindahl, P. A. *Journal of the American Chemical Society* **1997**, *119*, 3959.
(85) Maynard, E. L.; Sewell, C.; Lindahl, P. A. *Journal of the American Chemical Society* **2001**, *123*, 4697.
(86) Tan, X. S.; Loke, H. K.; Fitch, S.; Lindahl, P. A. *Journal of the American Chemical Society* **2005**, *127*, 5833.
(87) Saveant, J.-M. *Chemical Reviews* **2008**, *108*, 2348.
(88) Bonam, D.; Ludden, P. W. *Journal of Biological Chemistry* **1987**, *262*, 2980.
(89) Bonam, D.; Lehman, L.; Roberts, G. P.; Ludden, P. W. *Journal of Bacteriology* **1989**, *171*, 3102.
(90) Drake, H. L. *Journal of Bacteriology* **1982**, *149*, 561.
(91) Tolman, W. B. *Angewandte Chemie-International Edition* **2010**, *49*, 1018.
(92) Tavares, P.; Pereira, A. S.; Moura, J. J. G.; Moura, I. *Journal of Inorganic Biochemistry* **2006**, *100*, 2087.
(93) Lu, W. P.; Ragsdale, S. W. *Journal of Biological Chemistry* **1991**, *266*, 3554.
(94) Ho, B. K.; Gruswitz, F. *Bmc Structural Biology* **2008**, *8*, 49.
(95) Cracknell, J. A.; Wait, A. F.; Lenz, O.; Friedrich, B.; Armstrong, F. A. *Proceedings of the National Academy of Sciences of the United States of America* **2009**, *106*, 20681.
(96) Evans, R. M.; Parkin, A.; Roessler, M. M.; Murphy, B. J.; Adamson, H.; Lukey, M. J.; Sargent, F.; Volbeda, A.; Fontecilla-Camps, J. C.; Armstrong, F. A. *Journal of the American Chemical Society* **2013**, *135*, 2694.
(97) Stripp, S. T.; Goldet, G.; Brandmayr, C.; Sanganas, O.; Vincent, K. A.; Haumann, M.; Armstrong, F. A.; Happe, T. *Proceedings of the National Academy of Sciences of the United States of America* **2009**, *106*, 17331.
(98) Cokoja, M.; Bruckmeier, C.; Rieger, B.; Herrmann, W. A.; Kuehn, F. E. *Angewandte Chemie-International Edition* **2011**, *50*, 8510.
(99) Reda, T.; Plugge, C. M.; Abram, N. J.; Hirst, J. *Proceedings of the National Academy of Sciences of the United States of America* **2008**, *105*, 10654.
(100) Galan, B. R.; Schoeffel, J.; Linehan, J. C.; Seu, C.; Appel, A. M.; Roberts, J. A. S.; Helm, M. L.; Kilgore, U. J.; Yang, J. Y.; DuBois, D. L.; Kubiak, C. P. *Journal of the American Chemical Society* **2011**, *133*, 12167.
(101) DuBois, M. R.; DuBois, D. L. *Chemical Society Reviews* **2009**, *38*, 62.
(102) Crabtree, R. H. *The organometalic chemistry of the transition metal*; 5th ed.; Wiley, New York, 2009.
(103) Krishnan, S.; Armstrong, F. A. *Chemical Science* **2012**, *3*, 1015.
(104) Menon, S.; Ragsdale, S. W. *Biochemistry* **1996**, *35*, 15814.
(105) Santiago, B.; Meyer, O. *Fems Microbiology Letters* **1996**, *136*, 157.
(106) Roecker, L.; Meyer, T. J. *Journal of the American Chemical Society* **1986**, *108*, 4066.
(107) Halpern, J.; Taylor, S. M. *Discussions of the Faraday Society* **1960**, *29*, 174.
(108) Taylor, S. M.; Halpern, J. *Journal of the American Chemical Society* **1959**, *81*, 2933.
(109) Darensbourg, D. J.; Wiegreffe, H. P.; Wiegreffe, P. W. *Journal of the American Chemical Society* **1990**, *112*, 9252.
(110) Merrifield, J. H.; Gladysz, J. A. *Organometallics* **1983**, *2*, 782.
(111) Gu, W. W.; Seravalli, J.; Ragsdale, S. W.; Cramer, S. P. *Biochemistry* **2004**, *43*, 9029.

(112) Raaijmakers, H. C. A.; Romao, M. J. *Journal of Biological Inorganic Chemistry* **2006**, *11*, 849.
(113) Tiberti, M.; Papaleo, E.; Russo, N.; De Gioia, L.; Zampella, G. *Inorganic Chemistry* **2012**, *51*, 8331.
(114) Beley, M.; Collin, J. P.; Ruppert, R.; Sauvage, J. P. *Journal of the American Chemical Society* **1986**, *108*.
(115) Schmeier, T. J.; Dobereiner, G. E.; Crabtree, R. H.; Hazari, N. *Journal of the American Chemical Society* **2011**, *133*.